Effects of Rock and Fluid Properties on Seismic Dispersion and Attenuation in Sandstone

by
Qianqian Wei

A dissertation submitted to the Department of Earth and Atmospheric Sciences,
College of Natural Sciences and Mathematics
in partial fulfillment of the requirements for the degree of

DOCTOR OF PHILOSOPHY

in Geophysics

Chair of Committee: Hua-Wei Zhou

Committee Member: De-hua Han

Committee Member: Jiajia Sun

Committee Member: Hui Li

University of Houston
May 2021

ACKNOWLEDGMENTS

I would like to express my sincere gratitude to my advisor, Dr. De-hua Han, for his continuous support, guidance, and constructive suggestions throughout my Ph.D. program. I greatly admire his attitude, wisdom, and enthusiasm towards science, which will continue to inspire me in my future work. I would like to express my thankfulness to Dr. Hui Li for his suggestions and comments as a committee member and as the cooperator of my dissertation research. I would also like to thank my committee members, Dr. Hua-Wei Zhou and Dr. Jiajia Sun, for their generous time and constructive comments when reviewing my dissertation.

I am very grateful to Dr. Qiuliang Yao, Dr. Hui Li, Dr. Qi Huang, and Mr. Min Sun for their continuous work on developing and improving the Low frequency system. Without their success in improving the data quality, I could not have finished my PhD program.

Over my study at UH, it has been a great experience to be part of RPL research group. I will forever remember all the moments I spent together with the RPL colleagues, Mr. Min Sun, Mr. Frank Chen, Dr. Qiuliang Yao, Dr. Fuyong Yan, Dr. Yang Wang, Dr. Zhengwei Xu, Dr. Xuan Qin, Dr. Qi Huang, Dr. Hemin Yuan, Dr. Jiali Ren, and Mr. Teng Long. Special thanks to Mr. Min Sun, who always offered me supports of my research. I am very impressed by his kindness and willingness to help the students.

I could not have come this far without the endless love and support of my family. I would like to express the sincerest thanks to my parents and parents-in-law for their patience, and support. Last but not the least, I deeply indebted to my husband and my daughter for their endless love and accompany. I would not have finished the PhD program without the love, encouragement, and patience from my daughter. I dedicate this dissertation to my daughter with all my heart.

ABSTRACT

A better understanding of the relationship between dispersion/attenuation and rock/fluid properties is of great interest in improving hydrocarbon identification and reservoir characterization. Presently it is less investigated at seismic frequency range, limited by the reliable laboratory data measured under varying physical conditions. Additionally, the roles of fluid type and distribution in enhancing wave dispersion and attenuation are still poorly understood. With this concern, I perform three groups of laboratory measurements on wave dispersion and attenuation for typical porous sandstones at both seismic and ultrasonic frequencies and under vacuum-dry and fluid-saturated conditions. More specifically, sandstone samples are fully or partially saturated by a series of fluids: methane, butane, water, and glycerin, aiming to investigate effects of fluid viscosity and distribution on wave dispersion and attenuation.

The experimental data suggests that distinct dispersion and attenuation can be found even at vacuum-dry conditions, especially for sandstones with relatively high clay contents. This finding might contradict the previous knowledge of no dispersion and attenuation in dry rocks but has been extensively certified through a series of laboratory data in this study. Nevertheless, the comparison with fluid saturated data indicates that pore fluid related mechanisms are still the dominant cause for the dispersion and attenuation in sandstones. Significant dispersion and attenuation occur in the presence of relatively small amounts of gas both for partial glycerin and partial water saturation yet varying in their magnitudes and characteristic frequencies. Generally, the overall characteristic frequencies shift to a relatively lower frequency range with the decrease of rock permeability or the increase of fluid viscosity.

A complete attenuation curve is firstly observed in glycerin-saturated conditions at measured seismic frequency.

Based on porous modeling analysis, the mesoscopic fluid flow, in response to a heterogeneous fluid distribution in the pore space, might be the dominant mechanism accounting for the observed dispersion and attenuation in partially fluid-saturated rocks. The associations among velocity dispersion and wave attenuation, rock permeability, and fluid properties in the laboratory provide a potential indicator for the presence of fizz gas or high-permeability zones in fields during seismic surveys.

TABLE OF CONTENTS

LIST OF TABLES

LIST OF FIGURES

1. INTRODUCTION

1.1. Overview

Seismic survey is of great significance in hydrocarbon exploration and production, reservoir monitoring, CO_2 sequestration, and geothermal energy recovery, which relies on seismic waves travelling through the Earth's subsurface rocks. However, the subsurface rocks are generally porous, heterogeneous, and show viscoelastic properties. A wave propagating in such medium would induce velocity dispersion and wave attenuation (Goetz et al., 1979; Stewart et al., 1984). Dispersion is the variation of propagation velocity with frequency, while attenuation refers to the wave energy dissipation as seismic waves propagate through the subsurface. Given the velocity dispersion and wave attenuation contain the important signatures about rock and fluid properties (Goloshubin and Korneev, 2000; Castagna et al., 2003; Korneev et al., 2004; Chapman et al., 2006; Redmond, 2013), it is of considerable interest to investigate their relationships and identify the physical mechanisms.

1.1.1 Dispersion and attenuation in sedimentary rocks

The velocity dispersion and wave attenuation have been extensively observed and investigated in both field and laboratory conditions (Thomas, 1978; Goetz et al., 1979; Stewart et al., 1984; De et al., 1994; Murphy, 1982; Yin et al., 1992; Batzle et al., 2006; Tisato and Quintal, 2014; Spencer and Shine, 2016; Chapman et al., 2016, 2019; Pimienta et al., 2017; Yin et al., 2019; Li et al., 2020b). In general, the attenuation can be classified into two types: non-intrinsic attenuation and intrinsic attenuation. The key difference between these two types of attenuation lies in whether the kinetic energy would be converted into other forms of energy (e.g., thermal energy) or not. In most scenarios of the seismic exploration, both intrinsic and non-intrinsic attenuation simultaneously exist in the field data.

The non-intrinsic attenuation could be attributed to the geometric spreading and the wave energy partitioning. The geometric spreading occurs with the wavefront expansion of an elastic propagating wave, accompanied by a decrement of the wave energy. However, the decreasing energy induces the decrease of the wavefront amplitude instead of being transformed into other energy forms. The wave energy partitioning is occurring along with the processes of transmission, reflection, refraction, diffraction, and scattering when an elastic wave travels across an interface. At a planar interface, the incident wave partitions into multiple outgoing waves, accompanied by the decreasing wave amplitude. The relationship of the amplitude between incident and outgoing waves at a planar interface obeys the Zoeppritz equation (Aki and Ricard, 1980).

The intrinsic attenuation accounts for the conversion from seismic energy to other different types of energy (e.g., heat). Usually, this conversion arises from the inelasticity of subsurface rocks. The amount of energy loss is determined by the material's viscoelastic properties. The relationship between stress and strain in such medium does not obey the Hooke's law which only considers the effect of springs. Instead, it can be generally viewed as a spring-dashpot system. Three models are proposed to describe the viscoelastic behaviors between the stress and strain: Maxwell model, Kevin-Voigt model, and Zener model (Zener, 1948). The existence of the dashpot has two effects. First, the movement of the piston inside the dashpot will cause frictional energy loss, which subsequently is converted into heat. This is the root cause of the wave attenuation in so-called viscoelastic materials. Second, the stress exerted on the dashpot part is not proportional to the strain but associated with the rate of strain. In other words, the apparent stiffness of a dashpot depends on how fast it is deformed. Such time-dependent behavior is the major reason of the modulus (or velocity) dispersion in viscoelastic materials. For a purely linear, elastic material, the modulus dispersion should be related to the attenuation with the Kramers-Kronig equation (Toll, 1956), which basically illustrates that larger attenuation is associated to larger dispersion, whereas zero attenuation corresponds to no dispersion.

Furthermore, in geophysical field applications, the intrinsic dispersion/attenuation is closely related to the existence of hydrocarbon and can serve as a potential tool for reservoir characterization and hydrocarbon identification. In this dissertation work, I will mainly focus on investigating the intrinsic dispersion and attenuation of porous sandstones and their associations with rock and fluid properties. Thus, the dispersion and attenuation mentioned in the following contents refer to the intrinsic dispersion and attenuation.

1.1.2 Background literature

Many theoretical models seeking to understand the physical mechanism of wave dispersion and attenuation have been proposed. Early researchers believed that the friction-controlled sliding across the grain boundaries is the major cause of wave attenuation when a seismic wave passes through the rock (Walsh, 1966; Birch, 1975; Lockner et al., 1977; Johnston et al., 1979). As stated by Winkler et al. (1979), energy losses induced by frictional sliding only occur when the strain amplitude is greater than 10^{-6}. A propagating seismic wave is frequently characterized by a strain amplitude of 10^{-6} or below (Wideman and Major, 1967). Consequently, the frictional sliding at grain boundaries might not be the cause of velocity dispersion and wave attenuation in seismic explorations.

It has been increasingly believed that the wave-induced fluid flow (WIFF) at different scales is primarily responsible for the seismic wave attenuation in fluid-saturated sedimentary rocks (Biot, 1956; White, 1975; O'Connell and Budiansky, 1977; Cleary, 1978; Mavko and

Nur, 1979; Pride et al., 2004; Müller et al., 2010). The WIFF theories were first established by Biot in a series of papers (Biot, 1956a, 1956b, 1962). When the viscous fluid in pore spaces moves with respect to the host solid frame, a certain amount of energy will dissipate into heat, causing wave energy attenuation and velocity dispersion. In Biot's discussion, the fluid flow is induced by the pressure difference between the peak and trough of a passing plane seismic wave. The basic assumption of Biot's theory is that the material is homogeneous. However, in most cases, the observed dispersion and attenuation in sedimentary rocks are much stronger than those predicted by the Biot theory. Later, researchers found that the local heterogeneity can also generate pore pressure gradients and subsequently cause fluid flow (White, 1975; O'Connell and Budiansky, 1977; Cleary, 1978; Mavko and Nur, 1979; Pride et al., 2004). There are two types of heterogeneity inside a sedimentary rock. The first one is attributed to the different compliances of adjacent pores. When a seismic wave passes through, the fluid stored in cracks with greater compliance will be squeezed into pores with less compliance, generating a squirt flow (O'Connell and Budiansky, 1974, 1977; Mavko and Nur, 1975). The second type is ascribed to the compliance difference among various fluids. When two or more immiscible fluids with different compressibility coexist in the pore space (a typical case is the gas bubble within brine or oil), a passing wave will cause the phase boundary to oscillate, resulting in the dissipation from mechanical energy to heat (White, 1975). While the squirt flow models focus on heterogeneity at pore or grain scale, the compliance heterogeneity was extended into the mesoscopic scale in the double porosity and dual permeability model (Pride and Berryman, 2004).

The presence of WIFF is dominated by pore pressure gradients, which are caused by the heterogeneities either in the rock matrix or the saturating pore fluids. As a result, rock and fluid properties, such as permeability, pore structure, fluid viscosity, and fluid distribution, are expected to be sensitive to the velocity dispersion and wave attenuation (Zhao et al., 2017; Sarout et al., 2019). Effects of these parameters on the dispersion and attenuation have been experimentally investigated in the past decades (Tittmann et al., 1980; Murphy, 1982; Yin et al., 1992; Batzle et al., 2006; Tisato and Quintal, 2014; Spencer and Shine, 2016; Chapman et al., 2002, 2016; Pimienta et al., 2017; Yin et al., 2019; Li et al., 2020a). There are two basic experimental methods to make low-frequency measurements: resonant bar and forced-oscillation techniques. Resonant bar methods utilize a cylindrical or parallelepiped sample, usually driven into or through a resonant vibration with a sinusoidal force. Numerous modes of vibration are possible, including length deformations and flexural and torsional deformations. The attenuation can be determined by the width of the resonance frequency peak or by the decay of the resonation once the driving force is turned off. These techniques have the advantage of being simple and robust. Winkler et al. (1979), Clark (1980), and Murphy (1982) have used the resonant bar method to perform low-frequency measurements on a variety of sedimentary rocks. These resonance methods, however, have disadvantages. The rock samples must be sufficiently durable and homogeneous such that long, narrow bars can be machined. Larger samples result in lower frequencies.

The most frequently used method in low-frequency measurements is the forced-oscillation technique, allowing measurements over a wide frequency range and under varied ambient conditions. The forced-oscillation method is based on stress-strain relationship, which can measure the elastic and viscoelastic properties at seismic frequency bands. The elastic moduli are calculated from the ratio of the stress to the strain, while the attenuation is derived from the area of the hysteresis loop or the phase angle. During the measurements, a weak sinusoidal stress is applied to the sample and the induced deformation is monitored by the transducers. The strain amplitude induced by the sinusoidal stress is approximately 10^{-6}, which is similar to that of a seismic wave. Spencer (1981) first performed the forced-oscillation measurements with strain amplitude around 10^{-6} at frequencies below 100 Hz for both dry and water-saturated sandstones. This technique is further developed by Batzle et al. (2006) and Adam et al. (2009), who obtained several sets of velocity and attenuation data by measuring various reservoir rock samples at seismic frequencies. Following the measurement principles as used by Batzle et al. (2006), low-frequency measurement systems have been developed in some other research groups (Tisato and Quintal, 2013, 2014; Pimienta et al., 2014, 2015; Mikhaltsevitch et al., 2016; Zhao et al., 2017; Li et al., 2020b; Wei et al., 2021) to investigate the wave dispersion and attenuation characteristics.

1.2. Research challenges

Porous rocks are normally saturated with multiphase fluids underground (Zhao et al., 2017; Li et al., 2020a). When seismic waves pass through such subsurface rocks, it is unavoidable to create dissipative and dispersive responses. Besides the presence of multiphase fluids, the seismic dissipation and dispersion are highly associated with the intrinsic rock permeability and fluid viscosity, which determine the fluid mobility inside the rocks (Batzle et al., 2006). Moreover, it is of essential interest in investigating the effects of rock permeability, fluid viscosity, as well as fluid saturation on the seismic wave dissipation and dispersion in porous sandstones, given their significance in hydrocarbon exploration and production, reservoir monitoring, and geothermal energy recovery (Goodway et al., 2012; Zhao et al., 2017). However, both theoretical and experimental research of seismic wave dispersion and attenuation are still facing some critical challenges.

1. Many theories and models have been proposed for characterizing seismic dispersion and attenuation phenomenon in sedimentary rocks. But limited by lacking reliable laboratory data at seismic frequency bands, most of the theoretical models do not receive strong supports from experimental data. Given the high requirement of measurement precision and the complexity of laboratory measurements, there are limited teams capable of conducting low-frequency measurements worldwide so far. Therefore, a high-quality low frequency system, capable of precisely measuring intrinsic dispersion and attenuation at seismic frequency ranges, is necessary and meaningful.

2. Roles of rock and fluid properties in generating dispersion and attenuation are still poorly understood. Moreover, there exists a significant gap in explaining the existing seismic frequency data. Some contrasting conclusions have been inferred from previous measurements. Efforts must be made to precisely measure the velocity dispersion and wave attenuation at seismic frequency under varying physical conditions, such as different mineral contents, permeabilities, pore fluid viscosities, as well as effective pressures. Thus, we can develop robust relationship between dispersion/attenuation and rock/fluid properties.

3. It is particularly worth of mentioning the seismic dispersion and attenuation characteristics in partially saturated conditions. Since sedimentary porous rocks saturated with multiphases fluids are quite common in hydrocarbon reservoirs or engineering subjects: gas-brine-oil mixture in hydrocarbon reservoirs, CO_2-oil mixture for enhanced oil recovery (EOR), CO_2 mix with brine for CO_2 storage in saline aquifers, etc. (Zhao et al., 2017). Some experimental works have been done to examine the partial saturation effects on elastic properties of sedimentary rocks, aiming to better understand the seismic responses to partially saturated rock formations ((Murphy, 1982; Yin et al., 1992; Batzle et al., 2006; Tisato and

Quintal, 2014; Chapman et al., 2016, 2019; Mikhaltsevitch et al., 2016). However, to my best knowledge, most existing partial saturation experiments are carried out with water, while limited research have been done on other viscous fluids, which are also commonly encountered during the reservoir identification.

4. Today's challenging exploration requires us to integrate data from different frequency ranges for quantitative formation interpretations. However, the velocity dispersion makes the integration difficult. The low-frequency measurements together with ultrasonic measurements in the laboratory cover velocities at broad frequency bands. Practically, these measurements on core samples can provide important calibration points which facilitate the integration of acoustic data at different frequency scales. However, currently most groups conduct these two measurements in separate systems, which could be affected by artificial dispersion, resulting in ineffective comparisons.

1.3. Organization of the dissertation

The following dissertation comprises two major parts. The first part consists of Chapter 2 and Chapter 3, which mainly focus on the theoretical and experimental basis of seismic dispersion and attenuation. The second part consists of Chapter 4, Chapter 5, and Chapter 6, which concentrate on experimental studies, combined with theoretical analysis, to investigate the effects of rock and fluid properties on seismic dispersion and attenuation. The detailed outline is as follows:

In Chapter 2, I will review the fundamental dispersion and attenuation mechanisms, which may offer some insights for explaining experimental observations.

Chapter 3 introduces the principles and apparatus of the low frequency system built in the Rock Physics Lab of UH. Moreover, the specific procedure of sample preparation is described.

Chapter 4 investigates the effects of rock permeability on dispersion and attenuation in partially saturated sandstones at seismic frequencies. Comparison with theoretical and analytical models indicates the mechanism responsible for the observed frequency-dependent attenuation.

Chapter 5 reports the effects of fluid viscosity on dispersion and attenuation characteristics of fully saturated porous rocks. During this study, I successfully update the low frequency system and can measure the elastic properties of rock samples at both seismic and ultrasonic frequency range simultaneously. Following the update of my apparatus, I experimentally measured the elastic properties of the Berea sample saturated a series of fluids with varying viscosities (i.e., methane, butane, water, and glycerin).

In Chapter 6, I performed the laboratory measurements on the Berea sample under two partial saturation series with varying viscosities (e.g., water, glycerin). Specifically, for each saturation series, both the forced-oscillation and ultrasonic measurements are conducted at different saturation levels. Based on the measured results, I attempt to investigate the partial saturation effects on dispersion and attenuation.

2. THEORETICAL BACKGROUND

2.1. Introduction

Seismic waves propagating through the sedimentary rocks are intrinsically dispersive and dissipative due to the inelasticity of underground rock, which has been observed and recognized in field and laboratory data for years. Meanwhile, many theoretical models seeking to understand the physical mechanisms of wave dispersion and attenuation have been proposed. In this chapter, I will review some typical theories that explain the dispersion and attenuation at specific conditions. The assumption, physical meaning, and limitations of each model will be discussed.

2.2. Dispersion and attenuation mechanisms

2.2.1 Solid friction loss

Early researchers believe that the friction between the grain surfaces is the main contributor to the attenuation when seismic wave passing through the subsurface rock (Walsh, 1966). However, according to the measurements from Winkler and Nur (1979), the frictional energy losses in reservoir rocks occur only at strains greater than approximately 10^{-6} (Figure 2.1). While to my best knowledge, except for the cases in shallow weathering zone, the general seismic strain amplitudes encountered in typical exploration depth is less than the order of 10^{-6} (Wideman and Major, 1967). Therefore, the friction at grain boundary due to sliding should not be considered as the main source of attenuation and dispersion in seismic exploration.

Later studies showed that the primary dispersion and attenuation are induced from pore fluid related mechanisms. It is also increasingly believed that the wave-induced fluid flow (WIFF) at different scales is primarily contribute to the seismic wave attenuation in fluid-saturated sedimentary rocks (Biot, 1956; White, 1975; O'Connell and Budiansky, 1977; Cleary, 1978; Mavko and Nur, 1979; Pride and Berryman, 2003a, 2003b; Pride et al., 2004; Müller et al., 2010). In the past decades, more and more models have been proposed to account for the WIFF mechanisms.

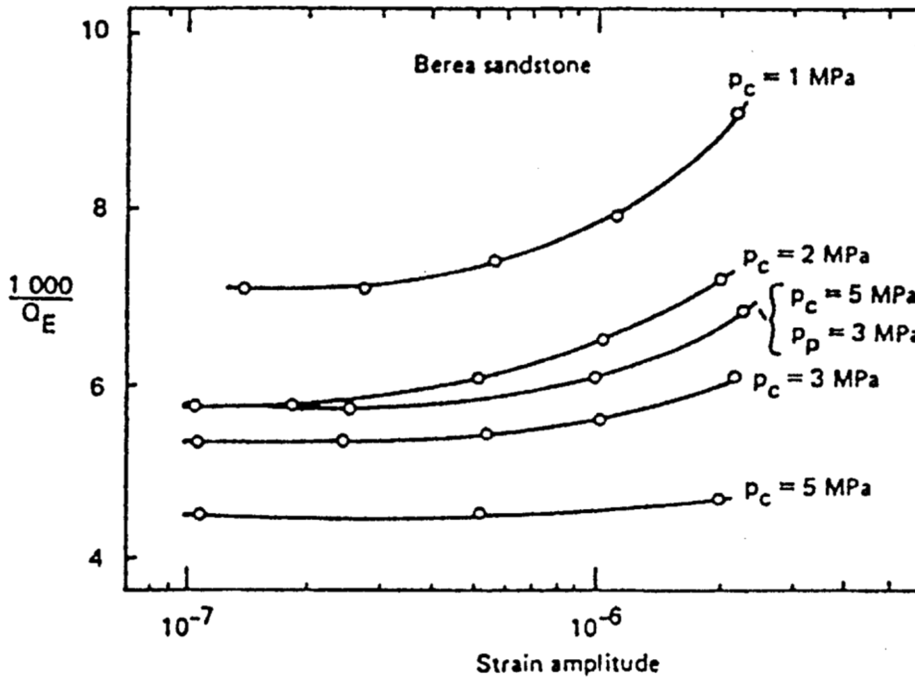

Figure 2.1 Intrinsic attenuation at different strain amplitudes and confining pressures.

2.2.2 Biot's Theory

The WIFF theories were first established by Biot in a series of papers (Biot, 1956a, 1956b, 1962). Biot theory considers frequency variations and allows for relative motion between fluid and rock framework. If a body wave propagates through a spatially homogeneous, permeable, and fluid-saturated rock, it will create pressure gradients between peaks and troughs of the wave. When the viscous fluid in pore spaces moves with respect to the host solid frame, a certain amount of energy will dissipate into heat, causing wave energy attenuation and velocity dispersion. Since this viscous-inertial attenuation and dispersion result from wavelength-scale flow, it is often called global or macroscopic flow.

To describe elastic waves in a system composed of porous elastic solid and viscous pore fluid, Boit introduced pore fluid parameters (such as fluid viscosity, density, and displacement) into the relationships of strain, stress, and displacement of the homogeneous and elastic solid material. He obtained two coupled wave equations to describe the wave propagation in the porous rock with the macroscopic fluid flow,

$$N\nabla^2 u + (A+N)\nabla\theta + Q\nabla\epsilon = \rho_u \ddot{u} + \rho_{u,U}\ddot{U} + b(\dot{u} - \dot{U}) \qquad (2.1)$$

$$Q\nabla\theta + R\nabla\epsilon = \rho_{u,U}\ddot{u} + \rho_U \ddot{U} - b(\dot{u} - \dot{U}) \qquad (2.2)$$

where b $(= \frac{\eta\phi^2}{\kappa})$ is the dissipative parameter (ϕ is the rock's porosity, κ is the rock permeability, and η is the fluid viscosity), u is the solid displacement vector, U is the fluid displacement vector, θ $(= \nabla \cdot u)$ is the divergence of the solid displacement, ϵ $(= \nabla \cdot U)$ is the divergence of the fluid displacement, A, N, Q and R are elastic constants, ρ_u, ρ_U, and $\rho_{u,U}$ are densities.

By solving two equations, characteristics of macroscopic fluid flow can be revealed. It is found that the phase velocity of waves increases slightly with the frequency while the absorption coefficient is proportional to the square of the frequency. The characteristic frequency f_c of Biot's theory is $\frac{\eta\phi}{2\pi\rho_f\kappa\xi}$, which may be considered as a frequency scale of the material. Here, ξ is the tortuosity (Biot, 1956a; Muller et al., 2010). One interpretation of this relation is that it is the frequency where viscous forces equal to the inertial forces. At the low frequency ($f \ll f_c$), the fluid movement is dominated by the viscous forces. While at high frequency ($f \gg f_c$), the inertia effect is the dominant factor in the fluid flow (Mavko and Jizba, 1994). For example, when the permeability decreases and viscosity increases, the characteristic frequency shifts to a higher frequency.

There are three waves exist in the rock with Biot's flow, one S-wave and two P-waves, denoted as fast P-wave and slow P-wave. The fast P-wave occurs when the overall solid and fluid motions are in phase whereas the slow P-wave appears when the overall solid and fluid motions have 180-degree phase difference. Meanwhile, both fast and slow P-waves have their own dispersion and attenuation features. The fast P-wave is slightly dispersive and dissipative. However, the slow P-wave is significantly frequency dependent with large attenuation. Typically, the slow P-wave will damp out in couple of cycles, thus being very difficult to observe in the conventional measurements and seismic data. Nevertheless, the slow P-wave is experimentally observed in a water-saturated porous glass by Plona (1980b) and a water-saturated sandstone at ultrasonic frequency band for the first time by Kelder and Smeulders (1997). Those observations greatly promoted the validation of Biot's theory.

According to later studies (Bourbié et al., 1993; Pride, 2005), the dispersion and attenuation caused by macroscopic fluid flow in typical rocks can only be significant at frequencies above 100 kHz, well outside the seismic exploration band. In addition, the magnitude of the velocity dispersion and wave attenuation predicted from Biot theory is smaller than those observed in lab measurement and seismic data. Therefore, the macroscopic fluid flow is not applicable to explain the dispersion and attenuation of seismic data. Nevertheless, Biot's theory provides us a fundamental framework to investigate the velocity dispersion and wave attenuation caused by the fluid flow. Based on this theory, later proposed models involve the heterogeneities on rock or fluid, and input additional parameters, such as pore aspect ratio, or bubble size.

2.2.3 Squirt flow

In contrast with Biot theory, squirt model describes the case that the pore pressure gradients and fluid flow are introduced from pore scale heterogeneity, particularly the scale of individual grains and pores. Thus, the squirt flow is also called the microscopic fluid flow.

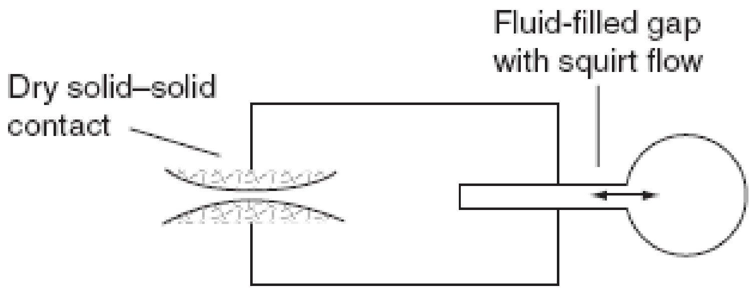

Figure 2.2 Schematic of a micromechanical model to describe the squirt-flow mechanism.

The microscopic scale type of heterogeneity was early recognized by O'Connell and Budiansky (1974, 1977). It mainly results from the different compliances of adjacent pores, such as the difference in pore shape or orientation. Figure 2.2 shows the schematic of a micromechanical model to describe the squirt flow mechanism (Mavko et al., 2009). When a seismic wave passes through rock, the fluids stored in those more compliant cracks are likely to be squeezed into those less compliant pores, generating pore pressure gradients and squirt flow. The relationship between the pore pressure and the fluid movement is given as following,

$$\rho \frac{\partial v}{\partial t} = -\frac{\partial P}{\partial x} + \eta \frac{\partial^2 v}{\partial y^2} \tag{2.3}$$

Here, ρ is the fluid density, P is the pore pressure, η is the fluid viscosity, and v is the fluid velocity along x direction. The associated characteristic frequency is $f_c = \varepsilon^3 K/\eta$. Here, ε is the crack aspect ratio, K is the frame bulk modulus. To thoroughly understand squirt flow related attenuation, it is necessary to qualitatively describe this physical mechanism. At a low frequency range $f < f_c$, the pore pressure increment caused by squirt flow has enough time to relax. At a high frequency $f > f_c$, the pore pressure increment cannot be totally balanced, and the fluid does not flow at all. For a rock, the confining pressure shrinks the rock volume, while the pore pressure has the opposite effect. In the poroelastic theory, the wave generates a confining pressure compressing the rock, but the pore fluid can resist the rock deformation. Therefore, the unrelaxed pore pressure makes the rock stiffer than the relaxed pore fluid. In the transition frequency band, the rock gradually becomes stiffer as the frequency increases. Because the pore fluid is viscous, the fluid vibration energy taking from the wave will transform into heat. In a specified frequency, the fluid flow will have resonance and absorb the most energy from the wave, and thus the wave attenuation reaches the maximum value.

The most important contribution of the squirt flow model is that it explicitly established the bridge between the rock frame heterogeneity and the wave attenuation. Moreover, the study on the squirt flow is continued by many other investigators to interpret the inelastic properties in fractured or cracked porous media (Mavko and Jizba, 1991; Dvorkin et al., 1995; Le Ravalec and Gueguen, 1996; Chapman, 2002; Lambert et al., 2006; Gurevich et al., 2009a, 2009b).

Due to the small heterogeneity scale and short diffusion time, it is usually considered that squirt flow attenuation mainly occurs at relatively higher frequency range, such as ultrasonic, and does not has significant effect in seismic or well-log frequency range. However, recent field or laboratory study shows that squirt flow can also play a role in seismic frequency in some unconventional rocks. Figure 2.3 shows the frequency dependence of P and S wave velocity of a tight gas sandstone with very low permeability. Cracks and fractures within the tight sandstone, along with other intergranular pores or micropores, constitute the necessary heterogeneities in pore scale, which are good candidates for the squirt flow. Meanwhile, with such low permeability, even though the heterogeneity size is very small, the relaxation time needed is long enough to shift the characteristic frequency to seismic frequency range.

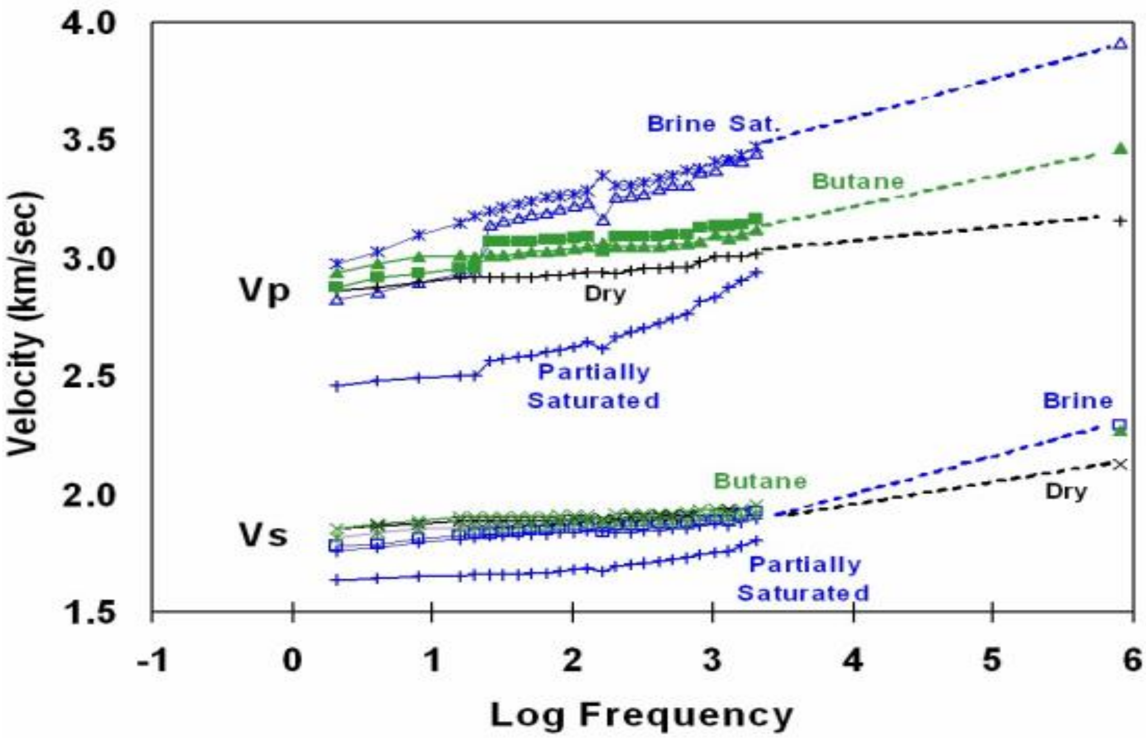

Figure 2.3 Frequency dependence of P and S wave velocity of a tight gas sandstone.

2.3.4 White's partial gas saturation model

Besides the Squirt flow (resulting from pore scale heterogeneity), WIFF can also occur on a scale larger than typical pore size but smaller than the wavelength, the so-called mesoscopic flow (Figure 2.4). In typical sedimentary rocks, mesoscopic flow can occur within a wide range of scales, from the largest pore size to the smallest wavelength, thus can cause wave attenuation in a broad frequency range. It is also increasingly believed that mesoscopic flow is a primary mechanism of fluid-related attenuation in the seismic frequency range (Pride et al., 2004). The lager degree of heterogeneity — the contrast between elastic properties of different regions of the rock, the more significant attenuation and dispersion can be induced.

Two most obvious scenarios that have received substantial attention in recent years are patchy saturation and fractured reservoirs.

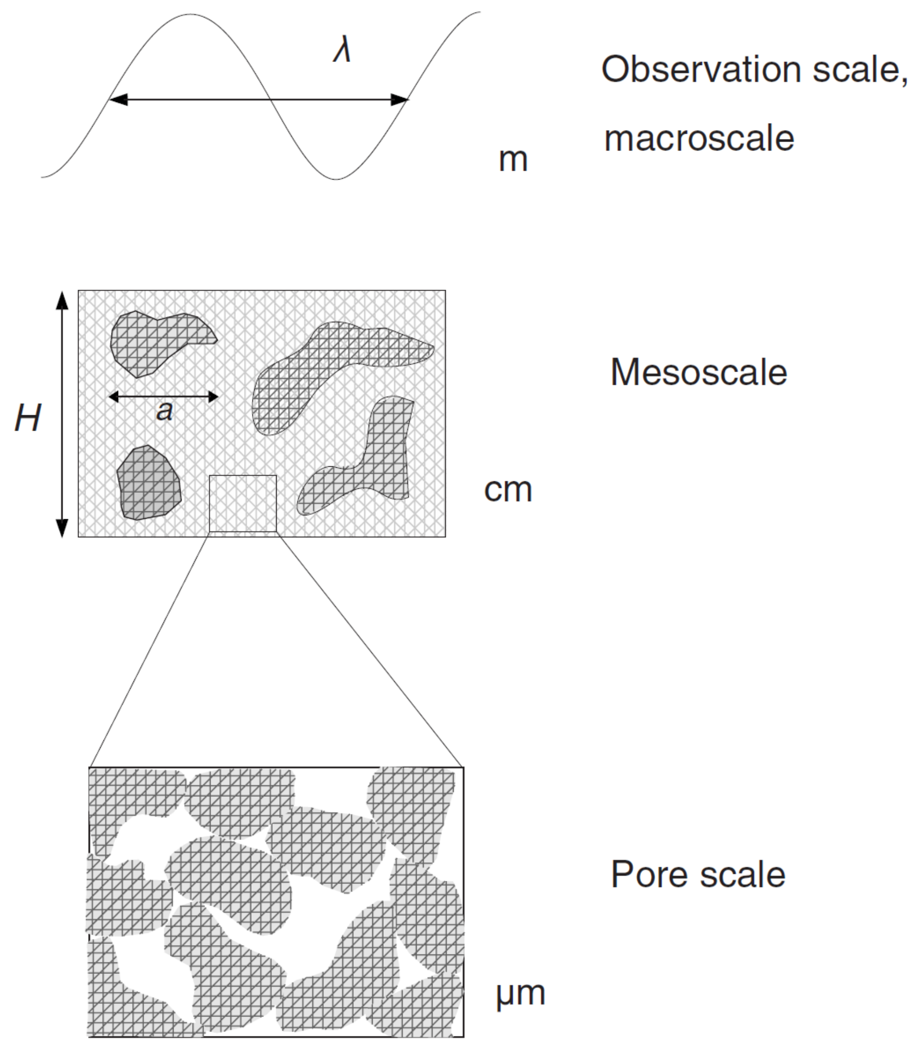

Figure 2.4 The scales that is typically relevant for wave-induced flow to occur at seismic frequencies.

When two immiscible pore fluids with substantially different compressibility form patchy saturation at the mesoscopic scale, the spatial pressure gradients induced by passing compressional wave will cause the phase boundary to oscillate and dissipate the wave energy. White (1975) modeled the patchy saturation effects by considering an idealized geometry. Spherical gas-filled pockets located at the corners of a cubic array with other parts saturated with brine (Figure 2.5). For simplicity, White treated the water and gas mixture inside the square as two concentric spheres. When a wave passes through the rock, a specified fractional volume change is impressed on the outer surface. The gas pocket is assumed to provide the release path for pressure gradient. The ratio of pressure amplitude to the fractional volume change yields the complex bulk modulus. With known density and shear modulus, velocity and attenuation compressional waves can be calculated.

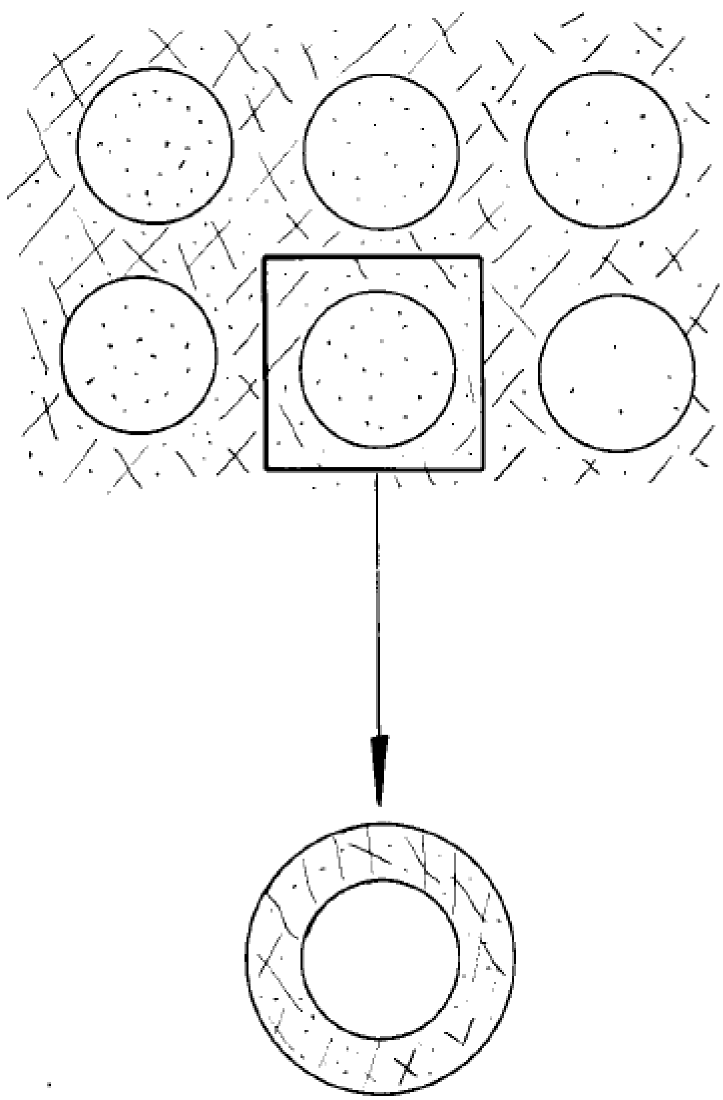

Figure 2.5 White’s partial gas saturation model.

Apparently, this model exhibits a relaxation phenomenon, and its characteristic frequency (or time) depends on the size of the gas pockets and the distance between them. When the oscillation period of passing wave is long compared to characteristic time, the fluid pressure can be relaxed, and the bulk modulus is independent of frequency. When the oscillation period is short, the pore pressure will be unrelaxed, where the bulk modulus is substantially the value computed as if there were no fluid flow. In the intermediate frequency range, pore fluids will vibrate with wave, and characterized by velocity dispersion and wave attenuation.

White (1975) conducted a numerical simulation to examine this model. Physical properties of the rock are porosity of 30%, grain density of 2.65 g/cc, bulk and shear modulus of rock frame are 38 GPa and 45 GPa. Several features can be found from the results. First, significant dispersion and attenuation occur in seismic frequency range (10-300 Hz). Second, P-wave velocity increases by 22% and the attenuation peak is 0.19. It also suggests that mesoscopic flow is a primary mechanism of fluid-related attenuation in the seismic frequency range.

2.3.5 Double-porosity dual-permeability model

White model characterizes the effect of fluid heterogeneous distribution on dispersion and attenuation at mesoscopic scale. Another obvious scenario of mesoscopic scale is heterogeneous porous structures. Berryman and Wang (2001) first introduced the idea of double porosity to represent the large contrast on the pore compressibility between two porous phases, such as matrix round pores and fractures. Elements of this double porosity are porous rock matrix intersected by fractures (Figure 2.6). Here, the fractures are much larger than the pore or grain size, but much smaller than the wavelength, which is distinguished with squirt flow model. Therefore, three types of macroscopic pressure are pertinent in such a model: external confining pressure pc; internal pressure of the matrix pore fluid pf1; and internal pressure of the fracture pore fluid pf2. Under the same confining pressure, fractures are more compliant than the matrix round pores. Then the pore pressure in the fractures will be higher than that in the round pores, which will force the fluid flow from the fractures toward to the stiffer round pores.

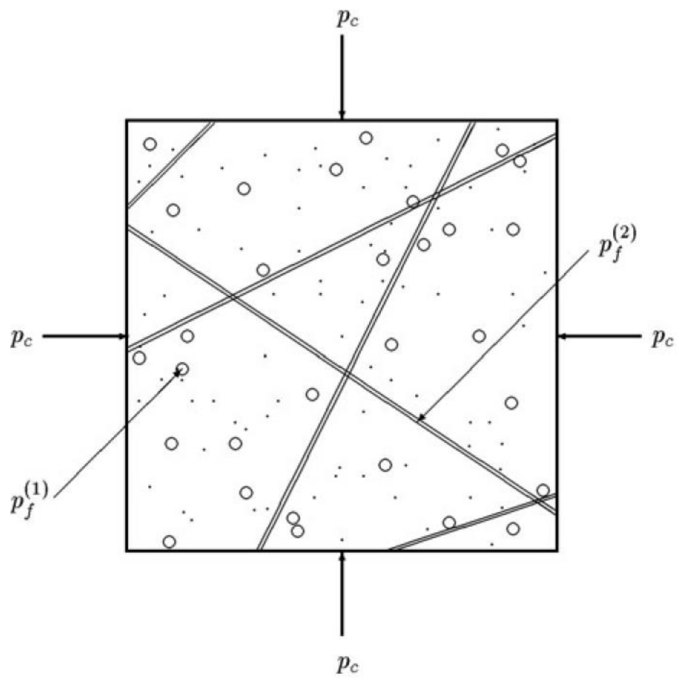

Figure 2.6 Double-porosity dual-permeability model.

Then the double porosity concept was further developed into double porosity and dual permeability model (Pride and Berryman, 2003). It generally characterizes the spatial variation of either rock frame or fluid compressibility in mesoscopic heterogeneity scale. Figure 2.7 shows the P-wave attenuation of a double-porosity composite saturating fluids with different viscosities. The three curves correspond to viscosities of 2×10^{-3} Pa*s (solid curve representing ambient water), 2×10^{-4} Pa*s (dashed curve representing hot water), and 5×10^{-3} Pa*s (dotted curve representing oil). The left peak of each curve corresponds to the characteristic frequency when the mesoscopic heterogeneity just has time to equilibrate in one cycle, while the right peak corresponds to the largest Biot loss, which occurs when the entire wavelength of fluid-pressure variation just equilibrates in a cycle. Also, it can be found that the effect of viscosity is to shift the attenuation peaks differently. For the mesoscopic heterogeneity, it has its own inherent characteristic frequency, which is inversely proportional to viscosity. Therefore, mesoscopic pressure gradient will equilibrate when the frequency is smaller than characteristic frequency and the attenuation peaks shift to lower frequency range with increasing viscosity. In contrast, for the Biot loss, the characteristic frequency has the opposite dependence on the fluid viscosity. The wavelength scale pressure gradient is equilibrating when the frequency is smaller than characteristic frequency and the attenuation peaks shift to higher frequency range with increasing viscosity.

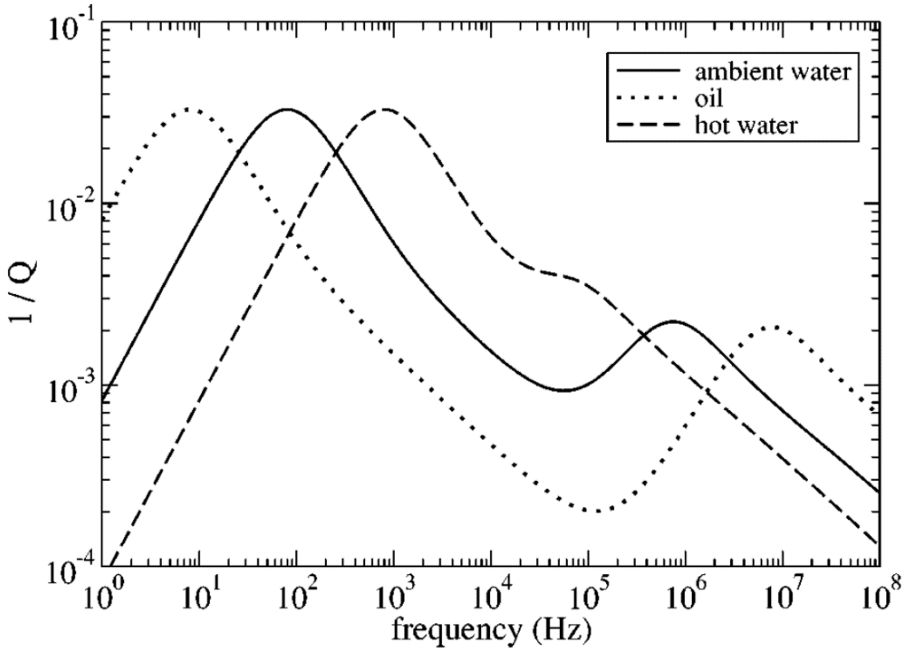

Figure 2.7 The P-wave attenuation of a double-porosity composite having different properties.

2.3. Summary

The presence of fluids in the pore space of rocks causes dispersion and attenuation by the wave-induced fluid flow mechanism (WIFF). WIFF's classification depends on the length scale of the pressure gradient, which can be classified into global flow (macroscopic fluid flow) and local flow (microscopic fluid flow and mesoscopic fluid flow).

The macroscopic fluid flow proposed by Biot generates viscous-inertial attenuation and dispersion at the wavelength-scale. However, macroscopic flow attenuation in typical rocks can only be significant at frequencies above 100 kHz, well outside the seismic exploration band. Meanwhile, the magnitude of the dispersion and attenuation predicated by Biot's theory is less than that observed in the real data. All the local fluid flow models consider that the wave-induced local pore pressure increments, due to heterogeneities of the pore fluid and/or the rock frame, account for the wave dispersion and attenuation in porous rocks. The squirt flow model and BISQ model investigate the heterogeneities in the microscopic scale, while White's model and the double-porosity dual-permeability model study the heterogeneities in the mesoscopic scale. It is usually considered that squirt flow attenuation mainly occurs at relatively higher frequency range, such as ultrasonic, and does not has significant effect in seismic or well-log frequency range. However, recent field or laboratory study shows that squirt flow can also play a role in seismic frequency in some reservoir rocks. Mesoscopic flow can occur within a wide range of scales, and cause wave attenuation in a broad frequency range. It is increasingly believed that mesoscopic flow is a primary mechanism of fluid-related attenuation in the seismic frequency range.

It is also worthwhile to notice the effects of viscosity and permeability on characteristic frequency, which largely dominates the features of velocity dispersion and wave attenuation. For instance, the Biot theory suggests the opposite dependence of characteristic frequency on the fluid viscosity with other attenuation models. Moreover, these two parameters are the main factors on which I will focus in low frequency measurements.

3. LOW FREQUENCY SYSTEM

3.1. Introduction

A low frequency system is essential to the experimental study of velocity dispersion and attenuation at seismic frequency. Following the forced-oscillation principles as used by Batzle et al. (2006), a well calibrated low-frequency measurement system has been developed in the Rock Physics Laboratory at the University of Houston (Yao, 2013; Li et al., 2020a), which can measure the elastic modulus and the corresponding attenuation of rocks under varying physical conditions at seismic frequency ranges (2-600 Hz). In this chapter, the evolution of the laboratory measurement methods of seismic dispersion and attenuation is reviewed firstly. Then I will introduce the forced-oscillation principles and present the low frequency system. Lastly, specific sample preparations for low frequency measurement are described.

3.2. Review on low frequency measurement

Laboratory measurements of the velocities of reservoir rocks are traditionally conducted at ultrasonic (MHz) frequency range. The wavelength of pulse is in mm range, which is much smaller than the typical core sample length (Figure 3.1). Through the pulse transmission technique (Yin, 1992), first-arrival travel times of P- and S-waves of rock samples can be recorded. P- and S-wave velocities can be calculated from the sample length and the first arrival times.

$$V = L/t \tag{3.1}$$

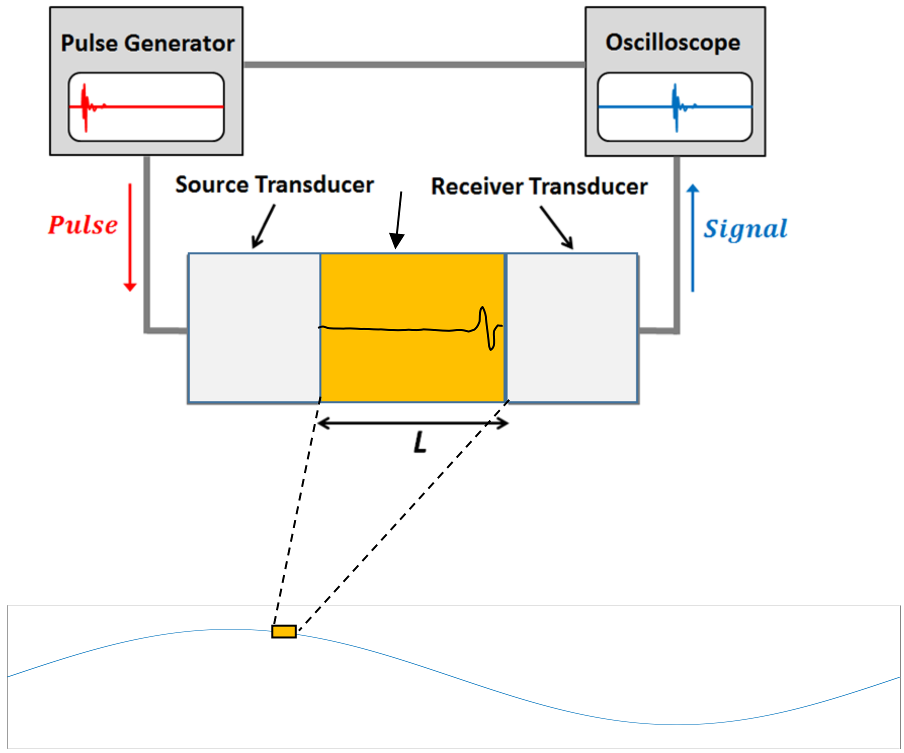

Figure 3.1 First arrival-pick up method in ultrasonic measurement.

However, if the measured frequency goes to the seismic frequency range (1-100Hz), the corresponding wavelength falls into tens to thousands of meters, which is much larger than the traditional length of a core sample. Therefore, a transient wave and first arrival pick up method is obviously not feasible anymore (Figure 3.1). Former researchers have been strived for years to indirectly measure the velocity and attenuation in relatively low-frequency range. Presently, there are two basic experimental methods, resonance-bar technique and forced-oscillation method.

3.2.1 Resonant bar method

Resonant bar utilizes a cylindrical or parallelepiped sample and is mechanically excited by a resonant vibration with a sinusoidal force. Young's modulus and shear modulus can be obtained from vibration modes of length deformation and flexural/torsional deformation. Attenuation is measured either from the width of the resonance frequency peak or from the decay of the resonation once the driving force is turned off (Murphy, 1982). These techniques have the advantage of being simple and robust. The drawback of this method is the necessity of very long samples to go sufficiently low in frequency, i.e., length of 85.3 cm for a sample of Amherst sandstone to achieve a frequency of 1260 Hz (Born, 1941). Murphy (1982) used the resonance-bar method to measure the extensional wave velocity and attenuation in partial-saturated sandstone at frequencies from 0.3 to 14 kHz. He found that the maximum attenuation is observed mainly in the presence of small percent of gas saturation. Yin et al. (1992) continued efforts with resonance bar and extend the frequency range a little bit wider into 0.3-14 kHz, making their results more meaningful for the well-logging data interpretation. However, constrained by the size and geometry of the sample, it is impossible to extend the measurement frequency range into the seismic band.

3.2.2 Forced-oscillation method

The forced-oscillation method is based on stress-strain relationship, and capable to measure the elastic and viscoelastic properties in seismic frequency. The ratio of the stress to the strain gives the moduli, and the area of the hysteresis loop or the phase angle between the stress and strain gives the attenuation. This experiment often takes the form of applying a weak sinusoidal stress to the sample and monitoring the deformation with the transducers. Meanwhile, the magnitudes of measured attenuation are relatively low (~0.01 – 0.1) and the amplitudes of strain are particularly low at the order of ~10^{-6} (i.e., similar orders of magnitude to seismic waves). Thus, it is experimentally challenging to perform forced-oscillation measurement. Spencer (1981) first successfully performed the forced-oscillation measurements with strain amplitude around 10^{-6} at frequencies below 100 Hz for dry and water-saturated sandstones. This technique is further developed by Batzle et al. (2006) and Adam et al. (2009), who obtained several sets of velocities and attenuation from various reservoir rocks at seismic frequencies (Figure 3.2).

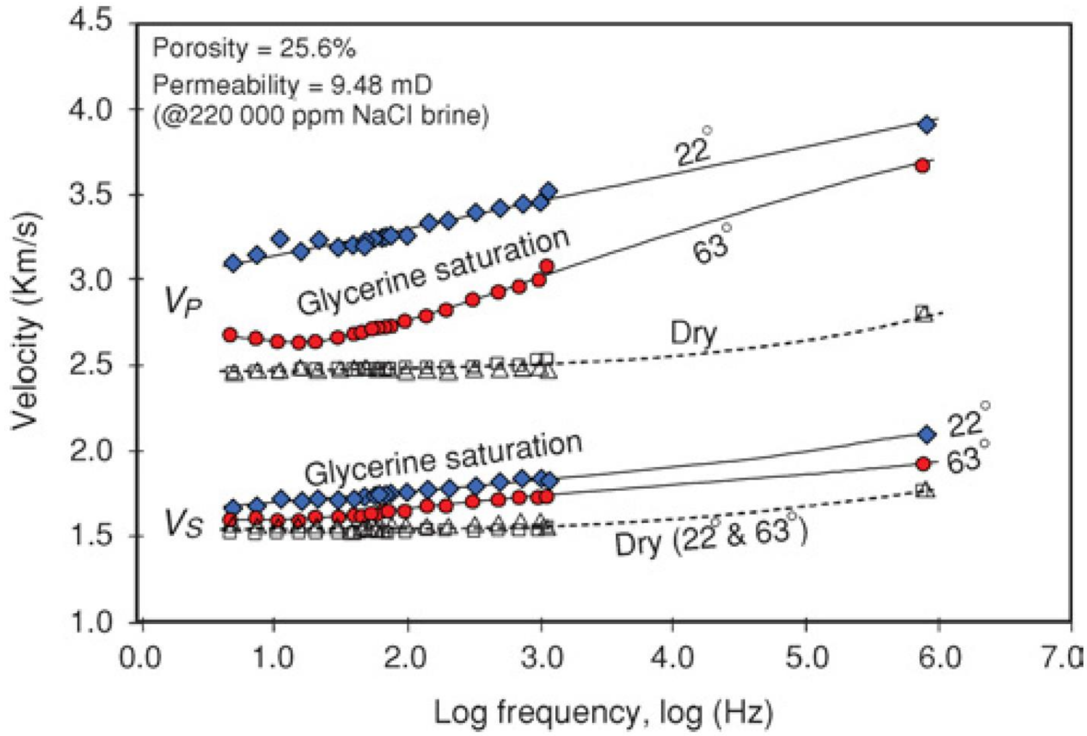

Figure 3.2 Compressional and shear velocities as a function of frequency and temperature for dry and glycerin saturated Foxhills Sandstone.

Following similar measurement principles as used by Batzle et al. (2006), a well-calibrated low-frequency measurement system has been developed in the Rock Physics Laboratory at the University of Houston (Li et al., 2020a), which is capable of measuring the elastic modulus and the corresponding attenuation of rocks under varying physical conditions at seismic frequency ranges (2-600 Hz).

3.3. Measurement principles

The principle of the forced-oscillation measurement is based on the Hooke's Law. Instead of measuring the velocity directly as ultrasonic measurement, two elastic constants (Young's modulus and Poisson's ratio) are measured. When a sinusoid stress field is applied vertically on the sample, the vertical and horizontal deformations are generated (Figure 3.3). By recording the stress σ, vertical strain $\varepsilon_{\perp}$ and horizontal strain $\varepsilon_{\parallel}$, Young's modulus and Poisson's ratio are obtained as:

$$E = \frac{\sigma}{\varepsilon_{\perp}} \tag{3.2}$$

$$\nu = -\frac{\varepsilon_{\parallel}}{\varepsilon_{\perp}} \tag{3.3}$$

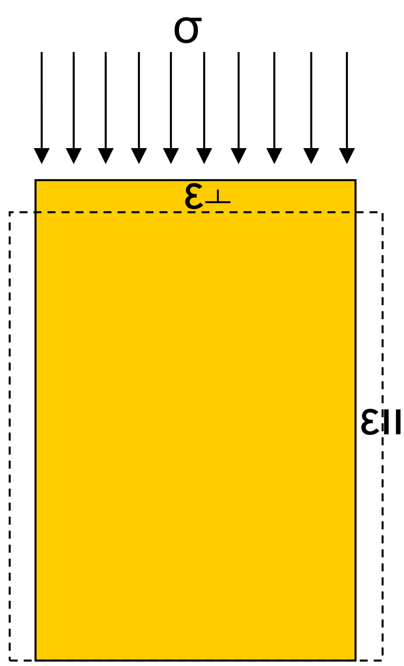

Figure 3.3 Principle of stress-strain relationship to measure elastic moduli of solid sample.

Since a sinusoidal oscillated (2–500 Hz) axial stress $\sigma(\omega)$ is applied in my low frequency measurement, the strains are frequency dependent $\varepsilon_{\perp}(\omega)$ and $\varepsilon_{\parallel}(\omega)$. Consequently, the frequency dependent Young's modulus $E(\omega)$ and Poisson's ratio $\nu(\omega)$ of measured sample can be obtained as

$$E(\omega) = \frac{\sigma(\omega)}{\varepsilon_{\perp}(\omega)} \tag{3.4}$$

$$\nu(\omega) = -\frac{\varepsilon_{\parallel}(\omega)}{\varepsilon_{\perp}(\omega)} \tag{3.5}$$

If the assumption of isotropic, homogeneous rock sample is valid, which means only two elastic constants are independent, bulk modulus $K(\omega)$/shear modulus $G(\omega)$ and P-wave velocity $Vp(\omega)$/S-wave velocity $Vs(\omega)$ can be further calculated from Young's modulus and Poison's ratio,

$$K(\omega) = \frac{E(\omega)}{3[1-2\nu(\omega)]} \qquad G(\omega) = \frac{E(\omega)}{2[1+\nu(\omega)]} \tag{3.6}$$

$$Vp\ (\omega) = \sqrt{\frac{K(\omega)+\frac{4}{3}G(\omega)}{\rho}} \qquad Vs\ (\omega) = \sqrt{\frac{G(\omega)}{\rho}} \tag{3.7}$$

where ρ is the bulk density of rock sample.

According to viscoelastic theory, the stress and strain are in phase for purely elastic materials,

$$\sigma(\omega) = \sigma_0 \sin(\omega t) \tag{3.8}$$

$$\varepsilon(\omega) = \varepsilon_0 \sin(\omega t) \tag{3.9}$$

In contrast, for purely viscous materials, the stress and strain have a phase lag of 90 degrees,

$$\sigma(\omega) = \sigma_0 \sin(\omega t) \tag{3.10}$$

$$\varepsilon(\omega) = \varepsilon_0 \sin(\omega t - \frac{\pi}{2}) \tag{3.11}$$

The reservoir rocks often show viscoelastic behavior, which takes place between pure elasticity and pure viscosity. Therefore, the phase difference θ of stress and strain of the rock sample ranges from 0 to 90 degrees,

$$\sigma(\omega) = \sigma_0 \sin(\omega t) \tag{3.12}$$

$$\varepsilon(\omega) = \varepsilon_0 \sin(\omega t - \theta) \tag{3.13}$$

If a wave propagates through the viscoelastic materials, there will be kinetic energy loss, which can be defined by the complex modulus as follows,

$$M = M_r + iM_i \tag{3.14}$$

$$M_r = \frac{\sigma_0}{\varepsilon_0}\cos\theta \tag{3.15}$$

$$M_i = \frac{\sigma_0}{\varepsilon_0}\sin\theta \tag{3.16}$$

where M_r and M_i represent the energy storage and the energy loss, respectively. Then quality factor Q can be calculated by the complex modulus (O'Connell and Budiansky, 1977),

$$Q_M = \frac{M_r}{M_i} = \frac{1}{\tan\theta} \tag{3.17}$$

In the low frequency measurements, phases of stress, vertical and horizontal strains will be recorded. Therefore, quality factors of Young's modulus and Poisson's ratio ($Q_E(\omega)$ and $Q_\nu(\omega)$) can be acquired by:

$$Q_E(\omega) = \frac{E_r(\omega)}{E_i(\omega)} \tag{3.18}$$

$$Q_\nu = \frac{\nu_r(\omega)}{\nu_i(\omega)} \tag{3.19}$$

The other quality factors, such as quality factors of shear modulus, P-wave modulus, and bulk modulus, are related to each other and can be calculated through these three equations (White, 1965; Winkler and Nur, 1979):

$$Q_S^{-1}(\omega) = Q_E^{-1}(\omega) - \frac{\nu(\omega)}{1+\nu(\omega)} Q_\nu^{-1}(\omega) \tag{3.20}$$

$$Q_P^{-1}(\omega) = \frac{1+\nu(\omega)}{[1-\nu(\omega)][(1-2\nu(\omega)]} Q_E^{-1}(\omega) - \frac{2\nu(\omega)[2-\nu(\omega)]}{[1-\nu(\omega)][(1-2\nu(\omega)]} Q_S^{-1}(\omega) \tag{3.21}$$

$$Q_K^{-1}(\omega) = \frac{3}{1-2\nu(\omega)} Q_E^{-1}(\omega) - \frac{2[1+\nu(\omega)]}{1-2\nu(\omega)} Q_S^{-1}(\omega) \tag{3.22}$$

Experimentally, instead of directly measuring the amplitude and phase of the applied stress, I use an aluminum or Titanium standard as a reference to calculate stress. The standard is stacked with the rock sample under the same uniaxial stress (Figure 3.4). The diameter of the standard is identical to that of the sample. Thus, the stress on the sample is approximately the same as the stress on the standard. In addition, the Young's modulus of aluminum or Titanium is known and does not change with frequency. Consequently, the frequency dependent Young's modulus $E(\omega)$and Poisson's ratio $\nu(\omega)$ of measured sample can be obtained by comparing the strains recorded in the sample and standard,

$$E_{sample}(\omega) = \frac{E^{standard} * \varepsilon_{\perp}^{standard}(\omega)}{\varepsilon_{\perp}^{sample}(\omega)} \tag{3.23}$$

where $E_{\perp}^{standard}$ and $\varepsilon_{\perp}^{standard}(\omega)$ are the Young's modulus and axial strain of the standard, respectively.

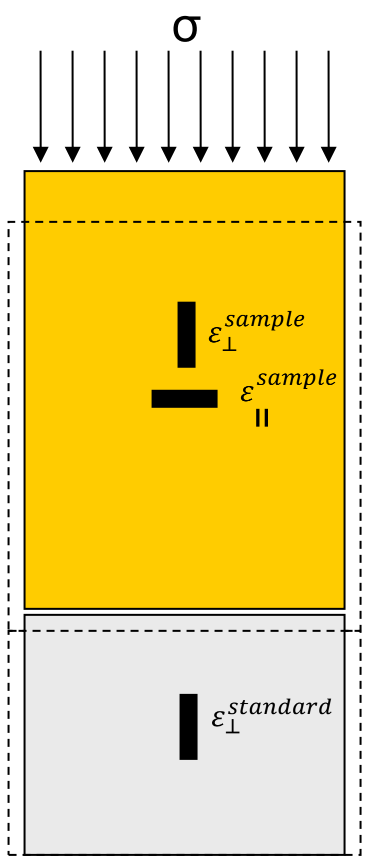

Figure 3.4 Uniaxial stress and generated strain on the rock sample and standard.

Since aluminum or Titanium is essentially elastic, its strain is exactly in phase with the stress. Thus, I use the phase of strain on the standard represents the phase of the applied stress. According to the vibration theory, under the same force, the sample's stress and the standard's stress are in the same phase, while the sample's strain and the standard's strain are in the different phases. In addition, both the standard and rock sample signals go through identical electronic paths; amplifier phase shifts and other noise cancel in the analysis (Batzle et al., 2006). Therefore, the quality factor of Young's modulus of the sample can be calculated by,

$$Q_E(\omega) = \frac{1}{\tan\theta} \tag{3.24}$$

where θ is the phase delay between the sample's strain and the standard's strain.

Several advantages are achieved for the relative stress measurement as opposed to the direct stress measurement. First, I use the same electronic instruments to measure the stress and strain, which can make the system compact and calibration much easier. Moreover, using strain instead of stress efficiently generates all recorded data in the same order of magnitude, which can largely reduce the random error and increase the data quality.

3.4. Low frequency apparatus

In order to obtain high quality data of low frequency measurement, the following requirements are expected for the low frequency system: 1. the measured frequency range includes typical seismic frequency band, several Hz to hundreds Hz; 2. the strains are the same order of magnitude as seismic waves, which is usually less than 10^{-6}; 3. high S/N ratio; 4. mechanical component includes pressure vessel, pore fluid lines as well as digital pump to simulate different underground geological conditions. The low frequency measurement system is designed to fulfill these requirements.

The low frequency system consists of mechanical component and electronic component (Figure 3.5). Mechanical component is developed to generate dynamic stress and strains on both rock sample and standard as well as to control measurement conditions such as saturations and pressures. While the electronic component is designed to convert electric signals to digitized data and process the data with high S/N ratio.

Figure 3.5 Low frequency system.

3.4.1 Mechanical component

The main part of the mechanical component is a triaxial cell (Figure 3.6), which is inside a pressure vessel. In order to measure the dispersion and the attenuation of the elastic moduli over a broad frequency range, we use the forced-oscillation method, combined with ultrasonic measurements in the triaxial cell.

Figure 3.7 is the schematic of mechanical component of low frequency system. First, to perform forced-oscillation measurements at seismic frequencies, I use a piezoelectric transducer (PZT) that is mounted between the end lap of the standard and the top-end of platform. Then rock sample and standard are stacked align upon the PZT. A relatively small, deviated stress of ~2 MPa is maintained on the sample column in order to have a good contact. During the measurement, the piezoelectric transducer is driven by a harmonic current wave to excite a sinusoidal oscillated (2–600 Hz) axial force to the sample column. The magnitude of strain amplitudes is maintained at the level of 10^{-7}, leading to a linear stress-strain response for the tested sample. The axial and radial strain amplitudes are recorded from strain gauges attached to the surface of sample.

Figure 3.6 Main part of the mechanical component.

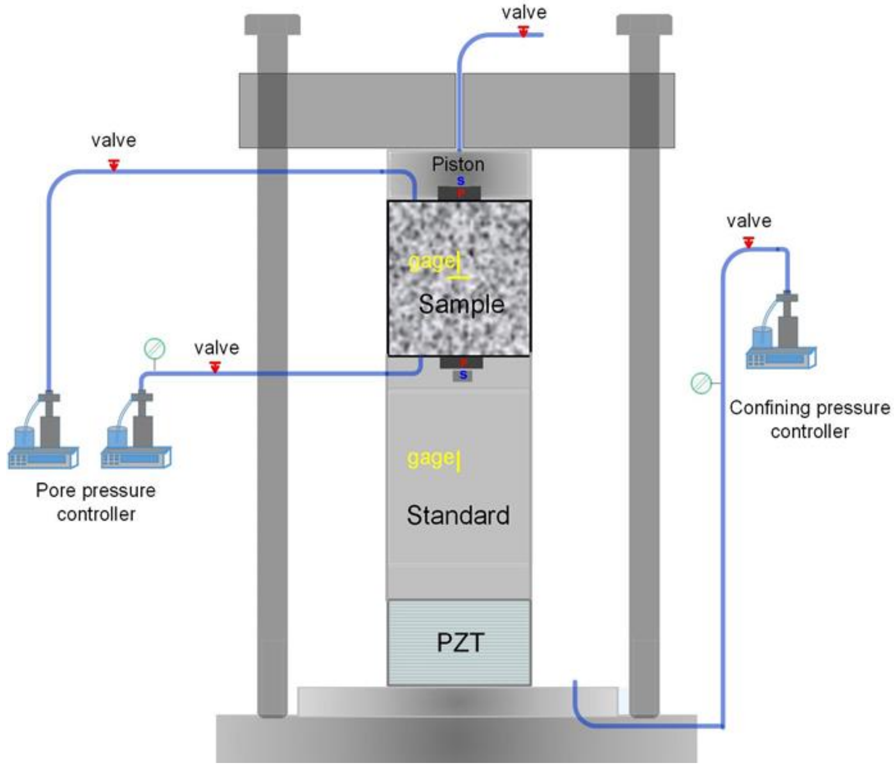

Figure 3.7 Schematic of mechanical component of low frequency system.

In addition to the forced oscillations for low frequency measurements, the system enables ultrasonic measurements. Two pairs of piezoelectric transducers (PZTs) for P- and S-waves were embedded in the top and bottom endcaps, respectively, acting as transmitters and receivers, as shown in Figure 3.7. The central resonant frequency for all PZTs is about 1 MHz. Prior to measuring rock samples, the system delay times for P- and S-waves are obtained by contacting endcaps housing PZTs together. Through the pulse transmission technique (Yin, 1992), first-arrival travel times of P- and S-waves of rock samples can be recorded along with the experimental measurements. Thus, P- and S-wave velocities can be calculated from the sample length and the first arrival times after being corrected for system delay times. The errors caused by manually picking up the first arrival times are approximately ± 1% for P-waves and ± 2% for S-waves.

During the measurement, the forced-oscillation device operates inside a pressure vessel. Silicon oil is used as a confining pressure medium, and confining pressures can be set as high as 48 MPa. The pore pressure is applied and controlled by a digital pump, with various fluids as desired by experiment specific purposes. The fluid saturation also can be manipulated by the volume of the injected fluid. All the forced-oscillation measurements are carried out at room temperature. Therefore, with this low frequency measurement system, the dispersion and attenuation can be measured at different saturations and pressures.

3.4.2. Electronic component

Figure 3.8 shows the schematic of electrical component of low frequency system. The strain gauge signals are input into a Wheatstone bridge arrangement, whose outputs are the voltage waveforms recording the amplitude and phase information of the strains.

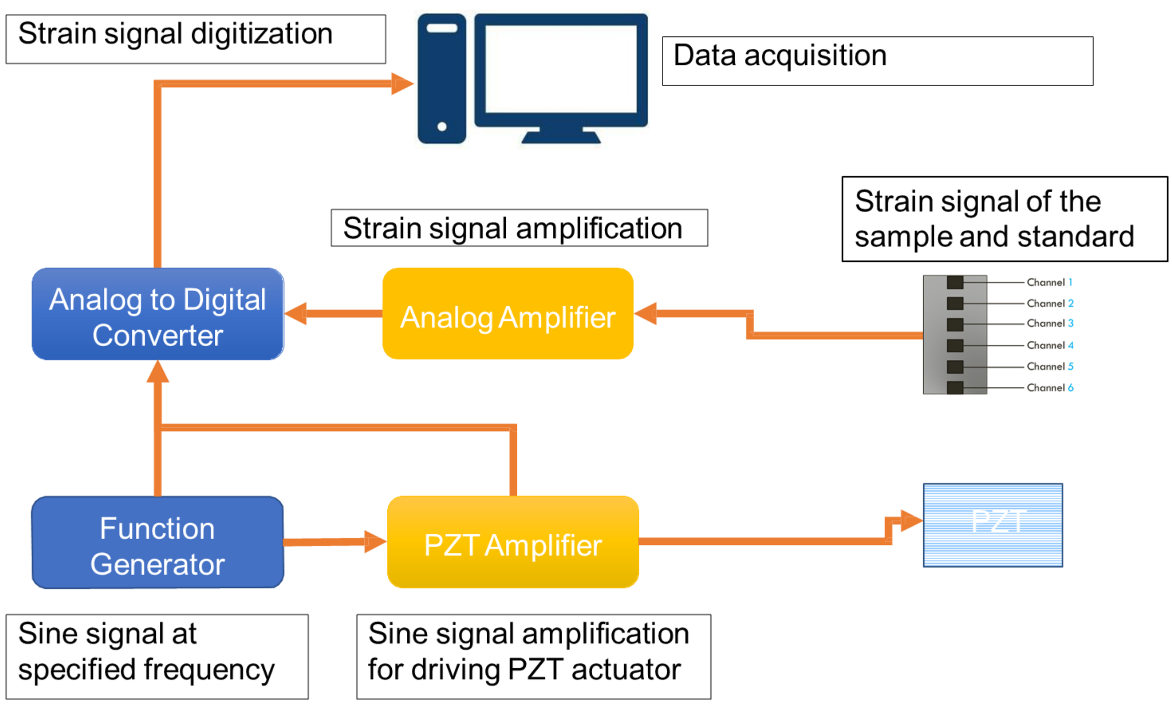

Figure 3.8 Schematic of electronic component of low frequency system.

Since the output voltage is in micro range, it can be easily disturbed by the environmental electromagnetic noise, which may be hundred times higher than the signal.

Therefore, astrain amplifier is used to amplify the strain signal 196 times as opposed to original signal. Then, the amplified analog output is converted to digital signal by an analog-to-digital converter. Finally, the digital signal is input into the computer with a dedicated data acquisition program, which is written by Qi Huang based on LabView. In virtue of this program, the calculation of moduli, velocities, and their attenuations are automatically accomplished in the computer. Meanwhile, frequency points and the strain amplitude can be chosen manually. The stored data is waveforms of each channel at each preset frequency point.

3.4.3 Calibration

System calibration is essential for ensuring the accuracy of the measurement. I worked with Huang (2018) and conducted several calibration measurements on low frequency system. An Aluminum sample and a Titanium standard are used for the system calibration. Young's modulus of the Aluminum sample is a constant of 69 GPa and being frequency independent. Meanwhile, the attenuation of the Aluminum is fairly small, which may beyond the system's limit. Therefore, the calibration aims to measure the sample's Young's modulus at 69 GPa in 2-500 Hz and the sample's attenuation within the error limit.

To verify Young's modulus measured by strain gauges, I use a PCB Piezotronics 208C02 force transducer, which is placed in the middle of the sample and standard, to calculate the ratio of the stress and the strain. In the calibration process, Channels 1 & 2 are vertical strains of the Aluminum sample, and Channels 5 & 6 represent the vertical strains of the Titanium standard. Together with the force transducer measurement, four Young's moduli are acquired (Figure 3.9). E1(FT) and E2(FT) are Young's modulus calculated from the stress (measured by force transducer) and strains of Aluminum, while E1(SG) and E2(SG) are the Young's modulus calculated by the strain ratios of Channels 1 & 5, and Channels 2 & 6. Figure

3.9 shows that Young's modulus measured by two methods is close to 69 GPa, which verifies the reliability of strain gauges. The strain gauges can be used to calculate Young's modulus within ± 0.4% error. The extensional attenuation is obtained by the strain phase difference between the standard and sample. From Figure 3.10, one can see the attenuation is quite small (<0.0035).

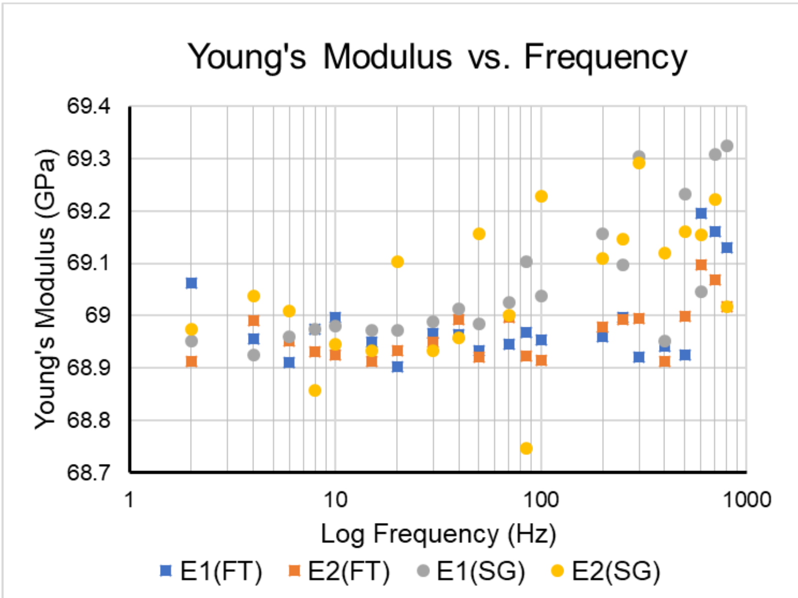

Figure 3.9 Young's modulus of the Aluminum sample.

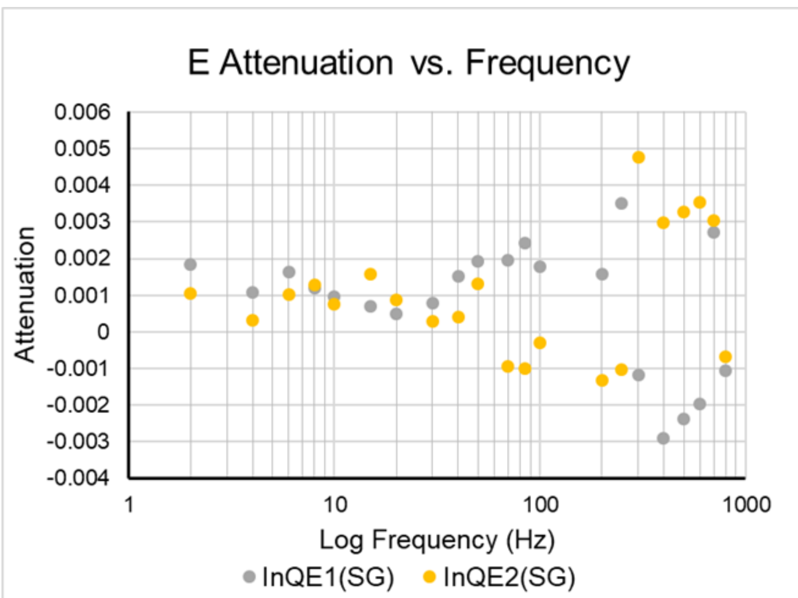

Figure 3.10 Extensional Attenuation of the Aluminum sample.

Furthermore, a comparison with other low frequency systems is conducted to verify the system reliability. Several groups have measured the dispersion and attenuation of Lucite, one kind of viscous material (Batzle et al.,2006; Madonna et al., 2011; Pimienta et al., 2015). Therefore, I compared the results with other groups (Figure 3.11, 3.12). Significant dispersion of Young's modulus of Lucite can be observed. Due to the system variety, the measurement frequency ranges of different groups vary from 0.005 Hz to 6000 Hz. Although there are differences existing in the low frequency system or Lucite sample, the measured Young's modulus by different groups shows similar behavior.

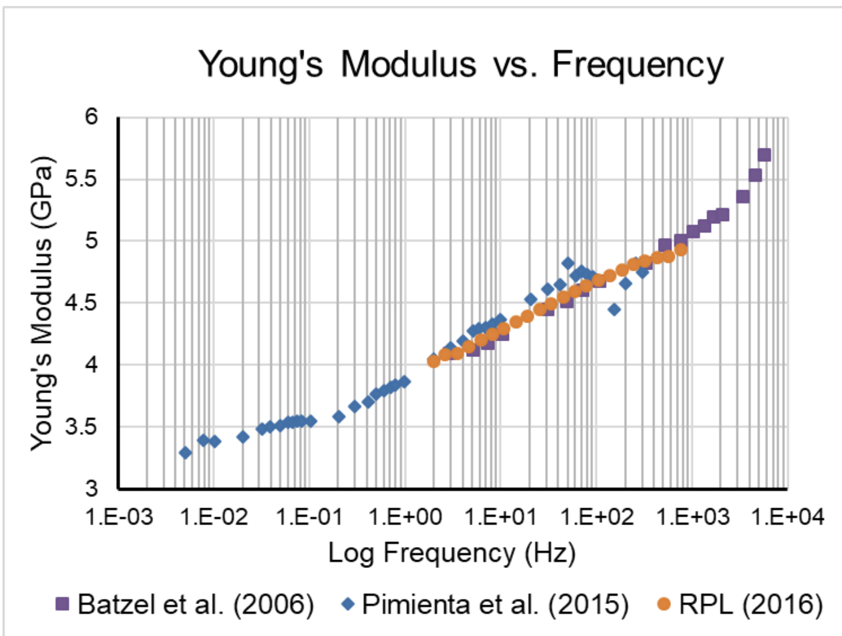

Figure 3.11 Measured Young's modulus of Lucite by different groups.

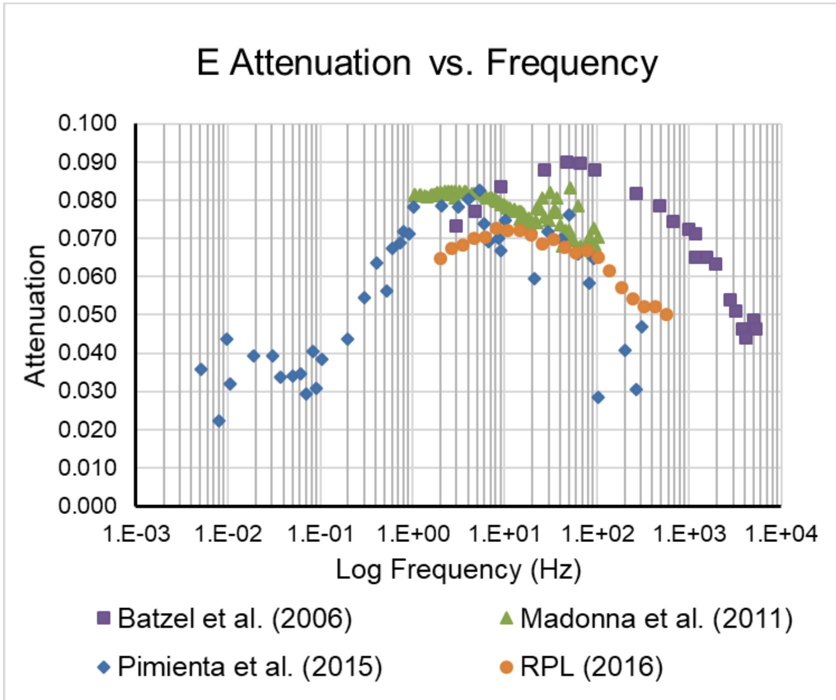

Figure 3.12 Measured Young's attenuation of Lucite by different groups.

Attenuation is the most difficult to be precisely measured in the low frequency measurement, because the phase difference between the standard and sample usually is so small that is not easy to differentiate from the waveform. For example, the attenuation of 0.017 means the phase lag is 1 degree (Figure 3.13). From figure 3.12, we can see that the measured extensional attenuation values range from 0.02 to 0.09 in the frequency range 0.005 Hz to 6000 Hz. Data reported by Batzel et al. (2006) shows an attenuation peak of 0.09 at 40 Hz, and the result of Madonna et al. (2011) suggests the attenuation peak is 0.075 at 4 Hz. Pimienta et al. (2015) reported that the peak attenuation is not noticeable to be determined due to the data quality. In the meantime, our result shows the maximum of attenuation 0.073 occurs at 8Hz. Overall, the extensional attenuation measured by different groups has a peak value in the same order. Through the system calibration, the stability and reliability of the low frequency measurement system have been verified to be good enough to measure the rock sample's elastic properties.

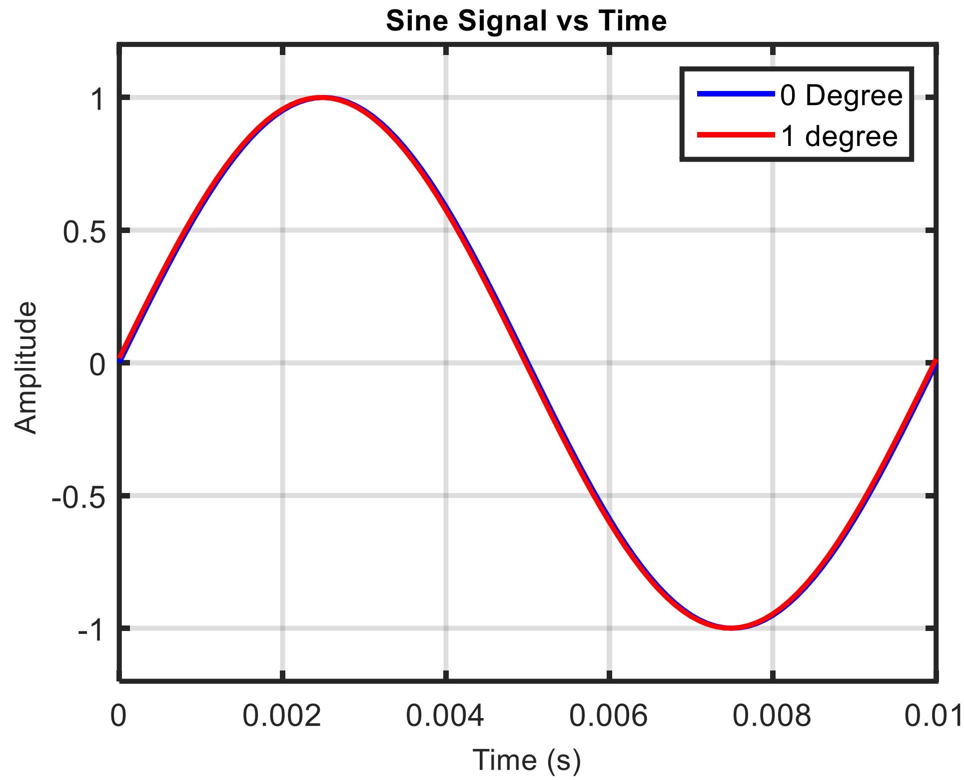

Figure 3.13 Two sine signals with 1-degree phase difference at 100 Hz.

3.5. Sample preparation

Dunn (1987) shown that open boundaries in the pore-fluid system can cause a fluid flow effect leading to an artificial dispersion. Moreover, strain gauges are very sensitive but also fragile instruments. Therefore, sample preparation of the low-frequency measurement is much more important and complicated than the conventional ultrasonic measurement. It is necessary to follow an efficient preparation approach to protect each measurement procedure from failure. Several precautions have been taken to seal the sample boundary and protect strain gauges from damage. First, I coat the epoxy-20to the curved surface of the oven-dried sample, to seal the sample boundary and provide a perfectly smooth surface for the strain gauge installation. Then strain gauges are attached to the seamless, thin-walled epoxy film (Figure 3.14). Moreover, to protect the strain gauges from short circuits caused by moisture during the measurement, I apply

M-Coat A to the strain gauges and terminals. Lastly, a rubber jacket is covered to the outermost of the sample and fitted the endplates (over an O-ring) to isolate it from the confining pressure.

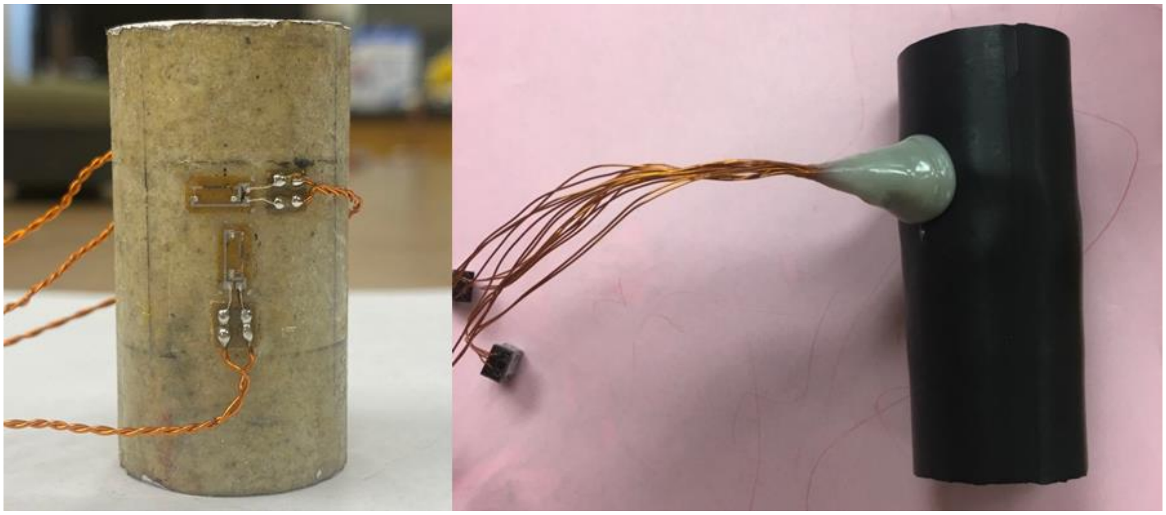

Figure 3.14 An example of the sample preparation in low frequency measurements.

4. EFFECTS OF ROCK PERMEABILITY ON DISPERSION AND ATTENUATION

4.1. Introduction

Effects of rock permeability on dispersion and attenuation have been, to a certain degree, experimentally investigated in recent years (Batzle et al., 2006; Spencer and Shine, 2016; Pimienta et al., 2017). Batzle et al. (2006) pointed out that rock permeability combined with fluid viscosity systematically affect the characteristic frequency of the P-wave relaxation. But they did not obtain the corresponding attenuation data. Pimienta et al. (2017) investigated frequency-dependent bulk modulus and attenuation in three sandstones with different permeability. They also found that the characteristic frequency of attenuation for each sandstone correlates well with its permeability. On the contrary, Spencer and Shine (2016)'s data illustrates that the relaxation of fluid-saturated sandstones shifts to a lower frequency range with the increase of fluid viscosity, but it does not show the dependence on permeability as predicted by Batzle et al. (2006) and Pimienta et al. (2017).

Considering the contrasting conclusions from previous measurements and the limited laboratory seismic frequency data, this chapter aims to further investigate the effects of rock permeability on dispersion and attenuation at seismic frequencies. Two typical outcrop sandstones, Bentheimer and Bandera, are chosen to conduct low-frequency measurements. Samples have similar porosity of ~20% but different permeabilities of 1830 mD and 33 mD. First, the rock samples and experimental procedures are described. Then, the frequency-dependent elastic properties are reported under dry and fluid saturated conditions. Ultimately, interpretations are suggested and discussed.

4.2. Experimental methodology

4.2.1 Sample description

Bentheimer and Bandera sandstone samples have similar porosity of ~20% but different permeabilities of 1830 mD and 33 mD, respectively. The mineral compositions of two samples are characterized using the in-house X-Ray diffraction (XRD) analysis, the results of which are shown in Table 4.1. Bentheimer sandstone is fairly clean, dominated by quartz with a volume fraction of 97.7%. In contrast, Bandera sandstone consists of a mixture of quartz (64.5%), plagioclase (17.1%), dolomite (10.8%), and clay (7.6%). The clay content in Bandera sandstone is visibly greater than that in Bentheimer sandstone. Meanwhile, the thin section images are taken under plane-polarized light to analyze the granular microstructures, as shown in Figure 4.1. Solid grains in Bentheimer sandstone (Figure 4.1a) are weakly cemented and well sorted. The grains are mainly rounded with an average radius of ~100 μm. The pore spaces, impregnated with blue epoxy, are homogeneously distributed and moderately well-interconnected. In Figure 4.1b, both grain and pore sizes of Bandera sandstone are smaller than those of Bentheimer sandstone. Solid grains are sub angular or surrounded, mostly cemented with argillaceous clay. Despite of serving as cementation materials, some amounts of clay minerals fill the pore spaces, resulting in poor pore connectivity. Given the significant difference of two sandstones in mineral compositions and pore connectivity, it is expected that there exist different dispersion and attenuation behaviors in two samples.

Table 4.1 Mineralogical compositions of two sandstone samples based on XRD analysis.

Sample	Quartz (wt.%)	Orthoclase (wt.%)	Plagioclase (wt.%)	Dolomite (wt.%)	Clay (wt.%)
Bentheimer	97.7	1.8	0	0	0.5
Bandera	64.5	0	17.1	10.8	7.6

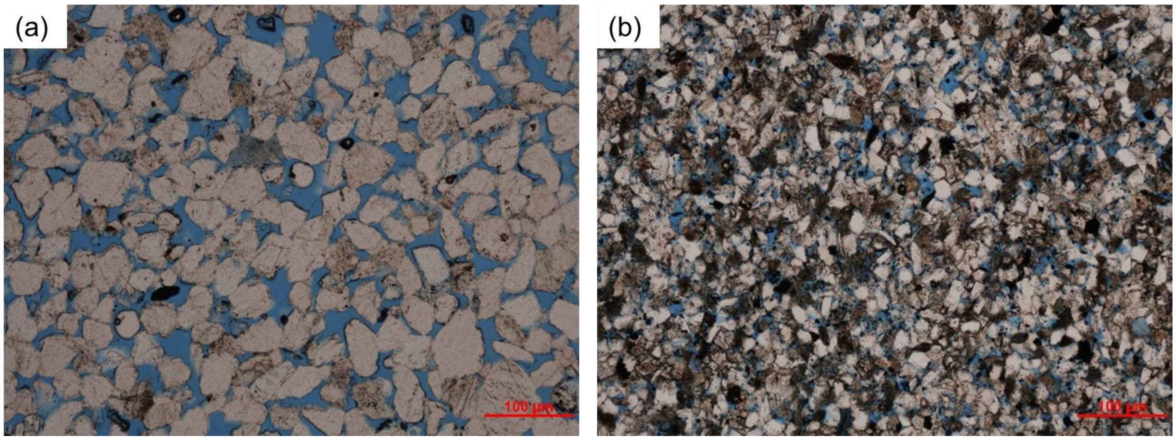

Figure 4.1 Thin section images of Bentheimer (a) and Bandera (b) sandstone at the same scale.

4.2.2 Experimental procedures

Two samples are firstly performed under the vacuum-dry condition at different confining pressures (6.9 MPa, 13.8 MPa, and 20.7 MPa). Then I employ the imbibition method to inject water into the rock sample. Meanwhile digital pump is used to manipulate the flow rate of water to precisely quantify the partial water saturation ranging from 0% to 100%. During the measurements under different water saturations, the effective pressure is kept at a constant value of 20.7 MPa. For saturation levels less than 100%, confining pressure and pore pressure are set as 20.8 MPa and 0.1 MPa, respectively. At 100% saturation, the pore pressure is increased up to 6.9 MPa, and the confining pressure is correspondingly set as 27.6 MPa. All measurements are conducted at room temperature.

4.3. Experimental results

4.3.1 Frequency dependence of elastic properties in dry rock

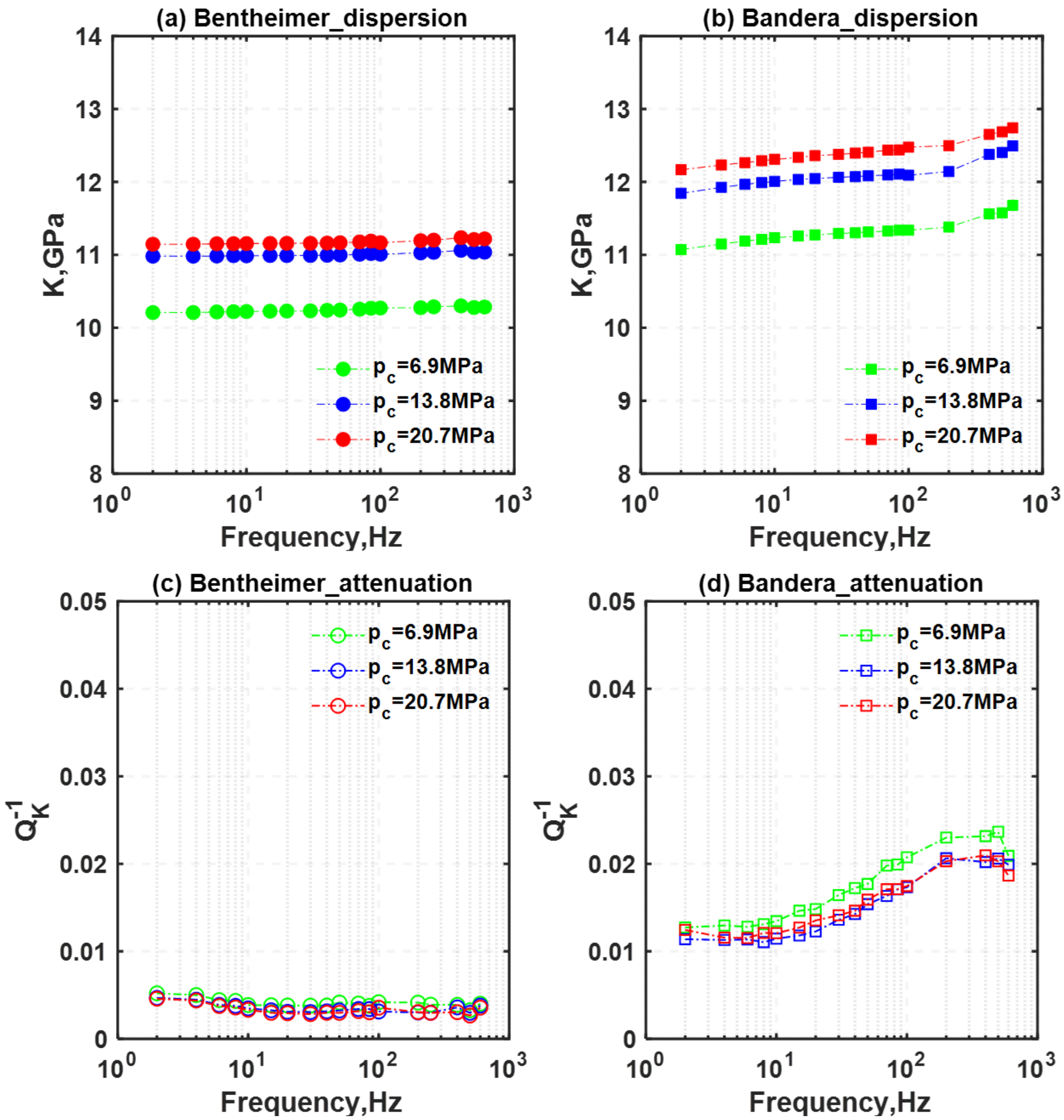

Figure 4.2 Frequency dependence of the bulk modulus K and attenuation $Q_K{}^{-1}$ for (a)/(c) dry Bentheimer and (b)/(d) dry Bandera sandstone.

Figure 4.2 shows the bulk modulus K and attenuation $Q_K{}^{-1}$ as a function of the frequency ranging from 2 to 600 Hz under different confining pressures for two sandstone samples. Overall, at any confining pressure condition, the bulk modulus for Bentheimer sandstone almost keeps constant, whereas the bulk modulus for Bandera sandstone presents an increasing trend over the applied frequency range. In addition, as shown in Figures 4.2c and 4.2d, the bulk attenuation for Bentheimer sandstone is quite smaller and almost independent of frequency. However, the bulk attenuation for Bandera sandstone is noticeable and increases with the increasing frequency. By comparing, both the bulk modulus and attenuation of Bandera sandstone are more sensitive to frequency than those of Bentheimer sandstone.

In Figures 4.2a and 4.2b, the bulk modulus of both samples increases with the increasing confining pressure. The increment when the confining pressure rises from 6.9 MPa to 13.8 MPa is much larger than that when the confining pressure increases from 13.8 MPa to 20.7 MPa. In Figures 4.2c and 4.2d, the bulk attenuation is insensitive to the applied confining pressure for Bentheimer sandstone but decreases with the increasing confining pressure for Bandera sandstone, especially when the confining pressure increases from 6.9 MPa to 13.8 MPa.

4.3.2 Low frequency data of partial saturated samples

Figure 4.3 shows the bulk modulus K and attenuation ${Q_K}^{-1}$ of Bentheimer and Bandera sandstone as a function of the frequency at varying water saturation degrees. In the whole measurement, the effective pressure is kept at 20.7 MPa. In Figure 4.3a, the bulk modulus of Bentheimer sandstone almost remains constant over the applied frequency range, no matter what saturation state the sample is. However, the magnitude of the bulk modulus is dependent on the saturation degree. When Bentheimer sandstone changes from the vacuum-dry to partially saturated condition, the bulk modulus demonstrates a somewhat decreasing trend. However, as the water saturation approaches 100%, the bulk modulus jumps from ~11 GPa to ~15 GPa. Despite the effects of saturation degree, the bulk attenuation of Bentheimer sandstone is quite small in the whole imbibition process, as shown in Figure 4.3c.

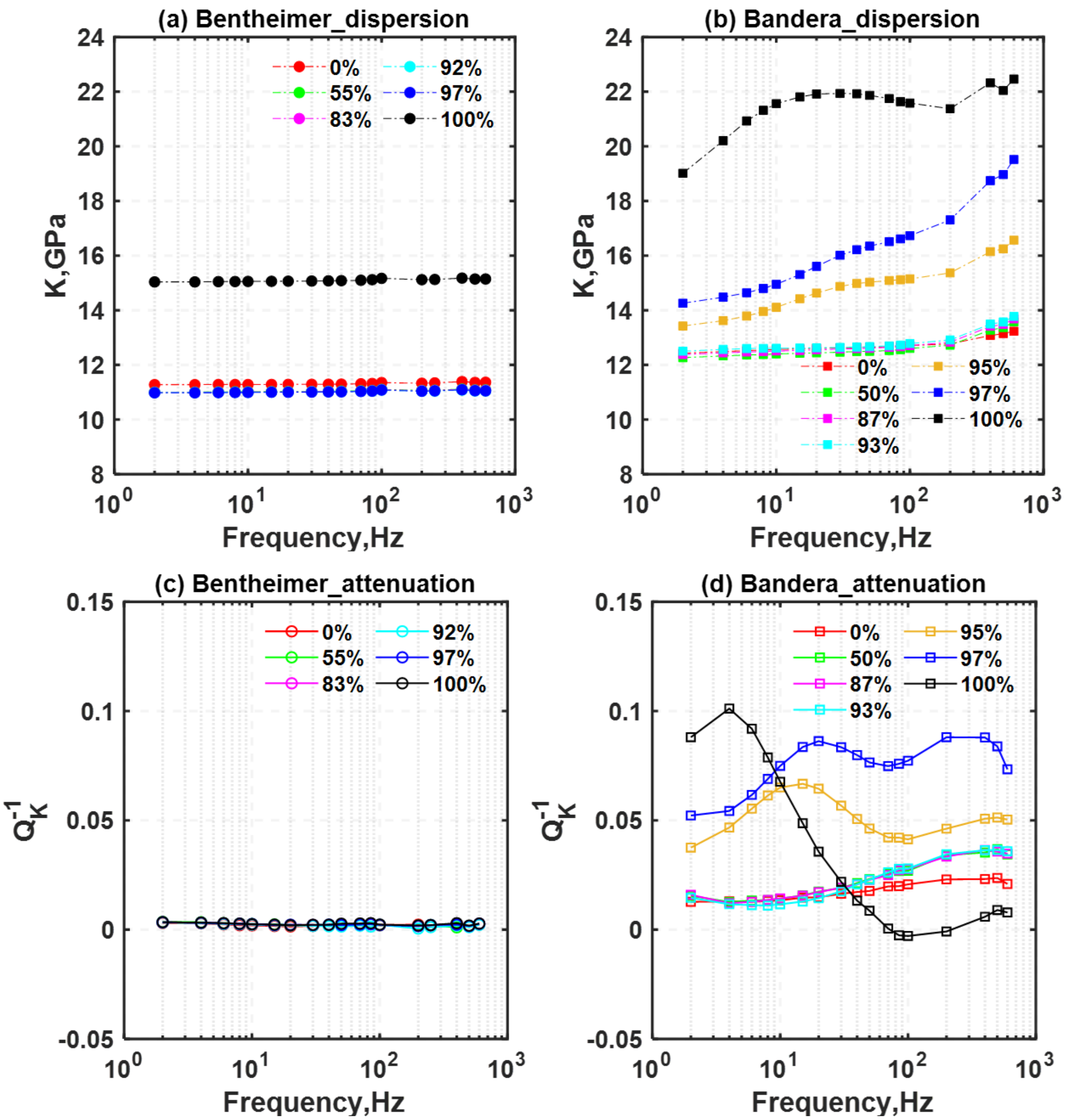

Figure 4.3 Bulk modulus K and attenuation $Q_K{}^{-1}$of Bentheimer (a)/(c) and Bandera sandstone (b)/(d) as a function of frequency at varying water saturation degrees.

In contrast to Bentheimer sandstone, Bandera sandstone shows more complicated dispersion and attenuation behaviors, as shown in Figures 4.3b and 4.3d. In Figure 4.3b, the bulk modulus of Bandera sandstone displays an increasing trend with the increasing frequency, indicating noticeable dispersion. The frequency-dependent bulk modulus is also associated with the saturation conditions. When the water saturation is below or equal to 93%, the bulk modulus dispersion is not noticeable until the frequency reaches 100 Hz. By further increasing water saturation to 95%, significant dispersion is observed with a bulk modulus increment of ~3 GPa over the applied frequency range. With continued imbibition, the maximum dispersion is achieved at the water saturation level of 97%, accompanying with the bulk modulus increasing by 5.3 GPa. When the sample is fully saturated by water, there is a sharp increment in the magnitude of the bulk modulus, accompanying with a different frequency-dependence. In contrast to the dispersion at other saturation conditions, the dispersion zone at fully water saturation tends to move towards lower frequency. In Figure 4.3d, ${Q_K}^{-1}$of Bandera sandstone shows a causal relationship with the dispersion behavior, that is, large dispersion correlates with high attenuation and peak attenuation occurs at the point where the bulk modulus increases rapidly.

4.4. Discussion

4.4.1 Role of mineral content

Data in Figure 4.2 suggests that two dry samples exhibit similar pressure dependence of the bulk modulus and attenuation. The bulk modulus increases with the growing confining pressure, whereas the bulk attenuation has a trend to decrease with the increasing confining pressure, especially at relatively low-pressure levels. The pressure-dependent behavior might be attributed to the closure of soft pores or pre-existing cracks and the enlargement of grain-to-grain contacting area (Wang et al., 2020) when the confining pressure increases from 0 to 13.8 MPa. Subsequently, the rock becomes stiffer and stiffer, resulting in the increase of bulk modulus and the decrease of attenuation. When the confining pressure is beyond 13.8 MPa, compliant pores or grain contacts tend to have a weak impact on the bulk modulus. The bulk dispersion and attenuation subsequently are not sensitive to the increasing confining pressure.

For effects of the applied frequency, both dispersion and attenuation of the bulk modulus is quite small in dry Bentheimer sandstone, but are noticeable in dry Bandera sample, as seen in Figure 4.2. The different frequency-dependent behaviors in two sandstones might be explained by their distinct mineral contents, which would express elasticity or inelasticity. As stated by Heyliger et al. (2003) and Brown et al. (2016), from the first order, properties of solid minerals, like quartz or feldspar, are in accordance with the assumption of linear elasticity. As a result, Bentheimer sandstone, which is dominated by quartz (97.7%), to some extent, can be considered as an elastic material, presenting quite small dispersion and attenuation. In contrast, for Bandera sandstone, besides the elastic minerals, there is appreciable quantity of clay minerals (8%). The elastic properties of clay mineral are ambiguous due to the difficulties caused by their intrinsic properties (Vanorio et al., 2003). It is impossible to acquire a single clay crystal to measure its acoustic properties because of the small grain size of clay minerals. Meanwhile, the dispersion and attenuation caused by the viscous behavior of clay contents are seldom investigated either, especially at seismic frequency ranges (Le et al., 2012). Nevertheless, effects of clay contents on the rock properties can be summarized as follows: 1. create micropores with diameter less than 1 μm; 2. fill the pores and throats with small particles; 3. reduce the permeability; 4. increase the specific surface area. These effects may collectively cause the dispersion and attenuation in the seismic frequency band. Klimentos and McCann (1990) investigated the relationship between attenuation and varying clay contents at 1 MHz in water-saturated sandstones. Their result suggests that the quality factor is inversely proportional to the increasing weight fraction of clay minerals. Based on above analysis, it can be proposed that clay contents are responsible for the observed dispersion and attenuation of dry Bandera sandstone at seismic frequency.

4.4.2 Comparison of low frequency data with Gassmann model

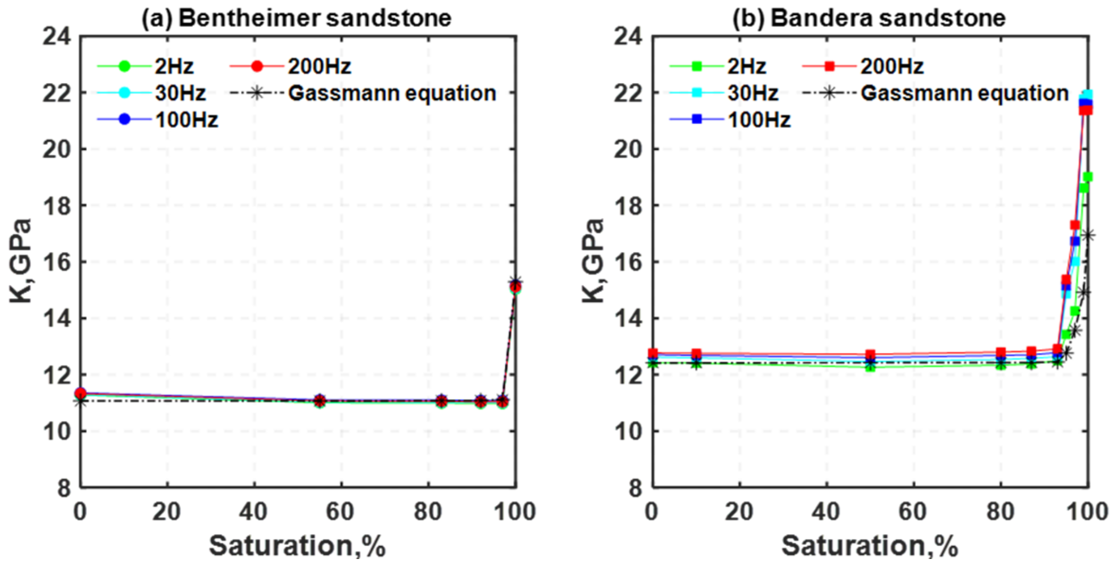

Figure 4.4 Comparisons of the bulk modulus at seismic frequencies with that predicted by Gassmann equation for (a) Bentheimer and (b) Bandera sandstone.

The well-known Gassmann equation (Gassmann, 1951) has been widely used to quantify the amount of the fluid effect in a homogeneous porous medium as follows,

$$\frac{K_{sat}}{K_0 - K_{sat}} = \frac{K_{dry}}{K_0 - K_{dry}} + \frac{K_{fl}}{\phi(K_0 - K_{fl})} \tag{4.1}$$

$$G_{sat} = G_{dry} \tag{4.2}$$

where K_{dry} is the effective bulk modus of dry rock, K_{sat} represents the effective bulk modulus of fluid saturated rock, K_0 is the effective bulk modulus of rock minerals, K_{fl} is the effective bulk modulus of pore fluids, ϕ is the rock porosity, G_{sat} and G_{dry} are the shear modulus of fluid saturated rock and dry rock, respectively.

Gassmann's equation assumes that rock matrix is homogenous and isotropic. Pore fluids have achieved an equilibrated state, giving rise to identical pore pressure inside the rock sample (Zhao et al., 2020). Therefore, it generally describes the lower bound of elastic moduli of a fluid-filled porous rock. Figure 4.4 compares the bulk modulus at seismic frequencies with that predicted from Gassmann equation for Bentheimer and Bandera sandstone, respectively. Overall, for Bentheimer sandstone, Gassmann estimation highly agrees with the measured seismic frequency data (Figure 4.4a). This is caused by the fact that Bentheimer sandstone, with homogeneously distributed and well interconnected pores, will have its pore fluid easily equilibrated within the measured frequency ranges (2-600 Hz). In this case, rock elastic properties can be represented by the effective-fluid model (Gassmann equation). For Bandera sandstone (Figure 4.4b), when the water saturation is less than 93%, the measured bulk moduli at seismic frequencies match well with those predicted by Gassmann equation. However, with further increasing water saturation, the bulk modulus exhibits noticeable dispersion, accompanying with an apparent deviation from the Gassmann estimation. Additionally, the deviation presents an increasing trend with the increasing frequency, as shown in Figure 4.4b. Considering the complicated pore structure of Bandera sandstone, the large dispersion is likely to be caused by the combined effects of rock permeability, gas saturation, as well as the fluid-rock interaction.

4.4.3 Effects of rock permeability

The frequency-dependent behaviors of Bandera sandstone with partial water saturation, as shown in Figures 4.3b, 4.3d, and 4.4b, illustrate three pore fluid status: relaxed, unrelaxed, and transition status (Mavko and Jizba, 1991; Batzle et al., 2006). The key parameter that dominates pore fluid status is the characteristic frequency f_c, which can represent the relaxation time of the pore fluid. Considering the primary wave-induced fluid pressure diffusion taking place at mesoscopic scale, the corresponding characteristics frequency is expressed as (Pride et al., 2004):

$$f_c = \frac{\kappa K_{fl}}{\eta {L_c}^2} \tag{4.3}$$

where κ is the permeability, K_{fl} is the fluid bulk modulus, $\eta$is the viscosity, and L_c is the critical fluid-diffusion relaxation scale. Figure 4.5shows the general feature of fluid-related wave dispersion and attenuation signatures based on the three typical fluid pressure relaxation status.

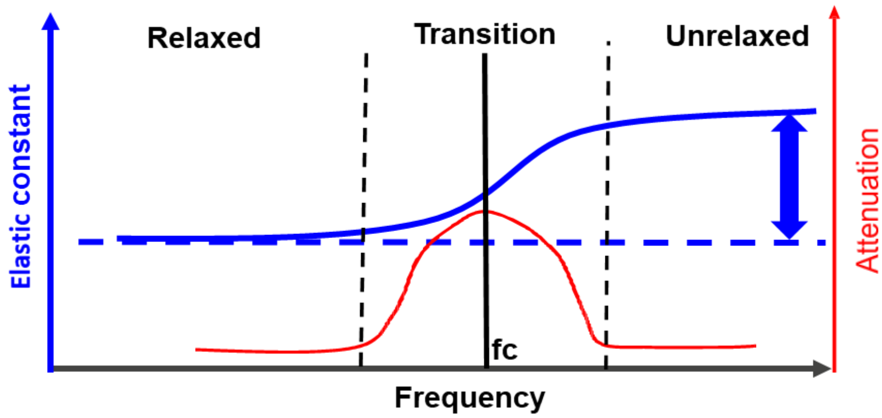

Figure 4.5 General feature of fluid-related dispersion and attenuation of elastic properties.

On the one hand, when the measured frequency f is sufficiently lower than the rock's characteristic frequencyf_c, the forced-oscillation induced pore pressure gradients would have enough time to completely equilibrate within the pore space and reach a relaxed status. In this case, the elastic modulus of the rock can be well predicted by the Gassmann-Wood equations. On the other hand, when the experimental frequency is much larger than f_c, the pore fluid will not have sufficient time to diffuse and remain in an unrelaxed status. In this case, the pore fluid is prone to increase the rock stiffness. In addition, there exists a transition zone from a relaxed to an unrelaxed status (Figure 4.5), during which the pore pressure gradients will be partially equilibrated. As a result, a substantial change of elastic moduli can be obtained within the transition frequency ranges. Meanwhile, the oscillatory fluid flow resulting from unequilibrated pore pressures will consume energy produced by the oscillated force, giving rise to apparent attenuation (Yin, 1992).

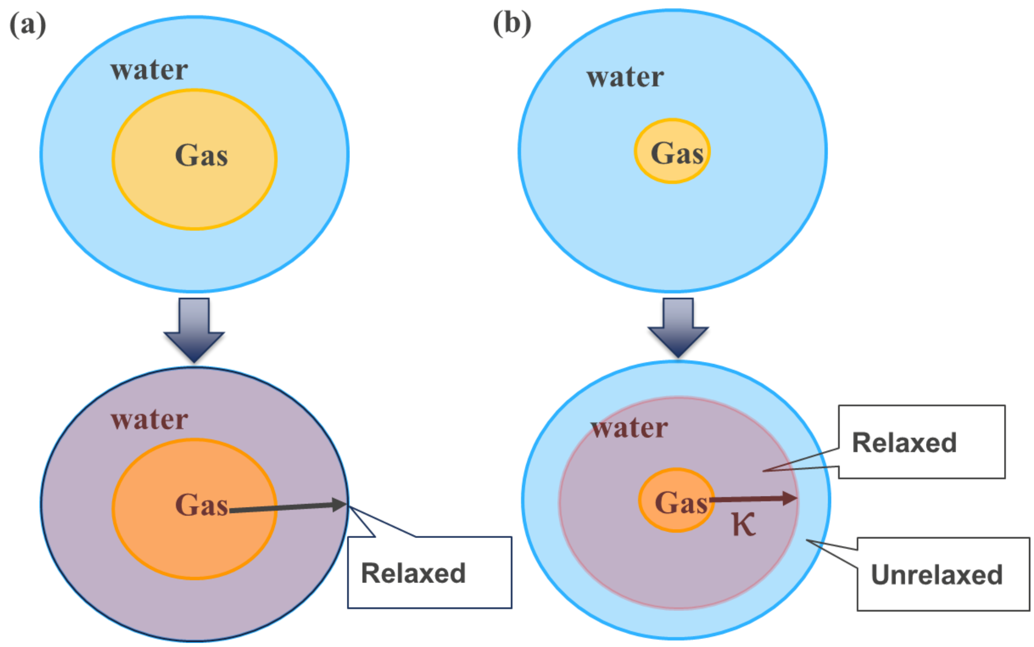

Figure 4.6 Simple schematics to interpret the combined effects of rock permeability and gas saturation on the frequency-dependent behaviors of elastic moduli.

Based on above analysis, rock permeability and gas saturation associated with characteristic frequencies would play an important role in the frequent-dependent behaviors of elastic moduli. For simplicity, I use two schemetics, as illustrated in Figure 4.6, to qualitatively interpret our experimental observations. The spherical gas-filled pocket is located at the center of the water-saturated sphere. Since gas has extremely higher compressibility than water, a release path for pore pressure gradients would be formed (White, 1975). When the gas saturation is larger than certain percent of pore volume (e.g. 50%), as shown in Figure 4.6a, gas can substantiallydominate pore fluid relaxation by providing quick and short release path for pore pressure gradients. Thus, the pore fluid can be relaxed quicklyeither in Bentheimer or Bandera sandstone,resulting in negligible dispersion and attenuation at measured frequency range, as shown in Figure 4.3. In Figure 4.6b, when the gas saturation is less than a few percent of pore volume (e.g. 5%), the gas effect would gradually decrease. The rock frame properties are expected to play important roles in the pore fluid relaxation. For the case of Bentheimer sandstone with higher permeability and better pore connectivity, the pore fluid can easily reach a relaxed status even though only 3% gas occupies the pore space, resulting in small attenuation and dispersion in Figures 4.3a and 4.3c. In contrast, for Bandera sandstone with lower permeability and worse pore connectivity, the gas-water communication becomes difficult. As a result, pore pressure gradients need more time to reach an equilibrated state. At the applied frequency ranges, only parts of the pore fluid can reach a relaxed status. Therefore, in Figures 4.3b and 4.3d, when the water saturation is 95% or 97%, distinct bulk attenuation and dispersion can be observed.

4.5. Summary

In this study, a series of low-frequency measurements are performed on two sandstones with different permeability to investigate the effects of rock permeability on bulk dispersion and attenuation in partially saturated rocks. The experiments are conducted at frequencies ranging from 2 Hz to 600 Hz under both vacuum-dry and partially water-saturated conditions. At vacuum-dry conditions, the bulk dispersion and attenuation in Bandera sandstone with more clay contents are distinctly larger than those in Bentheimer sandstone, suggesting clay contents might contribute to the inelasticity of the rock frame.

At partially water-saturated conditions, the bulk dispersion and attenuation in Bentheimer sandstone are relatively small in the whole imbibition process. The bulk modulus predicted by the Gassmann equation highly agrees with that measured at seismic frequencies, suggesting that a relaxed status of pore fluids is reached for the partially saturated Bentheimer sandstone. By comparing, Bandera sandstone shows complicated dispersion and attenuation behaviors. When the water saturation is below 93%, bulk dispersion and attenuation are not noticeable. However, when the water saturation is beyond 93%, bulk dispersion and attenuation become significant, accompanied by apparent bulk modulus deviations from Gassmann's estimations. The mismatching between the measured data and the Gassmann prediction can be attributed to the combined effects of rock permeability and fluid saturation. As gas saturation is larger than a few percent (~5%), gas with relatively high compressibility dominates the pore-fluid relaxation by providing a quick and short communication path for pore pressure gradients. As a result, dispersion and attenuation are not significant when the water saturation is below 95%. With continued water injection, the gas effect gradually decreases. The rock permeability begins to dominate the pore-fluid relaxation. For Bandera sandstone with relatively low permeability, a partially relaxed status is reached with apparent attenuation and dispersion.

5. EFFECTS OF FLUID VISCOSITY ON DISPERSION AND ATTENNUATION

5.1. Introduction

The magnitude and frequency dependence of attenuation not only depend on the rock matrix properties, but also on the physical properties of the saturating pore fluids, notably the fluid viscosity. Experimentally, effects of fluid viscosity on dispersion and attenuation have been investigated in recent years (McKavanagh and Stacey, 1974; Batzle et al., 2006; Subramaniyan et al., 2015; Pimienta et al., 2015, 2017; Mikhaltsevtich et al., 2015, 2016; Spencer and Shine, 2016). Fluids with varying viscosities, such as gas with low viscosity or glycerin with high viscosity, are used to conduct the measurements of elastic properties at seismic frequencies, allowing for a better resolution with respect to dispersion and attenuation characteristics. Batzle et al. (2006) pointed out that fluid viscosity combined with rock permeability systematically affects the characteristic frequency of P-wave relaxation. Spencer and Shine (2016) conducted low frequency measurements under fully saturated conditions with a series of pore fluids. The fluids cover a relatively wide range of viscosities from 0.071 to 1064 cP. They reported that relaxations of viscous fluid-saturated sandstone samples shift to a lower frequency range with increasing fluid viscosity at the frequency range of 1 - 200 Hz.

Even though there has been a relatively surge in the availability of laboratory data from fluid-saturated sandstones at seismic frequencies (<100 Hz), measurements of rock samples saturated with varying viscous fluids are still limited. Meanwhile, comparing experiments is challenging given the variation in microstructure between samples and the use of different low frequency apparatus. Furthermore, fewer studies performed the measurements of low frequency and ultrasonic simultaneously, which investigate the dispersion and attenuation characteristics in a broader frequency range, facilitating the integration of acoustic data at different frequency scales.

In this chapter, to contribute to the available data and current knowledge, I present the joint measurements of frequency-dependent elastic properties at both seismic (i.e., f $\in$[2; 400] Hz) and ultrasonic (i.e., f ~ 1 MHz) frequency ranges on a Berea sandstone sample. The experiments were performed under dry and a series of fully fluid-saturated conditions with varying fluid viscosity (e.g., Butane C4, water, and glycerin). Firstly, I provide a description of the sample and the experimental procedure. Then the results of modulus dispersion and corresponding attenuation at different conditions are reported. Finally, the discussion focuses on the physical mechanisms responsible for the observations.

5.2. Experimental methodology

5.2.1 Physical properties of rock sample and fluids

In this work, a typical Berea sandstone sample is selected to conduct the forced-oscillation measurement at varying conditions. The rock sample exhibits relatively high porosity of 20%, and medium permeability of 153 mD. The cylindrical sample is 50.7 mm in length and 37.8 mm in diameter. It is a relatively clean, quartz dominant sandstone (i.e., 91.7% volume content of quartz), with minor amounts of clay, orthoclase, and plagioclase (Table 5.1). Additionally, Berea sandstone is documented to be isotropic and homogeneous at the sample scale, and well-characterized of elastic properties (Christensen and Wang, 1985; Winkler, 1985; Mavko and Vanorio, 2010; Chapman et al., 2016; Pimienta et al., 2014, 2016; Spencer and Shine, 2016). The microscopic images of the Berea sandstone sample are shown in Figure 5.1. From the low magnification image (Figure 5.1a), one can see that this sample is fine grained and has an average grain size of approximately 25 µm. The sand grains are well sorted and well rounded. Intergranular pores are moderately well interconnected, and the average pore size is 10μm. In the high magnification image (Figure 5.2b), the grains are cemented by Quartz and suture lines between grains can be observed, and clay contents exhibit pore lining and pore filling morphologies.

Table 5.1 Mineralogy of the Berea sandstone (unit: wt %).

Quartz	Orthoclase	Plagioclase	Analcite	Anhydrite	Clay
91.7	2.3	1.2	0.6	0.5	3.7

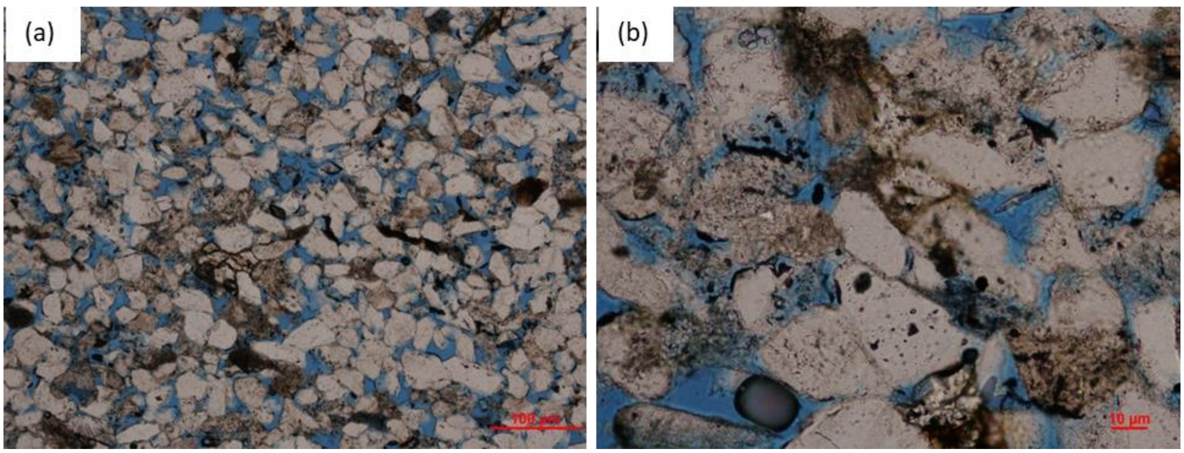

Figure 5.1 Microscopic images of the thin section of the Berea sample.

All measurements are conducted at room temperature. Physical properties of the saturated pore fluids at room temperature as a function of effective pressures are plotted in Figure 5.2. From Figure 5.2c, one can see that the selected fluids cover a relatively wide range of viscosities from ~0.1 to 1420 cP. As viscosity of glycerin is three orders of magnitude higher than that of water, and four orders higher than that of C4, it is expected that the chance of observing different frequency regimes is greater when C4, water, and glycerin are successively used as pore fluids. Noticeably, C4 has a specific property that it can be liquefied at a pressure larger than about 3.5 atmospheres (≈ 51 Psi) at room temperature (NIST Chemistry Web Book). This property of C4 makes the measurements much easier to conduct, because C4 is in liquid status at measured pore pressure (7 MPa ≈ 1000 Psi). Meanwhile, it can be vent out through the pore pressure line when I finish the C4 measurements. Thus, there is no need to flush C4 out by another fluid. In addition, glycerin can immediately and fully dissolve in water and the viscosity of pore fluids dramatically decreases to 1 cP (water's viscosity). Therefore, glycerin can be rinsed by water, and the same sample can be used in the series of hydrostatic cycles.

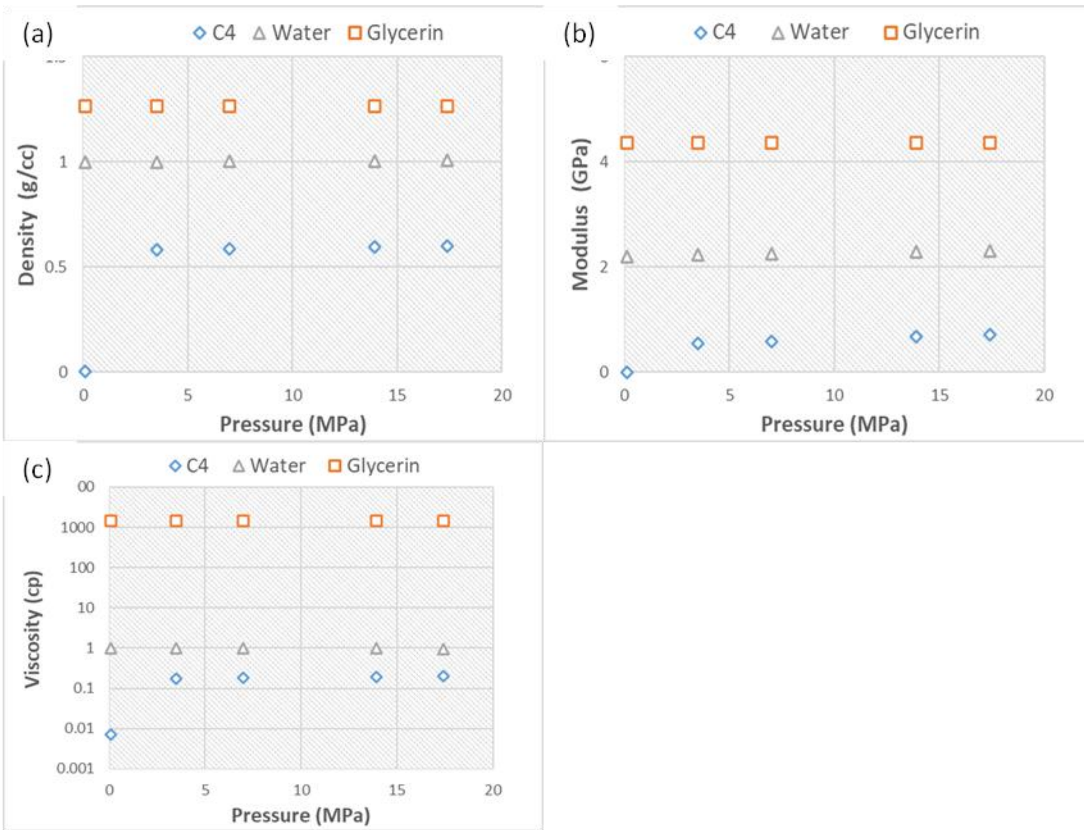

Figure 5.2 Density (a), Bulk modulus (b), and viscosity (c) properties as a function of pressure for three saturated pore fluids at room temperature.

5.2.2. Experimental procedure

A procedure is devised to conduct low frequency and ultrasonic measurement simultaneously on Berea sandstone using different fluids at different pressures. First the oven-dried sample is measured, with confining pressure Pc increased from 0 up to ~21 MPa at a step of ~ 7 MPa. Then, considering the fluid feature and data consistency, a series of fluid saturated measurements (C4-, glycerin-, and then water-saturated) are successively carried out on Berea sample to explore the effect of viscosity. The fully saturated measurements are performed at a constant pore pressure of ~7 MPa, and the confining pressure Pc is increased from 10.45 MPa to 27.6 MPa at a step of ~7 MPa. Therefore, Terzaghi effective pressure Pe = Pc − Pp is matched with dry measurement, which allows for comparison between dry and fluid-saturated data. In order to precisely illustrate the fluid properties at measured pore pressure of 7 MPa, I make a list in Table 5.2. Moreover, the detail of fluid-saturated procedure is described as follows,

First, the sample is fully saturated with C4, and conducted on the forced-oscillation and ultrasonic measurements at different confining pressures. Following the measurements with C4, the fluid pressure is reduced by opening the valve. Then C4 changes to the vapor state and is vented out through the pore fluid lines. Next, the sample is vacuum saturated with glycerin. Originally, I was trying to directly inject glycerin to the sample to obtain fully saturation. However, due to the high viscosity of glycerin and relatively medium permeability of the sample, the rock sample could not reach the fully saturated status, which is proved by comparing with Gassmann prediction. Therefore, I took the sample out of the system, and ascertained the fully glycerin saturation by following procedure: (1) immerse the sample in a cup of glycerin, with height of fluid higher than sample but lower than the jacket, (2) then put it in the oven, heat up to 50 ºC, and vacuum is applied with a vacuum pump, (3) measure sample weight to ascertain fully saturated, (4) setup the sample on the forced-oscillation system again, and increase the pore pressure up to ~7 MPa and hold constant for at least 12 h to ensure complete saturation of the pore space. Then I conduct low frequency and ultrasonic measurement on glycerin-saturated sample at same pressure conditions as C4. Water saturation is then obtained by directly injecting water into the glycerin filled sample. As glycerin can immediately and fully dissolve in water, I assume that full saturation of the water is obtained by flushing almost fifty times of the pore volume. Then the same measured procedure for full C4 or glycerin saturation is repeated.

Table 5.2 Fluid properties at a pressure of 7 MPa and at room temperature (20°C).

Pore fluid	Density (Kg/m^3)	Viscosity (cP)	Modulus (GPa)
C4	587	0.179	0.579
Water	1001	0.97505	2.243
Glycerin	1263	1420	4.35

5.3. Experimental results

5.3.1 Frequency dependence of elastic properties of Berea at Pe ≈ 7 MPa

Figure 5.3 shows the directly measured Young's modulus E, extensional attenuation Q_E^{-1}, and Poisson's ratio ν as a function of frequency for Berea sample under dry and varying fluid-saturated conditions at effective pressure of 7 MPa. For dry condition, both the measured E and ν show little frequency influence. Correspondingly, the Q_E^{-1} is relatively small (${Q_E}^{-1} < 0.01$), which confirms the general knowledge that the attenuation in dry and clean sandstone is negligible.

By comparing varying fluid-saturated conditions, a distinct difference between glycerin-saturated data and C4- or water-saturated results can be observed. Almost no frequency dependence is observed on Young's modulus (Figure 5.3a) under C4- or water-saturated conditions. In contrast, large frequency dependence is shown under glycerin-saturated condition. In this case, E increase with frequency from 31.8 GPa (2 Hz) up to a value of 34.0 GPa (400 Hz).

The corresponding measurements of Q_E^{-1} (Figure 5.3b) show a good causal relationship with the frequency dependence of E (Figure 5.3a). Particularly, attenuation is essentially negligible for C4 and water-saturated conditions, while being significant and frequency dependent under glycerin saturation. In this last case, an attenuation peak of Q_E^{-1}~ 0.022 is observed at ~ 20 Hz.

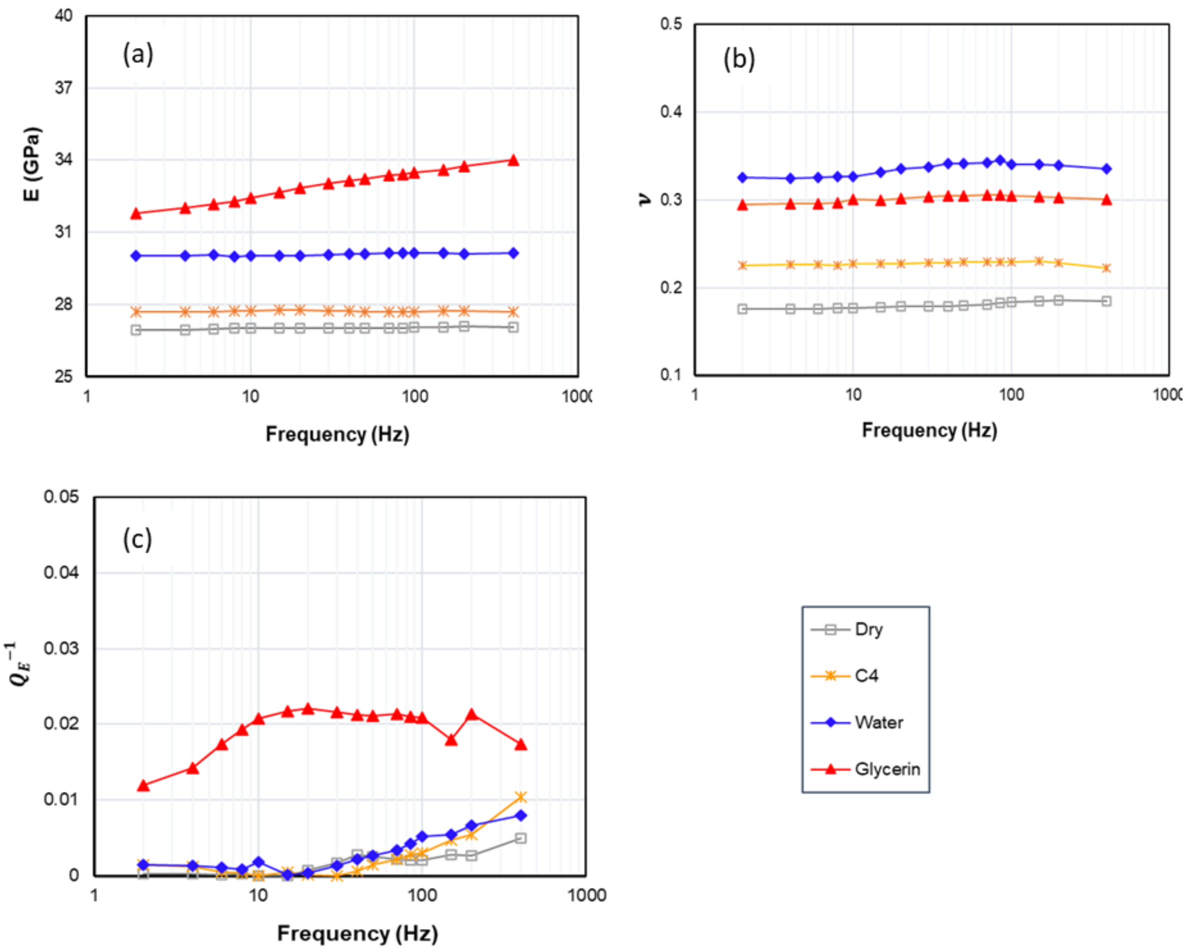

Figure 5.3 Frequency-dependence of (a) Young's modulus E, (b) Poisson's ratio ν and (c) Young's attenuation Q_E^{-1} of Berea sample under dry, C4, water, and glycerin saturated conditions at a pressure of P_{eff}=7 MPa.

Poisson's ratio changes with different pore fluids (due to different values of fluid modulus) but remains flat and nearly independent of frequency, even for glycerin-saturated situation. It follows the well-known relations between isotropic elastic moduli that other modulus ratios (e.g., P/G and K/G) will likewise be nearly independent of frequency and there will be similar dispersions in the P-wave, bulk, and shear moduli (Spencer and Shine, 2016).

5.3.2 Pressure effect on the frequency dependence of elastic properties

Sample saturated with C4 and water shows a very small variation of E with frequency. By contrast, it shows notable dispersion and attenuation under glycerin saturation. I further investigate the effect of effective pressure on the frequency dependence of elastic properties of glycerin-saturated and water-saturated rock.

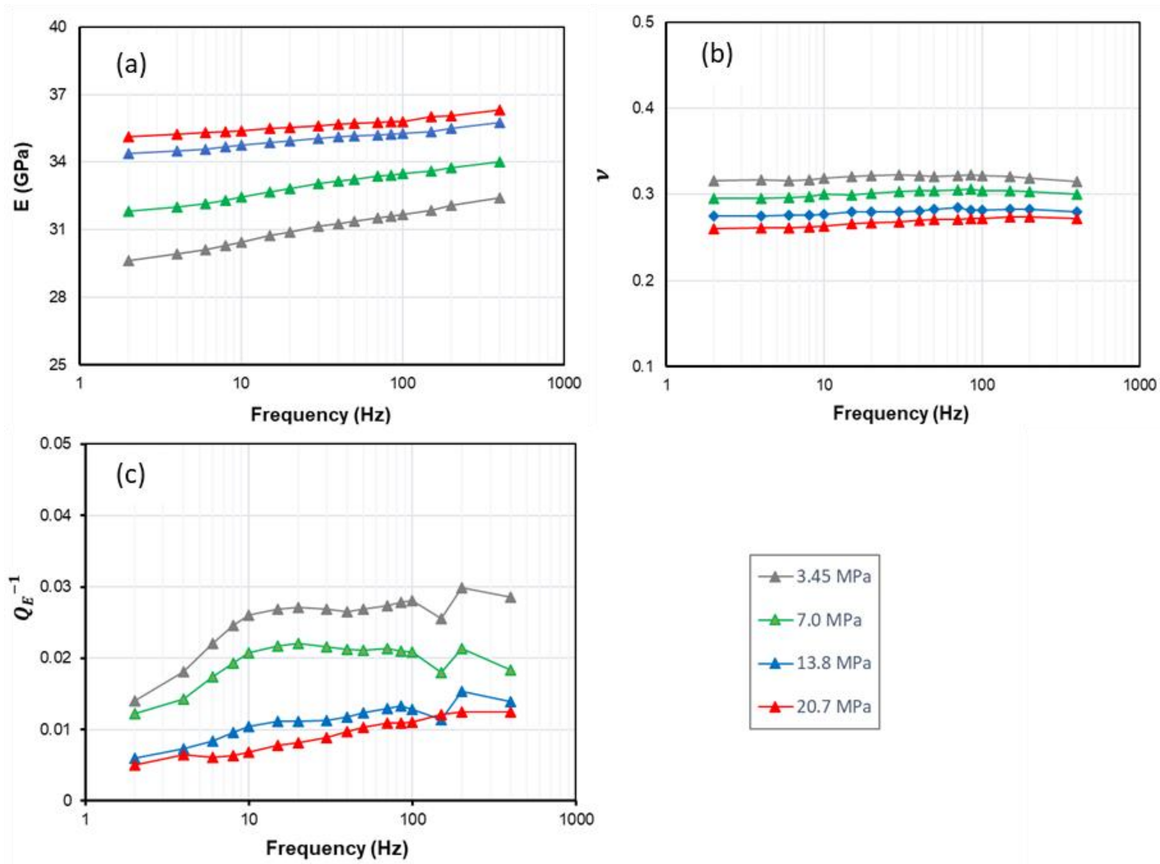

Figure 5.4 Pressure-dependence of (a) Young's modulus E, (b) Poisson's ratio ν and (c) Young's attenuation Q_E^{-1} under glycerin-saturated conditions.

A clear dependence to the effective pressures is observed in the glycerin-saturated data (Figure 5.4a, 5.4b and 5.4c). With increasing effective pressure, the amplitude of Young's modulus increases, which ranges from ~29 to ~36 GPa. Moreover, the frequency dependence of Young's modulus varies with effective pressure. At low effective pressure, Young's modulus increases notably with frequency. This frequency dependence, however, is significantly damped by the increase in the effective pressure. The measured attenuation Q_E^{-1} shows a good causal relationship with E. Significant frequency-dependent attenuation is measured at low effective pressure. Increasing the effective pressure results in a clear decrease of Q_E^{-1}. Again, almost no frequency dependence is observed in Poisson's ratio at different effective pressures. The value of Poisson's ratio decreases with increasing effective pressure.

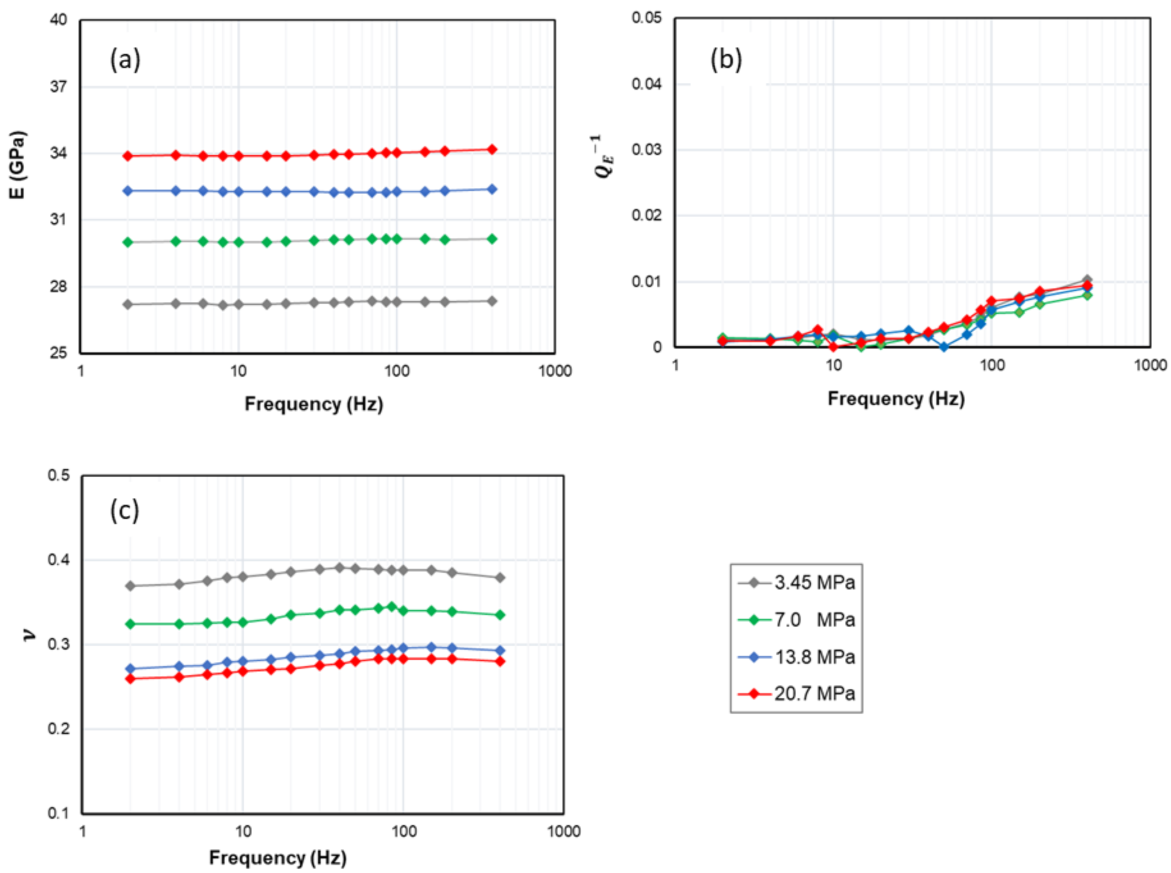

Figure 5.5 Pressure-dependence of (a) Young's modulus E, (b) Poisson's ratio ν and (c) Young's attenuation Q_E^{-1} under water-saturated conditions.

Figure 5.5 shows the Young's modulus (E), Poisson's ratio (ν) and attenuation (Q_E^{-1}) as a function of the frequency under different confining pressures for water-saturated Berea samples. Overall, the amplitude of Young's modulus increases with increasing effective pressures (Figure 5.5a). However, at any confining pressure condition, the Young's modulus almost keeps constant with no dispersion. The corresponding measurements of Q_E^{-1} (Figure 5.5b) show a good causal relationship with the frequency dependence of E. Attenuation is essentially negligible for water-saturated conditions. Again, almost no frequency dependence is observed in Poisson's ratio at different effective pressures. The value of Poisson's ratio decreases with increasing effective pressure.

5.4. Discussion

5.4.1 Comparison of seismic frequency data with ultrasonic data

Figure 5.6 shows the measured frequency-dependent Young's modulus E of Berea sample under dry, C4, water and glycerin saturated conditions in seismic and ultrasonic frequency range. By comparison, dry, C4, and water saturated rocks show negligible dispersion in the whole frequency range.

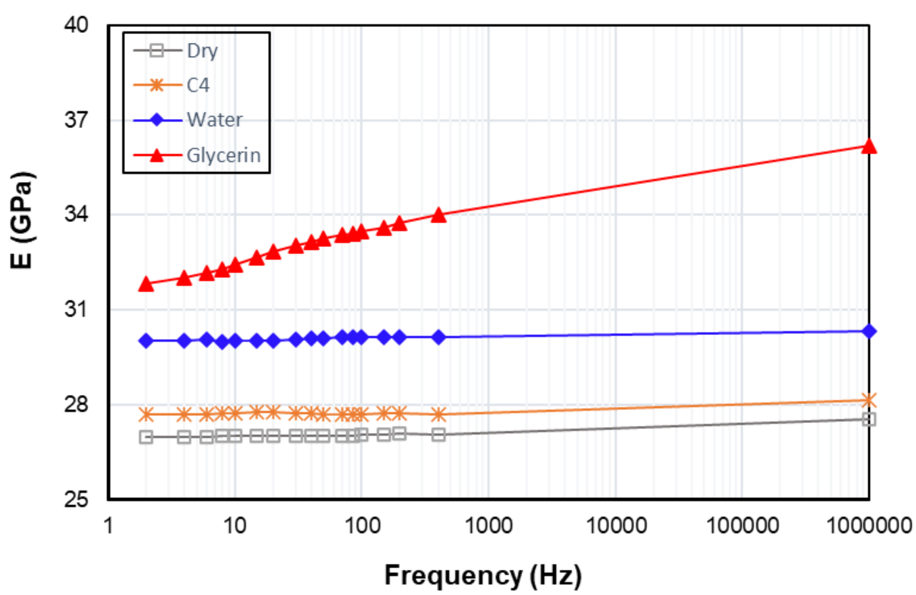

Figure 5.6 Comparison of frequency-dependent Young's modulus E of Berea sample under dry, C4, water and glycerin at a pressure of P_{eff}=7 MPa in seismic and ultrasonic frequency range.

While glycerin saturated rocks display a gradually increasing trend with the increasing frequency, indicating noticeable dispersion. When the rock sample is fully saturated by one fluid, the heterogeneous distribution of the pore fluid disappears. If the rock frame is less heterogeneous, which is the case for Berea sandstone, and fluid viscosity is low, one can therefore expect attenuation to be negligible and frequency independent (White, 1975). This can explain the observed negligible dispersion in dry, C4, and water saturated rocks. However, for rocks saturated with high viscous glycerin, pore fluid mobility (Batzle et al., 2006) is thus much lower than that of C4 or water saturated rock, and more time is needed for pore fluid to relax. Then its relaxation frequency will shift to lower frequency range, resulting in significant dispersion and attenuation at seismic frequencies.

Again, I compare the frequency dependent Young's modulus E under glycerin-saturated (Figure 5.7) and water-saturated (Figure 5.8) conditions at different effective pressures in seismic and ultrasonic frequency range. Overall, the Young's modulus of glycerin saturated rock becomes less dispersive with increasing effective pressures. At high frequencies, the young's modulus is less sensitive to the effective pressures than that at seismic frequencies. In contrast, the Young's modulus of water-saturated rock generally shows negligible dispersion in the whole frequency range. Nevertheless, there is a slight trend that the dispersion increases with decreasing effective pressure, especially for frequency ranging from 400Hz to MHz. These pressure-dependent behaviors might be attributed to the closure of soft pores or pre-existing cracks and the enlargement of grain-to-grain contacting area (Wang et al., 2020) when the effective pressure increases from 3.5 to 20.7 MPa. Subsequently, the rock becomes stiffer and stiffer, resulting in the increase of Young's modulus. Meanwhile, the closure of soft pores or pre-existing cracks will lead to better grain contact and more homogeneous rock frame. Thus, dispersion becomes smaller with increasing effective pressure.

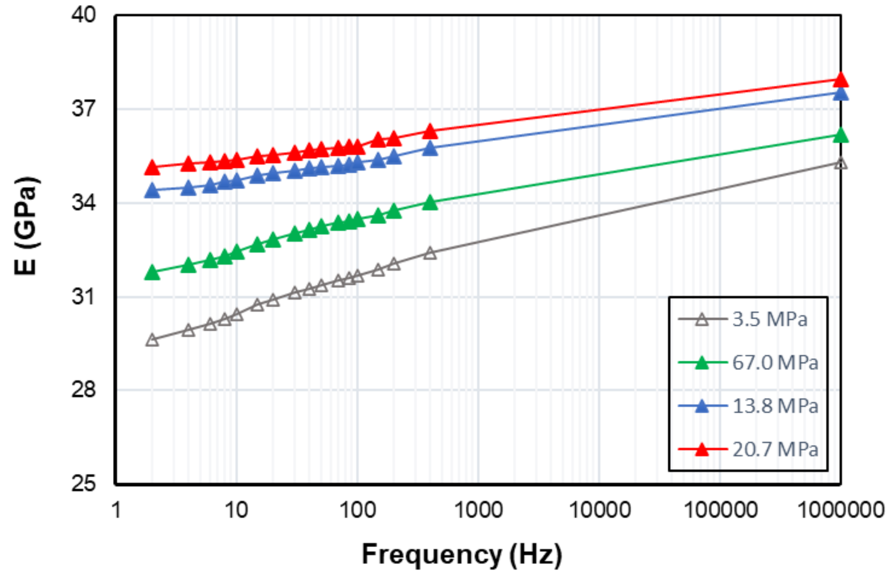

Figure 5.7 Comparison of frequency-dependent Young's modulus E under glycerin-saturated conditions at different effective pressures in seismic and ultrasonic frequency range.

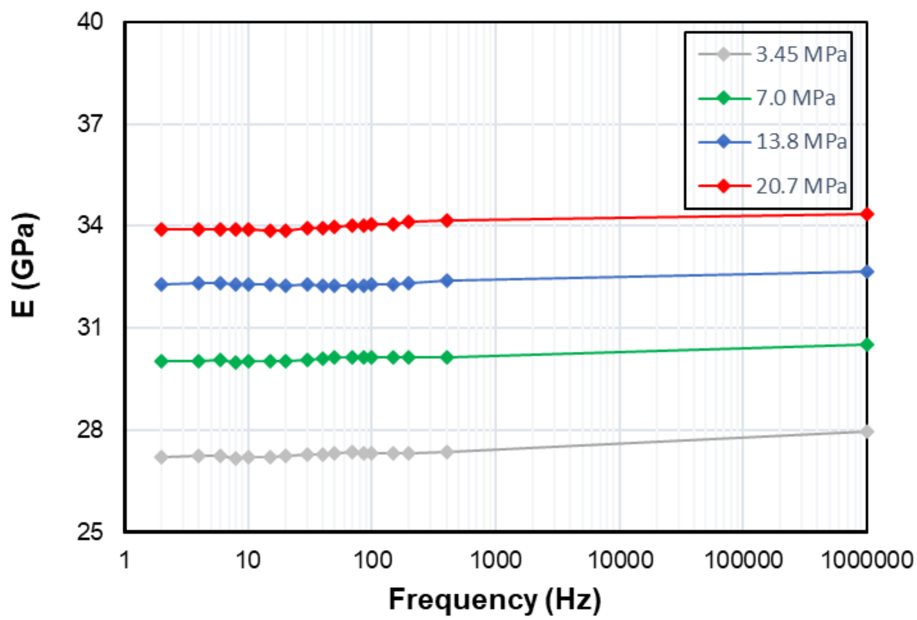

Figure 5.8 Comparison of frequency dependent Young's modulus E under water-saturated conditions at different effective pressures in seismic and ultrasonic frequency range.

5.4.2 Attenuation mechanism analysis

As detailed in Müller et al. (2010), various theories have been developed to describe those different mechanisms. In fully saturated homogeneous rocks, only two mechanisms (Cleary, 1978; Gardner, 1962; Mavko and Nur, 1979; O'Connell and Budiansky, 1977) are expected to occur over the allowed frequency range (e.g., Adelinet et al., 2010; Fortin et al., 2014; Sarout, 2012): Biot-Gardner flow or squirt flow. These two commonly used mechanisms tie attenuation to viscosity. Biot theory (Biot, 1956) describes the viscous-inertial attenuation and dispersion resulting from wavelength-scale flow, it is often called global or macroscopic flow. It gives a characteristic frequency for the fast-compressional wave, which is proportional to the fluid viscosity. According to later studies (Bourbié et al., 1987; Pride, 2005), the dispersion and attenuation caused by macroscopic fluid flow in typical rocks can only be significant at frequencies above 100 kHz, well outside the seismic exploration band. In addition, the magnitude of the velocity dispersion and wave attenuation predicted from Biot theory is smaller than those observed in lab measurement and seismic data. Therefore, the macroscopic fluid flow is not applicable to explain the dispersion and attenuation of seismic data.

In contrast, Squirt flow, arising from microscopic compressibility heterogeneities in the rock, is one of the dominant mechanisms for wave attenuation in fluid-saturated rocks. Numerous theoretical models (e.g., O'Connell and Budiansky, 1977; Mavko and Jizba, 1991; Chapman et al., 2002; Gurevich et al., 2010; Adelinet et al., 2011) have been developed to explain laboratory observations at sonic and ultrasonic frequencies. The characteristic frequency of squirt flow is $f_c = \varepsilon^3 K/\eta$. Here, ε is the crack aspect ratio, K is the frame bulk modulus. A key effect predicted by this theory is that the viscosity controls at which frequency the attenuation peak occurs. It is inversely proportional to fluid viscosity. A higher viscosity implies a slower fluid flow and a slower equilibration of the pressure gradients. The order-of-magnitude shifts to lower frequencies of the attenuation peak. Considering the features observed in my experiments that only glycerin-saturated (high viscosity) rocks show significant dispersion and attenuation at seismic frequency, squirt flow may be the potential mechanism that can interpret my observations.

5.5. Summary

Aiming to investigate the dispersion and attenuation characteristics of rocks saturated with varying viscous fluids, I present the joint measurements of frequency-dependent elastic properties at both seismic (i.e., $f \in [2; 400]$ Hz) and ultrasonic (i.e., $f \sim 1$ MHz) frequency ranges on a Berea sandstone sample. The experiments were performed on the dry and a series of fully fluid-saturated conditions with varying fluid viscosity (e.g., C4, water, and glycerin) and submitted to a range of effective stresses.

Data suggests that fluid viscosity systematically affects the frequency dependence of elastic properties. Low viscosity fluid (such as methane, butane, and water) permits pore pressure equilibration either between pores or between heterogeneous regions of the rock and results in a negligible dispersion and attenuation at measured seismic frequency range. In contrast, high viscosity, thus low fluid mobility, can produce strong dispersion and attenuation within the seismic band. Confining pressure appears to highly damp these frequency effects. Combined with ultrasonic measurements, I can investigate the frequency dependence of elastic properties over a broader frequency band. By comparison, dry, C4, and water saturated rocks show negligible dispersion in the whole frequency range. While glycerin saturated rocks display an increasing trend with the increasing frequency, indicating noticeable dispersion. Based on porous modeling analysis, the squirt flow, in response to a heterogeneous pore, can be a dominant mechanism accounting for the observed dispersion and attenuation in fully glycerin-saturated rocks.

6. EFFECTS OF PARTIAL SATURATION ON DISPERSION AND ATTENUATION

6.1. Introduction

Sedimentary porous rocks saturated with multiphases fluids are quite common in hydrocarbon reservoirs or engineering subjects: gas-brine-oil mixture in hydrocarbon reservoirs, CO2-oil mixture for enhanced oil recovery (EOR), CO2 mix with brine for CO2 storage in saline aquifers, etc. (Carcioneet al., 2006; Zhao et al., 2017). When seismic waves pass through such subsurface rocks, it is unavoidable to create dissipative and dispersive responses. Some experimental works have been done to examine the partial saturation effects on dispersion and attenuation of elastic properties at seismic frequency range, aiming to better understand the seismic response to partially saturated rock formations (Murphy, 1982; Yin et al., 1992; Batzle et al., 2006; Tisato and Quintal, 2014; Chapman et al., 2016; Mikhaltsevitch et al., 2016). Murphy (1982) analyzed the partial water saturation effect in Massilon sandstone, and the results suggested that the maximum attenuation occurs at a few percent of gas saturation. Yin et al. (1992) measured extensional attenuation on Berea sandstone and concluded that extensional attenuation is significantly influenced by the degree of saturation as well as saturation history and boundary flow conditions. Chapman et al. (2016) also studied the effects of the degree of water saturation on the wave attenuation in Berea sandstone. They found that attenuation peaks are observed at the nearly full degree of water saturation. Moreover, the overall attenuation magnitude increases with increasing water saturation and its peak shifts to lower frequency range. Li et al. (2020b) conducted the forced-oscillation measurements on tight sandstone samples at the seismic frequency range of 1-1000 Hz at partial water-saturated conditions. They claimed that the observed attenuation in partially saturated rock is attributed to the combined mechanisms of microscopic (squirt) flow and mesoscopic flow.

Indeed, those laboratory measurements provide strong evidence that the degrees of fluid saturation have a significant influence on wave dispersion and attenuation of rock samples. However, to our best knowledge, most existing partial saturation experiments are carried out with water (low viscosity of 1 cP), limited research has been done on rocks that partially saturated with varying viscous fluids, which are also commonly encountered during the reservoir identification. Consequently, to better understand the seismic response to partially saturated rock formations with high viscous fluids, it is necessary to conduct laboratory investigations at seismic frequencies, which, to a certain degree, can assist us to better understand the seismic field data.

In this chapter, I report the joint measurements of frequency-dependent elastic properties at both seismic (i.e., $f \in [2; 400]$ Hz) and ultrasonic (i.e., $f \sim 1$ MHz) frequency ranges under two partially fluid-saturated conditions (e.g., water, glycerin) in Berea sandstone. Firstly, the physical properties of rock sample and fluid are introduced. Secondly, the experimental procedure is briefly described. Thirdly, the forced-oscillation measurements of Berea sandstone are reported at varying saturation levels and fluid types. Then, I interpret the measured data by comparing with theoretical model and discuss possible underlying attenuation mechanisms.

6.2. Experimental methodology

In this work, I use the same Berea sandstone sample as described in Chapter 5. Then I perform the laboratory measurements on this Berea sample under two partial saturation series with varying viscosity (e.g., water, glycerin). Specifically, for each saturation series, both the forced-oscillation and ultrasonic measurements are conducted at different saturation levels.

Considering the fluid feature and data consistency, the drainage procedure is designed to conduct fluid saturation during the laboratory measurements. First, the oven-dried Berea sample is measured, with confining pressure of 13.7 MPa. Next, I fully saturated the Berea sample with glycerin. Following the measurements with the fully glycerin-saturated condition, methane (C1) is next quantitatively injected into the fully glycerin-saturation sample, estimating the saturation levels of glycerin according to the volume of the withdrawn glycerin. Here, the saturated glycerin is flooded by injecting C1. During the desaturation process, I keep constant pore pressure of 7 MPa and fixed confining pressure of 20.7 MPa, respectively. All measurements are performed at room temperature.

After accomplishing glycerin saturation measurements, we successively start to conduct forced-oscillation measurements at varying levels of water saturation. Water is directly injected into the rock sample with fully filled glycerin and C1. Chemically, glycerin will immediately and fully dissolve in water so that the viscosity of pore fluids (dissolved glycerin-water) dramatically decreases to 1 cP (water's viscosity). Meanwhile, to achieve a fully water-saturated sample as much as possible, the glycerin and C1 saturated sample is flooded almost fifty times to reach 100% water saturation. Then the same measurement procedure as glycerin saturation is repeated. As the viscosity of glycerin or water is several orders larger than that of C1 (Table 6.1), it is expected that glycerin or water cannot be flushed out anymore when fluid saturation is less. Therefore, the forced-oscillation measurements are conducted at the saturation levels ranging from 50% to 100%.

Table 6.1 Pore fluid properties at a pressure of 7 MPa and at room temperature (20°C).

Pore fluid	Density (g/)	Viscosity(cP)	Modulus (GPa)
C1	0.052	0.012652	0.00976
Water	1.001	0.97505	2.243
Glycerin	1.263	1420	4.35

6.3. Experimental results

6.3.1. Frequency-dependent elastic properties measured from forced-oscillation

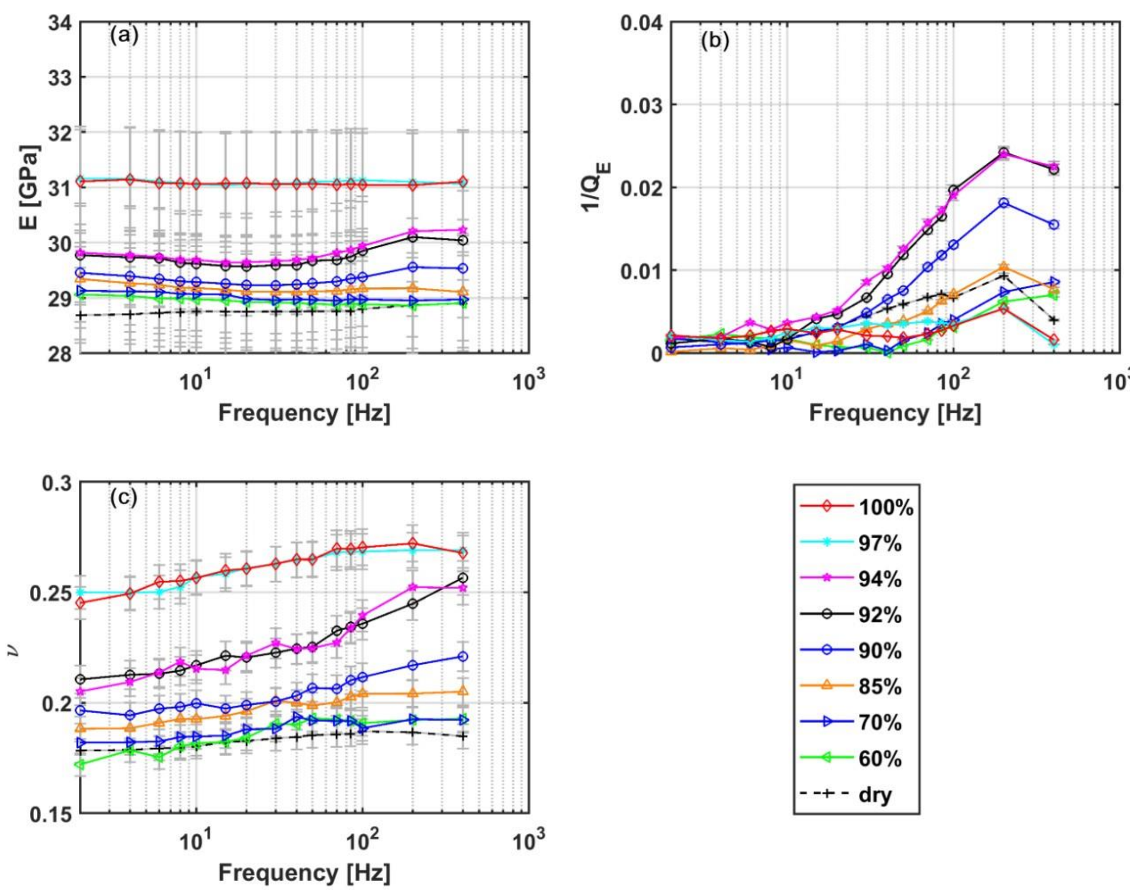

Figure 6.1 Measured frequency dependence of (a) Young's modulus, (b) extensional attenuation, and (c) Poisson's ratio of Berea sandstone from forced oscillations at varying degrees of water saturation.

Figure 6.1 shows the measured Young’s modulus E, extensional attenuation Q_E^{-1}, and Poisson’s ratio ν as a function of frequency at varying degrees of water saturation. For dry condition, both the measured E and ν show little frequency influence. Correspondingly, the

Q_E^{-1} is relatively small (${Q_E}^{-1} < 0.01$), which confirms that the dominant attenuation mechanisms are pore-fluid related.

At nearly full water saturation, Young's modulus (Figure 6.1a) remains flat and almost independent of frequency. As water saturation is reduced to 94% and 92%, Young's modulus drastically decreases and becomes frequency dependent, with an increment of 0.9 GPa between 40Hz and 400Hz, which is also the largest dispersion observed in water saturation series. By further reducing water saturation to 90%, both the amplitude and frequency dependence of Young's modulus decrease. Below 85% water saturation, the amplitude of Young's modulus slightly decreases but frequency dependence becomes negligible.

The corresponding measurements of extensional attenuation (Figure 6.1b) show a good causal relationship with the frequency dependence of Young's modulus (Figure 6.1a). Extensional attenuation is essentially small (${Q_E}^{-1} < 0.01$) for water saturation less than 85% or larger than 97%, while being significant and frequency dependent between 90% and 94%. The highest attenuation is measured at 92% or 94% with a peak of ~0.0234 at ~200 Hz.

Similar to Young's modulus, the Poisson's ratio (Figure 6.1c) shows almost no dispersion below 85% water saturation and significant dispersion between 90% and 94%, but a slight disagreement subsists at nearly full saturation, where Poisson's ratio shows noticeable dispersion.

In contrast with water saturation conditions, for any glycerin saturation levels (60%-100%), Young's modulus exhibits dispersive behavior, with larger dispersion magnitude and wider dispersion range (Figure 6.2a). At nearly full glycerin saturation, Young's modulus shows notable dispersion, with an increment of ~1.3 GPa between 2Hz and 400Hz. As glycerin saturation is reduced to 94% and 92%, Young's modulus drastically decreases. Particularly, the largest dispersion is observed, with an increment of 2.85 GPa between 2 Hz and 400 Hz. For glycerin saturation less than 85%, Young's modulus continues to decrease but still retains noticeable frequency dependence.

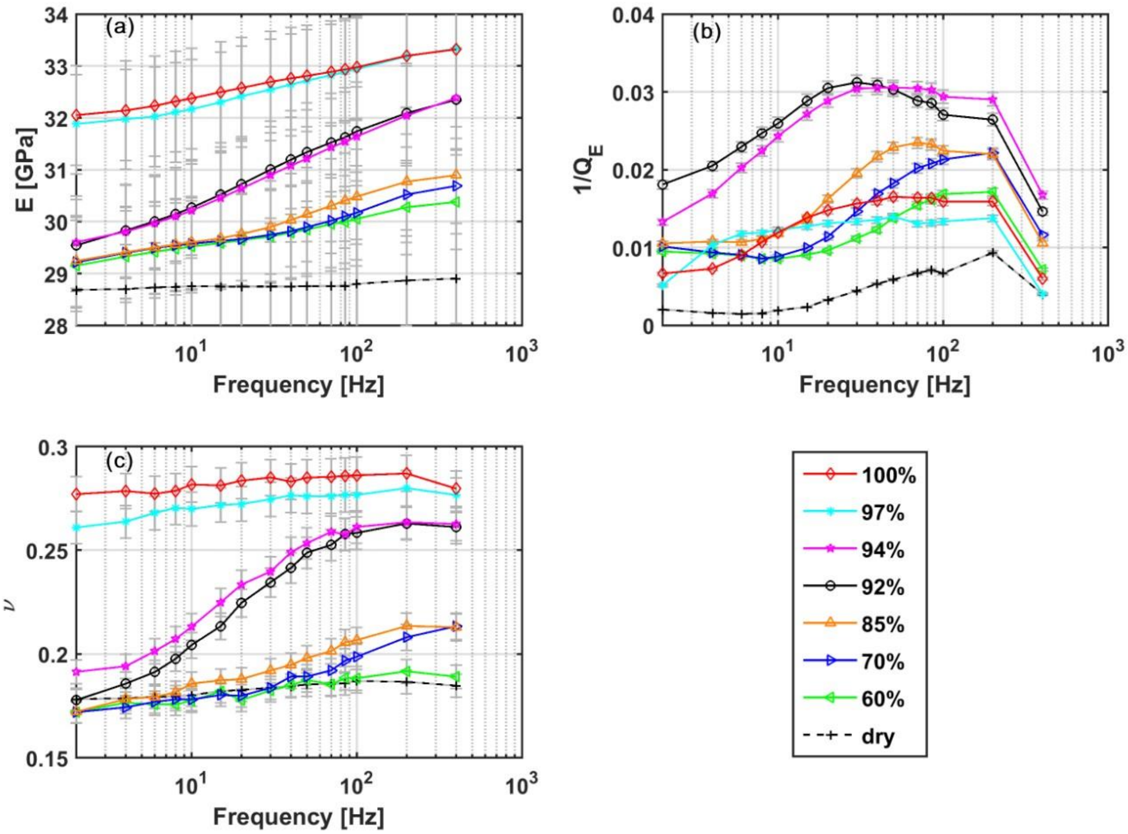

Figure 6.2 Measured frequency dependence of (a) Young's modulus, (b) extensional attenuation, and (c) Poisson's ratio of Berea sandstone from forced oscillations at varying degrees of glycerin saturation.

The corresponding measurements of extensional attenuation (Figure 6.2b) show a good causal relationship with the frequency dependence of Young's modulus (Figure 6.2a). For any glycerin saturation levels in our measurements, attenuation is significant, yet varying in magnitude. Relatively lower attenuation is observed at nearly full saturation. While as glycerin saturation is reduced to 94%, attenuation abruptly increases. The highest attenuation is measured at 92% or 94% with a peak of ~0.032 at ~30 Hz. Particularly, as saturation decreasing from 92% to 60%, the overall attenuation progressively decreases and its peak shifts to higher frequencies. Compared with water saturation data, the overall extensional attenuation peak with glycerin saturation shifts to lower frequency range.

Poisson's ratio (Figure 6.2c) shows different character of frequency dependence comparing with Young's modulus. At nearly full and 60% glycerin saturation, Poisson's ratio shows very weak frequency dependence. Significant dispersion is observed between 70% and 94% glycerin saturation. Particularly, largest dispersion is measured at 92%, where Poisson's ratio drastically increases with frequency, ranging from 0.18 at 2 Hz to 0.26 at 200 Hz.

6.3.2. Frequency dependence of translated elastic properties

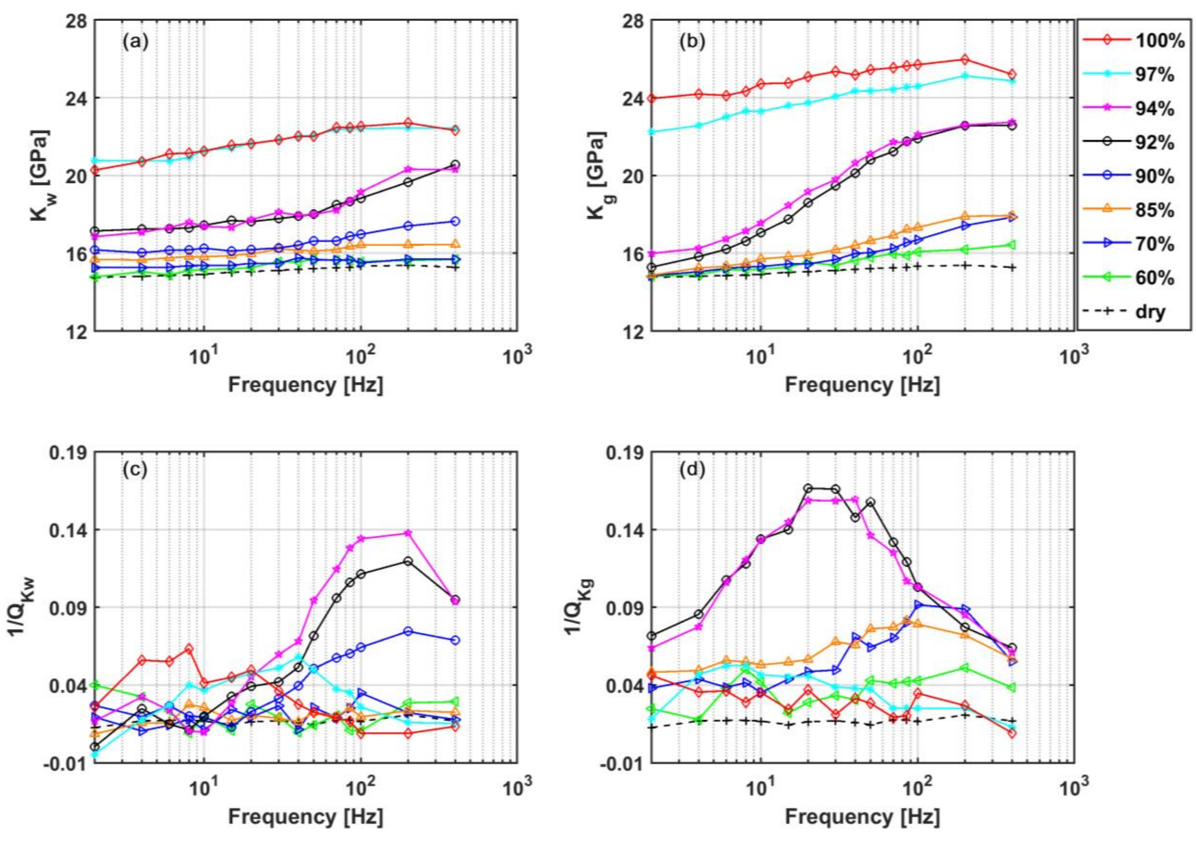

Figure 6.3 The frequency dependence of bulk modulus K (a, b) and attenuation (c, d) calculated from the complex Young's modulus and Poisson's ratio for water saturation and glycerin saturation, respectively.

Bulk modulus is more sensitive to the pore fluid properties than Young's modulus. Therefore, under the assumption of isotropy and homogeneity of Berea sample, as shown in Figure 6.3, translated bulk modulus and bulk attenuation for water saturation ($K_w, {Q_{Kw}}^{-1}$) and glycerin saturation ($K_g, {Q_{Kg}}^{-1}$) are calculated, respectively.

As observed in Figure 6.3a and 6.3b, K_w are systematically lower (~15%) than K_g when saturation levels approaching 100%. Moreover, when saturation levels are at 92% - 94%, the largest dispersion of bulk modulus is observed at about 200 Hz for water saturation, but at about 30 Hz for glycerin saturation. Correspondingly, bulk attenuation in Figures 6.3c and 6.3d displays a good causal relationship with bulk modulus for both water and glycerin saturation conditions. Specifically, bulk attenuation is relatively lower at nearly full saturation while being significant and frequency dependent as saturation reduces to 94%. The highest ${Q_{Kw}}^{-1}$ is observed at 94% with a peak of ~0.14 at ~200 Hz, while the peak of ${Q_{Kg}}^{-1}$ is occurred at 92% with a value of 0.17 at ~30 Hz. Notably, for glycerin saturation conditions, as saturation degrees decreasing from 92% to 60%, the ${Q_{Kg}}^{-1}$ progressively decreases, and its peak tends to shift to higher frequencies. In contrast, we did not observe such a peak shift for ${Q_{Kw}}^{-1}$.

Figure 6.4 shows the frequency dependence of shear modulus G and attenuation calculated from the complex Young's modulus and Poisson's ratio for water saturation (Figure 6.4a, 6.4c) and glycerin saturation (Figure 6.4b, 6.4d), respectively. Both saturation series shows negligible shear dispersion and attenuation. By comparing the amplitudes of shear modulus of two saturation series, we can see G_w is nearly the same with that of dry sample. In contrast, G_g is not independent of fluid but increases a lot comparing with that in dry condition, indicating a viscous contribution to the shear modulus.

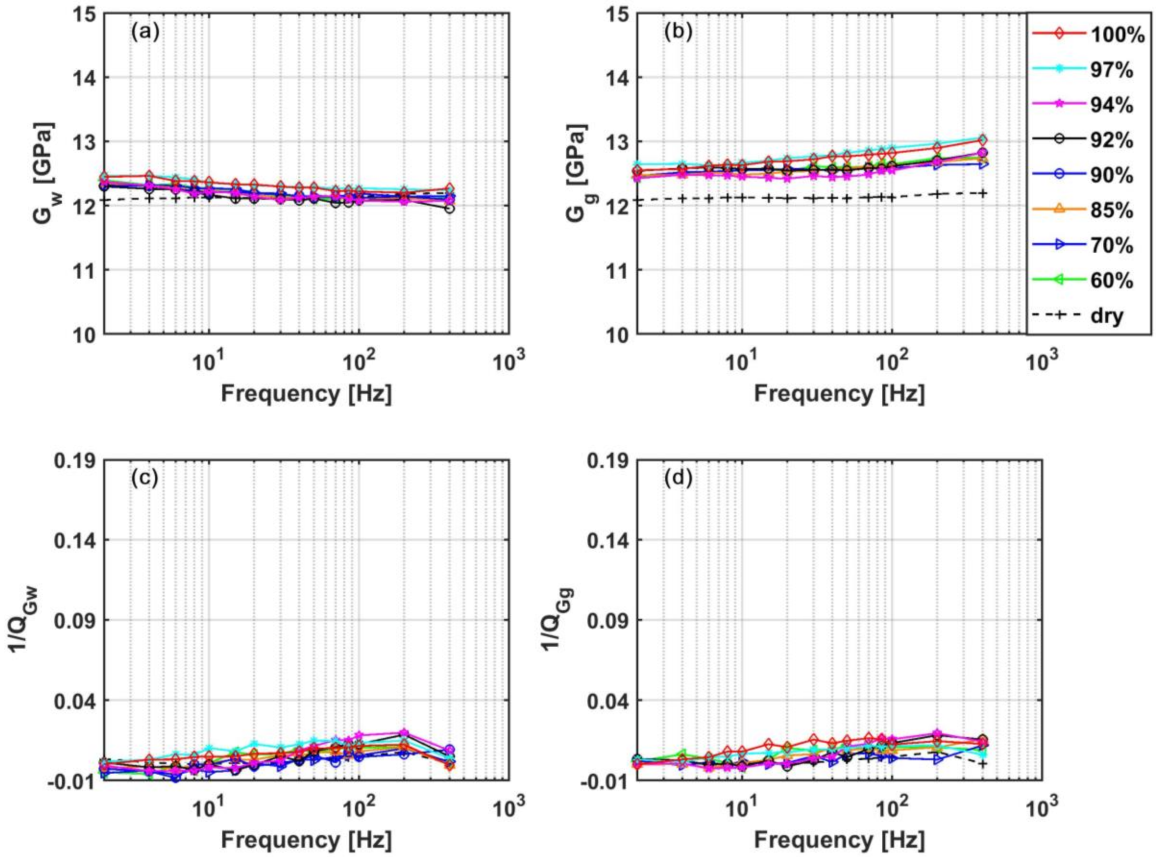

Figure 6.4 The frequency dependence of shear modulus G (a, b) and attenuation (c, d) calculated from the complex Young's modulus and Poisson's ratio for water saturation and glycerin saturation, respectively.

P-wave velocity (Vp) is further calculated and shown in Figure 6.5. The frequency dependence of Vp shows a similar behavior as that of bulk modulus. The amplitude, however, shows distinctly different trend with the change of saturation levels because of density effect. As water saturation is reduced from 100% to 70%, Vp_w has a trend to decrease. Below 70% water saturation, however, Vp_w begins to gradually increase. For glycerin saturation series, Vp_g drastically decreases as glycerin saturation reduced from 100% to 85%. Below 85% glycerin saturation, Vp_g seems to show opposite trend for frequencies beyond and below 60Hz, due to the combined effect of fluid saturation, density, and measured frequency.

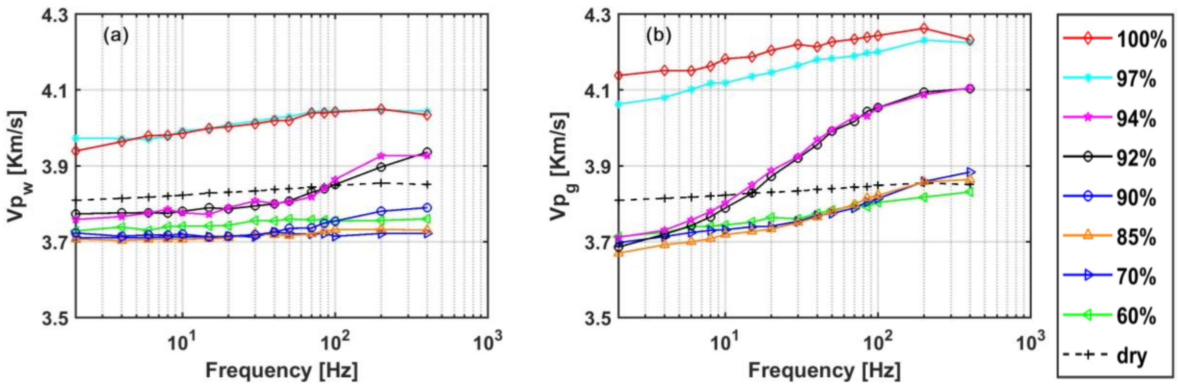

Figure 6.5 The frequency dependence of P wave velocity calculated from Young's modulus and Poisson's ratio for water (a) and glycerin (b) saturation, respectively.

6.4. Discussion

6.4.1. Comparisons to previous experimental studies

The experimental results show that the dispersion and attenuation of elastic properties vary with fluid types as well as saturation levels (Figure 6.1, 6.2, 6.3). Overall, dispersion and attenuation in glycerin saturation are much more significant and occur over broader saturation and frequency ranges than that in water saturation conditions. Notably, largest dispersion and attenuation effects occur in the presence of relatively small amounts of gas (~6% - 8%) both for glycerin and water saturation yet varying in their magnitudes and peak frequencies. Previous studies, especially for water saturation case, reported similar effects of fluid saturation and viscosity as observed in our study. However, partially glycerin-saturated data is still sparse in previous studies.

The measurements performed with dry Berea sandstone show negligible dispersion and attenuation (<0.01), which are agree with rock attenuation values (~0.01) found in the literature (Barton, 2006; Knopoff, 1965; Peselnick and Liu, 1987). At fully saturated conditions, weak dispersion and attenuation are observed both in water and glycerin saturation. Pimienta et al. (2015) measured frequency-dependence of bulk modulus and attenuation in Fontainebleau sandstone fully saturated with water or glycerin. Data indicates that significant dispersion and attenuation only exist in glycerin-saturated data at low effective pressure conditions. Weak dispersion and attenuation are observed at relatively high effective pressures (>10 MPa), which are substantially agree with our data measured at effective pressure of 13.8 MPa. Weak Squirt flow (Mavko and Jizba, 1991) or microscopic WIFF, due to negligible heterogeneities in the Berea or Fontainebleau rock pore structure, is accounted for these observations.

Under partially saturated conditions, Berea sandstone sample exhibits a strong frequency dependence and correspondingly large attenuation at water saturations ranging from 90% to 94%. Similar frequency response has been observed in several previous studies. Murphy (1982) reported a significant extensional attenuation at 75%-92% water saturation in partially saturated Massilon sandstones. Yin et al. (1992) observed an extensional attenuation peak in the case of high-water saturation (85% - 95%) in Berea sandstone sample. Chapman et al. (2016) measured attenuation in partially water-saturated Berea sandstone samples and found that attenuation is significant and frequency dependent at saturation levels between 91% and 97%. Moreover, increasing water saturation levels causes an increase in the attenuation magnitude and a shift of its peak to lower frequencies. Most of the authors attribute these water saturation effects to mesoscopic WIFF, in response to a heterogeneous water distribution in the sample (patchy saturation). For partially glycerin-saturated data, significant dispersion and attenuation are observed at saturations of 70%-94%, and maximum attenuation being found at 92-94% glycerin saturations. Meanwhile, attenuation peaks show a clear shift to lower frequency range comparing to that in water saturation cases. A complete attenuation curve is firstly observed in glycerin-saturated conditions at measured seismic frequency. Since few groups have performed measurements partially saturated with glycerin so far, we will need more data to verify these observations. Nevertheless, by comparing water saturation with glycerin saturation data, the combined effects of fluid saturation and viscosity on frequency dependence of elastic properties can be distinctly illustrated.

6.4.2. The comparison of experimental data with Gassmann model

Gassmann (1951) estimation describes the static or sufficiently low-frequency elastic properties of a fluid-filled porous rock. It generally represents the lower bound of elastic moduli. Figure 6.6 shows the comparison of Gassmann estimation with velocities (e.g., V_{pw}, V_{pg}) of Berea sandstone sample at both seismic and ultrasonic frequency band with partial water or glycerin saturation levels, respectively. Overall, both V_{pw} and V_{pg} are systematically higher at ultrasonic points (10^6 Hz) than those at seismic frequencies (2- 400 Hz) at entire saturation levels.

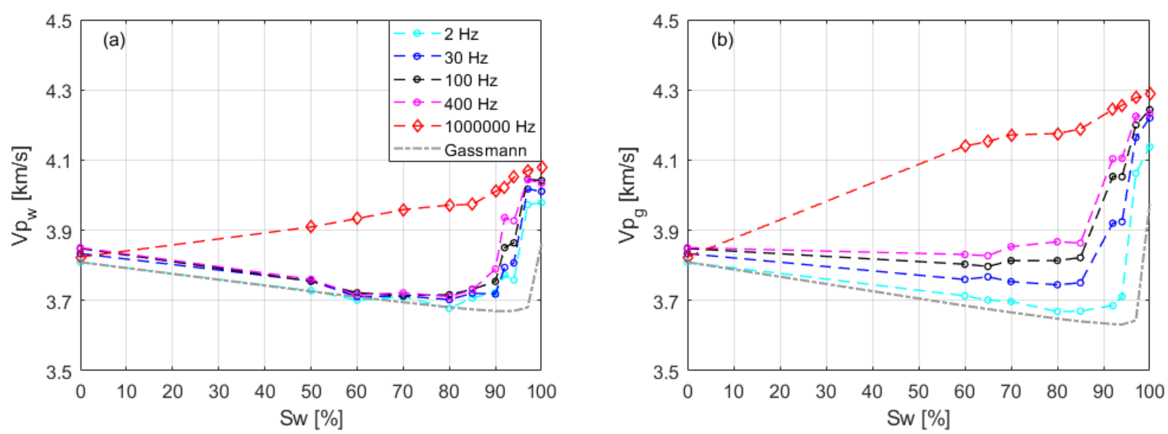

Figure 6.6 Comparison of measured data at seismic and ultrasonic frequencies with the Gassmann estimation at varying saturation degrees of (a) water and (b) glycerin.

At nearly full saturation, seismic-frequency velocities are slightly lower than the ultrasonic velocities. As water or glycerin saturation is reduced to 80%, V_{pw} and V_{pg} at ultrasonic frequency remain high and decrease slowly, while both V_{pw} and V_{pg} at seismic frequencies drop dramatically with decreasing saturation levels. Meanwhile, V_{pg} exhibits significant dispersion (~5% - 10%) at frequency range 2- 400 Hz at 80% - 94% glycerin saturation as opposed to V_{pw}, which shows relatively small dispersion (~5%) at narrow saturation range (92% - 94%). Moreover, the laboratory measurements of V_{pw} at the seismic frequency are well consistent with the Gassmann estimation, especially for relatively lower water saturation levels. In contrast, there is an apparent deviation between Gassmann estimation and laboratory measurements of V_{pg}.

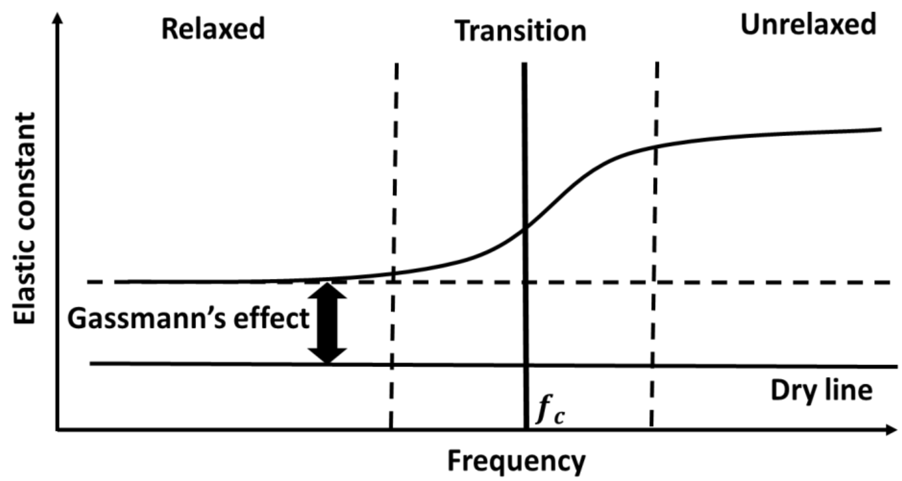

Figure 6.7 Generalized frequency dependence of elastic properties, illustrating three typical pore fluid status: relaxed, unrelaxed, and transition status.

These frequency-dependent behaviors of the data actually demonstrate three typical pore fluid status: relaxed, unrelaxed, and transition status (Batzle et al., 2006; Mavko and Jizba, 1991). The classification of pore fluid status is largely a scale related matter and determined by a key parameter characteristic frequency f_c, at which point the elastic constant changes most rapidly. As shown in Figure 6.7, when passing wave frequency f is sufficiently lower than f_c, the induced pore pressures reach completely equilibrated throughout the pore space of the rock, resulting in relaxed status of the pore fluid. In this case, rock elastic properties can be approximately described by the Gassmann equation. This seems to be the case for V_{pw} at seismic frequency, as well as V_{pg} at very low frequency (e.g., 2 Hz). Conversely, if the applied frequency is significantly higher than f_c, the pore fluid does not have enough time to equilibrate, resulting in unrelaxed status, where the pore fluid contributes to increase the total stiffness of the rock fluid system.

As is the case for ultrasonic measurements, where the frequency is too high for pore pressure to equilibrate, and pore fluid is prone to stiff the rock. Between relaxed and unrelaxed status, there exists a transition zone, where the induced fluid pressure inside the rock is partially equilibrated. A substantial change of velocities can be obtained by increasing the frequency, the so-called dispersion. According to the description of existing WIFF models (Müller et al., 2010), except for the viscous-inertial based Biot theory (Biot, 1956), which can only be significant at frequencies above 100 kHz, well outside the seismic frequency band (Pride, 2005; Müller et al., 2010), non-Biot WIFF models predict that the characteristic frequency is inversely proportional to fluid viscosity (Pride et al., 2004; White, 1975; O'Connell and Budiansky, 1977). Since the viscosity of glycerin is three orders larger than that of water, it is expected that the characteristic frequency (Pride et al., 2004) of glycerin saturated rock should theoretically shift towards to lower frequency range comparing with water saturated rock. This can explain why the larger dispersion of $V_{pg}$is observed at measured frequency range (2- 400 Hz), while V_{pw} at seismic frequency is well consistent with the Gassmann estimation. Consequently, Figure 6.7 might provide a general understanding of the observed frequency-dependent behavior based on WIFF.

6.4.3. Dispersion and attenuation mechanism analysis

Generally, for partial saturated rock, the pore scale heterogeneity and pore fluids distribution are always coupled together to control the wave dispersion and attenuation characteristics (Walsh, 1995; Rubino and Holliger, 2012; Ba et al., 2017).

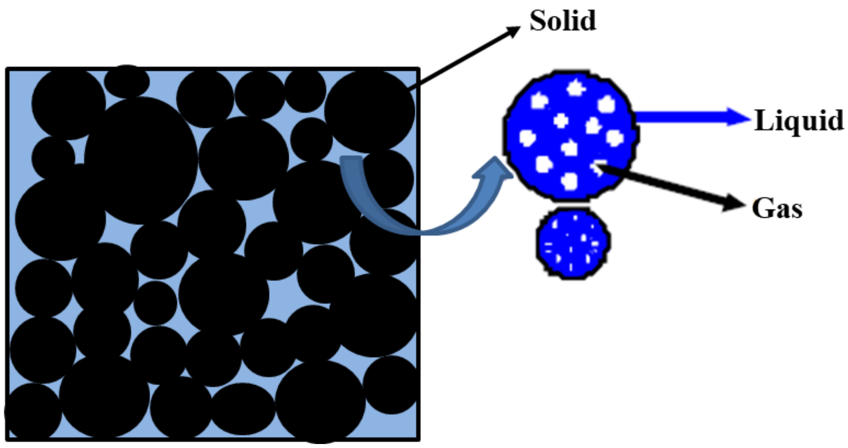

(a)Uniform saturation

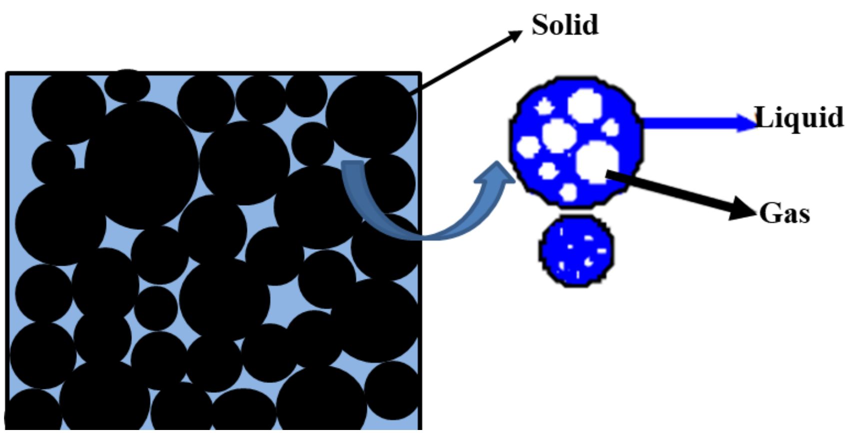

(b)Heterogeneous saturation

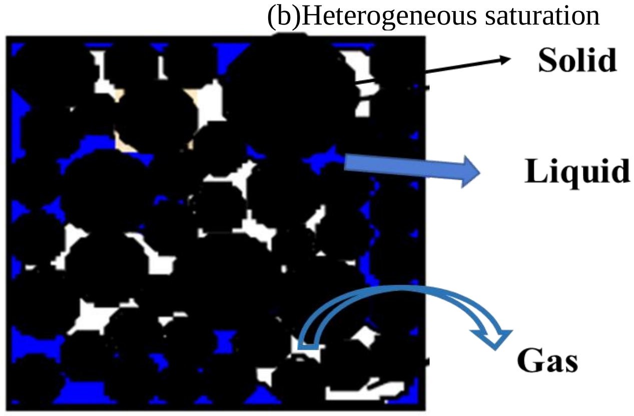

(c)Patchy saturation

Figure 6.8 Conceptual diagrams of different saturation states in pore space.

As discussed in the rock properties, the measured Berea sandstone is a relatively clean, quartz dominant sandstone and can be assumed homogeneous and isotropic at the sample scale. Besides, the gas pockets firstly invade larger pores and are sparsely distributed during the drainage process. Therefore, the heterogeneity of pore fluid distribution, sometimes referred to as patchy saturation, might offer insights into the dispersion and attenuation behaviors observed in Berea sandstone (Johnson, 2001; Masson and Pride, 2011).

Figure 6.8 shows the diagrams of different saturation states in pore space. (a) Uniform saturation indicates that gas saturation is same at any pore space. (b) Heterogeneous saturation means gas saturation is different at each pore space. (c) The presence of so-called patchy saturation, that is, spatially variable gas–liquid distributions in the form of local patches fully saturated with gas embedded in regions fully saturated with liquid.

The patchy model (White, 1975) associated with mesoscopic heterogeneities is considered to interpret the experimental data for both water- and glycerin-saturated cases. Given the rock and fluid properties as listed in sample description, the radius of the gas patch in partial water saturation is set as 1.8cm, which is approximately one third of the test sample length. Figure 6.9 shows the experimental data and modeling curve of extensional attenuation for partially water-saturated conditions.

Overall, White's patchy model is well consistent with the measured attenuation data. As observed, with increasing saturation levels, the attenuation magnitude tends to increase, and reaches the maximum value when the saturation degree is 94%, which highly coincides with the measured data. Moreover, the peak frequencies for modeling curves shift to a lower frequency with increasing saturation levels. This shift mainly results from the increase in the characteristic length of the heterogeneity scale (Dutta and Seriff, 1979). It is also necessary to point out that an apparent discrepancy exists at 97% water saturation, where the magnitude of modeling attenuation is significant, as opposed to negligible attenuation of measured data. One possible explanation of this discrepancy is that, during the real experiments, the first few-percent of gas may only occupy at the top of the sample as it was injected into the fully water saturated rock from the top pore pressure line, thus no patch is formed in the rock sample, resulting in similar attenuation characteristics as fully water saturation. Nevertheless, the measured attenuation can be well characterized by the white's model, suggesting that mesoscopic fluid flow is mainly account for the observed dispersion and attenuation in partially water-saturated cases.

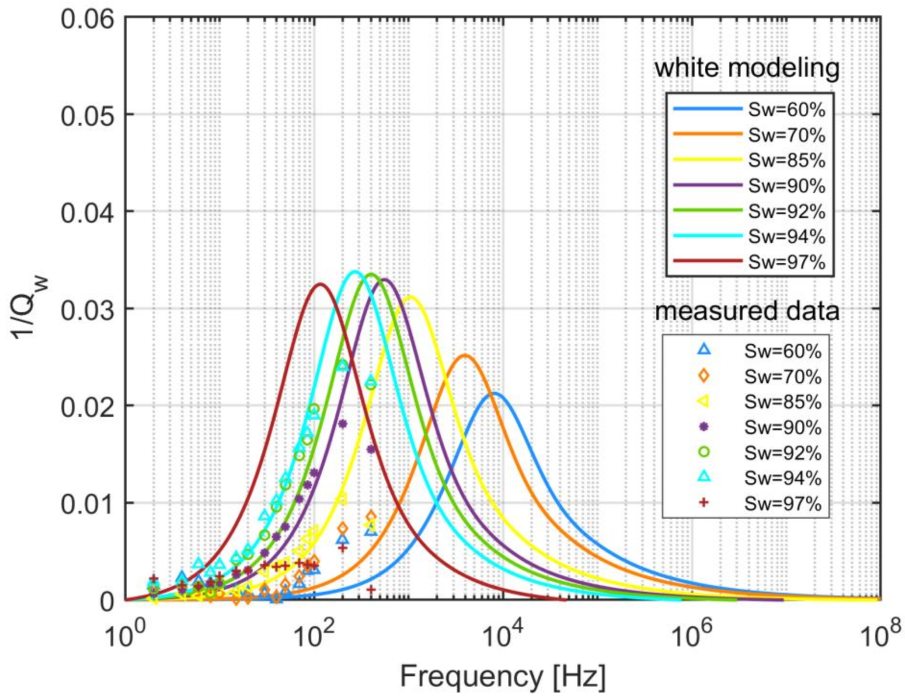

Figure 6.9 Comparison of measured extensional attenuation with the computed attenuation using the White model against frequencies at varying water saturation levels.

For partially glycerin-saturated state, considering the higher viscosity and lower compressibility of glycerin than that of water as listed in Table 6.1, I set the patch size as 0.8 cm. By comparing the behavior of the modeling extensional attenuation with changes in glycerin saturation to that of measured results (Figure 6.10), one can notice that both attenuations roughly occur in the same frequency range, from several Hz to hundreds Hz.

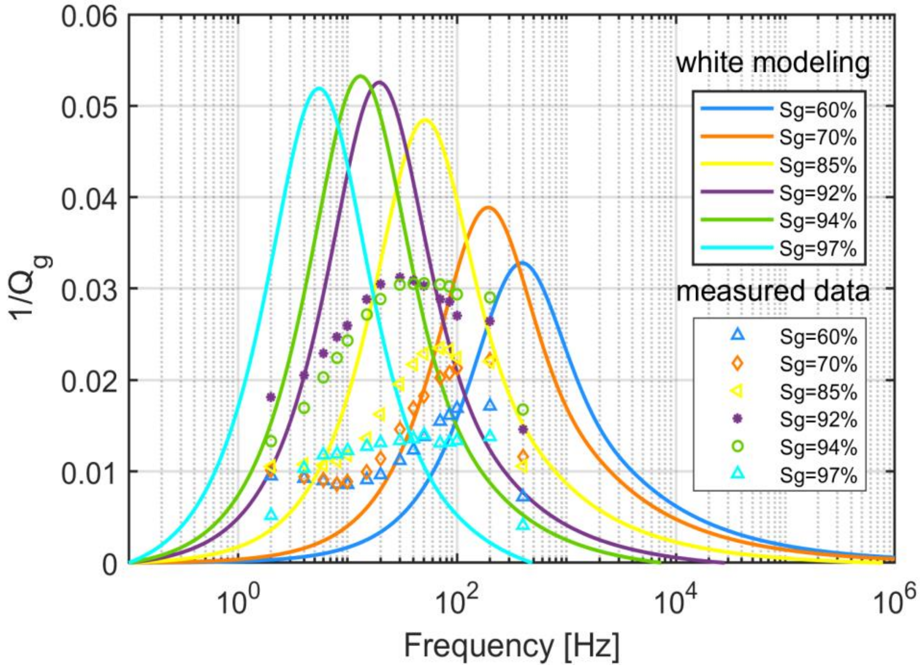

Figure 6.10 Comparison of measured extensional attenuation with the computed attenuation using the White model against frequencies at varying glycerin saturation levels.

The peak frequencies also seem to overlap and show a similar dependent relation with glycerin saturation levels. In addition, the magnitudes of modeling extensional attenuation gradually increase with increasing glycerin saturation degrees, and achieve a maximum value at 94% glycerin saturation, which is consistent with features of the measured attenuation magnitudes. Therefore, these characteristics suggest that the White model, to a certain degree, captures the dominant factors influencing the attenuation of the partially glycerin-saturated rock sample.

Besides the overall consistency, there have two apparent discrepancies existing between experimental data and modeling results. First, a similar discrepancy, as observed in water saturation case, also occurs at 97% glycerin saturation, where modeling attenuation is significant, while measured attenuation is negligible. The same interpretation might be applied to account for this discrepancy. Second, White's patchy model overestimates the extensional attenuation of the partially glycerin-saturated rock sample. This discrepancy is possibly caused by the fact that parameters in realistic Berea sample may be different from the model's assumption. For instance, if the realistic compressibility difference between two immiscible fluids is less than the model's estimation, it will induce relatively small pressure gradient between gas and glycerin. Then oscillatory fluid flow resulting from unequilibrated pore pressures will consume less energy from wave, finally leading to discrepancies between the modeling curves and experimental data.

It is also worth mentioning that the peak attenuation of partially water- and glycerin-saturated cases are both observed at ~ 94% saturation level, despite of the large difference of viscosity between water and glycerin. Moreover, viscosity as a key factor that controls the fluid mobility (Batzle et al., 2006), mainly affects the characteristic frequency range at which the peak attenuation occurs. As observed in figure 8 and 9, the characteristic frequencies of partially water-saturated case range between 10^2 Hz and 10^3 Hz, while shift to 10^1 Hz -10^2 Hz for partially glycerin-saturated conditions. This is mainly due to the increment of characteristic length of the heterogeneity size involving saturated glycerin with much higher viscosity (Dutta and Seriff, 1979; Zhao et al., 2017).

6.5. Summary

I experimentally investigated the elastic properties of the Berea sample at both seismic (i.e., f $\in$[2; 400] Hz) and ultrasonic (i.e., f ~ 1 MHz) frequency ranges under two partial saturation series with varying viscosities (e.g., ~1 cP for water, ~1400 cP for glycerin).The measured results show that elastic parameters (E, ν, Q_E^{-1}) are highly dependent on fluid viscosity as well as saturation levels.Significant dispersion and attenuation effects occur in the presence of relatively small amounts of gas (~6% - 8%) both for glycerin and water saturation yet varying in their magnitudes and characteristic frequencies. The overall characteristic frequencies of extensional attenuation with glycerin saturation shift to a lower frequency range comparing to that with water saturation. Specifically, the highest extensional attenuation (~0.024) of the measured sample is observed at 94% water saturation at ~200 Hz, while occurred at 92% with a peak of 0.032 at ~30 Hz for glycerin saturation. Based on porous modeling analysis, the mesoscopic fluid flow, in response to a heterogeneous fluid distribution in the pore space, can be a dominant mechanism accounting for the observed dispersion and attenuation in partial water or glycerin saturation cases.

7. CONCLUSIONS

Seismic waves propagating through the subsurface porous rocks are intrinsically dispersive and dissipative due to the inelasticity of the rock medium. A better knowledge of such intrinsic dispersion and attenuation is of great interest in improving reservoir characterization and hydrocarbon identification, because this phenomenon is intimately associated with rock and fluid properties. Many theories and models have been proposed for characterizing seismic dispersion and attenuation phenomenon in sedimentary rocks. But limited by lacking reliable laboratory data at seismic frequency bands, most of the theoretical models do not receive strong supports from experimental data. In addition, given the high requirement of measurement precision and the complexity of laboratory measurements, there are few teams capable of conducting low-frequency measurements worldwide so far. Therefore, the effects of rock and fluid properties on dispersion and attenuation at seismic frequency are still poorly understood.

Following the forced-oscillation principles as used by Batzle et al. (2006), a well calibrated low-frequency measurement system has been developed in the Rock Physics Laboratory at the University of Houston, which is capable of measuring the elastic modulus and the corresponding attenuation of rocks under varying physical conditions at seismic frequency ranges (2-600 Hz). In general, the error for the dispersion is roughly 0.4%. The average error for the attenuation is ±0.0035. Based on this system, I perform a series of laboratory measurements of elastic dispersion and attenuation on three typical sandstones (Bentheimer, Berea, and Bandera) with different permeabilities at both seismic (2-600 Hz) and ultrasonic (~1 MHz) frequencies, aiming to investigate the roles of rock and fluid properties in wave dispersion and attenuation. Samples are saturated by a series of fluids with varying viscosity (e.g., methane, butane, water, and glycerin). In addition, several partial saturation measurements are successfully carried out, especially partially saturated with high viscous fluid (e.g., glycerin). I interpret the measured data by comparing with theoretical model and discussing possible underlying attenuation mechanisms. Several conclusions are drawn as follows:

1. All the measured low frequency data show that intrinsic dispersion and attenuation are coupled phenomena. When the dispersion occurs, the attenuation takes place at the same time, vice versa. The maximum attenuation takes place at the point where the elastic property changes most rapidly with frequency.
2. Role of mineral content in frequency dependence of elastic properties in dry rock. At vacuum-dry conditions, the bulk dispersion and attenuation in sandstones with more clay contents are distinctly larger than those in quartz dominant and clean sandstone, suggesting clay contents might contribute to the inelasticity of the rock frame.
3. The rock permeability begins to dominate the pore-fluid relaxation only as gas saturation less than a few percent. For the case of higher permeability and better pore connectivity rock, the pore fluid can easily reach a relaxed status even though only 3% gas occupies the pore space, resulting in small attenuation and dispersion. In contrast, for sandstones with relatively low permeability, pore pressure gradients need more time to reach an equilibrated state. At the applied frequency ranges, only parts of the pore fluid can reach a relaxed status, accompanying with apparent attenuation and dispersion.

4. Fluid viscosity systematically affects the characteristic frequency of pore pressure relaxation. Low viscosity fluid (such as methane, butane, and water) permits pore pressure equilibration either between pores or between heterogeneous regions of the rock and results in a negligible dispersion and attenuation at measured seismic frequency range. In contrast, high viscosity, thus low fluid mobility, can produce strong dispersion within the seismic band.
5. Significant dispersion and attenuation effects occur in the presence of relatively small amounts of gas (~6% - 8%) both for partial glycerin and partial water saturation yet varying in their magnitudes and characteristic frequencies. The overall characteristic frequencies of extensional attenuation with glycerin saturation shifts to a lower frequency range comparing to that with water saturation. Based on porous modeling analysis, the mesoscopic fluid flow in response to a heterogeneous fluid distribution in the pore space, might be a dominant mechanism accounting for the observed dispersion and attenuation in partial water or glycerin saturation cases.

For future works, on the one hand, I need to measure more samples with different lithologies, such as tight sandstone, carbonate, and shale. Then try to establish a database, with which I can find more robust relationship between the dispersion/attenuation and rock's properties. On the other hand, I want to apply the newly experimental results and proved relationships to field data cases. Possible applications could be fizz gas identification, high-permeability zone detection, and reservoir production monitoring.

BIBLIOGRAPHY

Adam, L., Batzle, M., Lewallen, K. T., & van Wijk, K. (2009). Seismic wave attenuation in carbonates. *Journal of Geophysical Research: Solid Earth*, *114*(B6).

Adelinet, M., Fortin, J., & Guéguen, Y. (2011). Dispersion of elastic moduli in a porous-cracked rock: Theoretical predictions for squirt-flow. *Tectonophysics*, *503*(1-2), 173-181.

Adelinet, M., Fortin, J., Guéguen, Y., Schubnel, A., & Geoffroy, L. (2010). Frequency and fluid effects on elastic properties of basalt: Experimental investigations. *Geophysical Research Letters*, *37*(2).

Aki, K., & Richards, P. G. (1980). Quantative seismology: Theory and methods. *Quantative Seismology: Theory and Methods. by K. Aki and PG Richards. San Francisco: Freeman*.

Ba, J., Xu, W., Fu, L. Y., Carcione, J. M., & Zhang, L. (2017). Rock anelasticity due to patchy saturation and fabric heterogeneity: A double double-porosity model of wave propagation. *Journal of Geophysical Research: Solid Earth*, *122*(3), 1949-1976.

Barton, N. (2006). *Rock quality, seismic velocity, attenuation and anisotropy*. CRC press.

Batzle, M. L., Han, D. H., & Hofmann, R. (2006). Fluid mobility and frequency-dependent seismic velocity—Direct measurements. *Geophysics*, *71*(1), N1-N9.

Berryman, J. G., & Wang, H. F. (2001). Dispersion in poroelastic systems. *Physical Review E*, *64*(1), 011303.

Berryman, J. G., Pride, S. R., & Wang, H. F. (2002). A differential scheme for elastic properties of rocks with dry or saturated cracks. *Geophysical Journal International*, *151*(2), 597-611.

Biot, M. A. (1956a). Theory of propagation of elastic waves in a fluid-saturated porous solid. I. Lower frequency range. *The Journal of the acoustical Society of America*, *28*(2), 168-178.

Biot, M. A. (1956b). Theory of propagation of elastic waves in a fluid-saturated porous solid. II. Higher frequency range. *The Journal of the acoustical Society of America*, *28*(2), 179-191.

Biot, M. A. (1962). Mechanics of deformation and acoustic propagation in porous media. *Journal of applied physics*, *33*(4), 1482-1498.

Birch, F. (1975). Velocity and attenuation from resonant vibrations of spheres of rock, glass, and steel. *Journal of Geophysical Research*, *80*(5), 756-764.

Brown, J. M., Angel, R. J., & Ross, N. L. (2016). Elasticity of plagioclase feldspars. *Journal of Geophysical Research: Solid Earth*, *121*(2), 663-675.

Bourbie, T., & Gonzalez-Serrano, A. (1983). Synthetic seismograms in attenuating media. *Geophysics*, *48*(12), 1575-1587.

Carcione, J. M., Picotti, S., Gei, D., & Rossi, G. (2006). Physics and seismic modeling for monitoring CO_2 storage. *Pure and Applied Geophysics*, *163*(1), 175-207.

Castagna, J. P., Sun, S., & Siegfried, R. W. (2003). Instantaneous spectral analysis: Detection of low-frequency shadows associated with hydrocarbons. *The leading edge*, *22*(2), 120-127.

Chapman, M., Zatsepin, S. V., & Crampin, S. (2002). Derivation of a microstructural poroelastic model. *Geophysical Journal International*, *151*(2), 427-451.

Chapman, M., Liu, E., & Li, X. Y. (2006). The influence of fluid sensitive dispersion and attenuation on AVO analysis. *Geophysical Journal International*, *167*(1), 89-105.

Chapman, S., Tisato, N., Quintal, B., & Holliger, K. (2016). Seismic attenuation in partially saturated Berea sandstone submitted to a range of confining pressures. *Journal of Geophysical Research: Solid Earth*, *121*(3), 1664-1676.

Chapman, S., Borgomano, J. V., Yin, H., Fortin, J., & Quintal, B. (2019). Forced oscillation measurements of seismic wave attenuation and stiffness moduli dispersion in glycerine-saturated Berea sandstone. *Geophysical Prospecting*, *67*(4-Rock Physics: from microstructure to seismic signatures), 956-968.

Christensen, N. I., & Wang, H. F. (1985). The influence of pore pressure and confining pressure on dynamic elastic properties of Berea sandstone. *Geophysics*, *50*(2), 207-213.

Clark, V. A., Tittmann, B. R., & Spencer, T. W. (1980). Effect of volatiles on attenuation (Q− 1) and velocity in sedimentary rocks. *Journal of Geophysical Research: Solid Earth*, *85*(B10), 5190-5198.

Cleary, M. P. (1978). Elastic and dynamic response regimes of fluid-impregnated solids with diverse microstructures. *International Journal of Solids and Structures*, *14*(10), 795-819.

Dunn, K. J. (1987). Sample boundary effect in acoustic attenuation of fluid-saturated porous cylinders. *The Journal of the Acoustical Society of America*, *81*(5), 1259-1266.

Dvorkin, J., Mavko, G., & Nur, A. (1995). Squirt flow in fully saturated rocks. *Geophysics*, *60*(1), 97-107.

Fortin, J., Pimienta, L., Guéguen, Y., Schubnel, A., David, E. C., & Adelinet, M. (2014). Experimental results on the combined effects of frequency and pressure on the dispersion of elastic waves in porous rocks. *The Leading Edge*, *33*(6), 648-654.

Gardner, G. H. F. (1962). Extensional waves in fluid-saturated porous cylinders. *The Journal of the Acoustical Society of America*, *34*(1), 36-40.

Gassmann, F. (1951). Elasticity of porous media. *Vierteljahrsschrder Naturforschenden Gesselschaft*, *96*, 1-23.

Goloshubin, G. M., & Korneev, V. A. (2000). Seismic low-frequency effects from fluid-saturated reservoir. In *SEG Technical Program Expanded Abstracts 2000* (pp. 1671-1674). Society of Exploration Geophysicists.

Goetz, J. F., Dupal, L., & Bowler, J. (1979). An investigation into discrepancies between sonic log and seismic check spot velocities. *The APPEA Journal*, *19*(1), 131-141.

Goodway, B., Monk, D., Perez, M., Purdue, G., Anderson, P., Iverson, A., ... & Cho, D. (2012). Combined microseismic and 4D to calibrate and confirm surface 3D azimuthal AVO/LMR predictions of completions performance and well production in the Horn River gas shales of NEBC. *The Leading Edge*, *31*(12), 1502-1511.

Gurevich, B., Brajanovski, M., Galvin, R. J., Müller, T. M., & Toms-Stewart, J. (2009). P-wave dispersion and attenuation in fractured and porous reservoirs–poroelasticity approach. *Geophysical Prospecting*, *57*(2), 225-237.

Gurevich, B., Makarynska, D., & Pervukhina, M. (2009). Ultrasonic moduli for fluid-saturated rocks: Mavko-Jizba relations rederived and generalized. *Geophysics*, *74*(4), N25-N30.

Gurevich, B., Makarynska, D., de Paula, O. B., & Pervukhina, M. (2010). A simple model for squirt-flow dispersion and attenuation in fluid-saturated granular rocks. *Geophysics*, *75*(6), N109-N120.

Heyliger, P., Ledbetter, H., & Kim, S. (2003). Elastic constants of natural quartz. *The Journal of the Acoustical Society of America*, *114*(2), 644-650.

Huang, Q. (2018). *Velocity Dispersion and Wave Attenuation of Sandstone and Shale under Different Pressures and Saturations in Seismic Frequencies* (Doctoral dissertation).

Johnson, D. L. (2001). Theory of frequency dependent acoustics in patchy-saturated porous media. *The Journal of the Acoustical Society of America*, *110*(2), 682-694.

Johnston, D. H., Toksöz, M. N., & Timur, A. (1979). Attenuation of seismic waves in dry and saturated rocks: II. Mechanisms. *Geophysics*, *44*(4), 691-711.

Kelder, O., & Smeulders, D. M. (1997). Observation of the Biot slow wave in water-saturated Nivelsteiner sandstone. *Geophysics*, *62*(6), 1794-1796.

Klimentos, T., & McCann, C. (1990). Relationships among compressional wave attenuation, porosity, clay content, and permeability in sandstones. *Geophysics*, *55*(8), 998-1014.

Knopoff, L. (1965). Attenuation of Elastic Waves in the Earth. In *Physical Acoustics* (Vol. 3, pp. 287-324). Academic Press.

Korneev, V. A., Goloshubin, G. M., Daley, T. M., & Silin, D. B. (2004). Seismic low-frequency effects in monitoring fluid-saturated reservoirs. *Geophysics*, *69*(2), 522-532.

Lambert, G., Gurevich, B., & Brajanovski, M. (2006). Attenuation and dispersion of P-waves in porous rocks with planar fractures: Comparison of theory and numerical simulations. *Geophysics*, *71*(3), N41-N45.

Le Ravalec, M., Guéguen, Y., & Chelidze, T. (1996). Elastic wave velocities in partially saturated rocks: Saturation hysteresis. *Journal of Geophysical Research: Solid Earth*, *101*(B1), 837-844.

Le, T. M., Fatahi, B., & Khabbaz, H. (2012). Viscous behavior of soft clay and inducing factors. *Geotechnical and Geological Engineering*, *30*(5), 1069-1083.

Li, H., Wang, D., Gao, J., Zhang, M., Wang, Y., Zhao, L., & Yang, Z. (2020). Role of saturation on elastic dispersion and attenuation of tight rocks: An experimental study. *Journal of Geophysical Research: Solid Earth*, *125*(4), e2019JB018513.

Li, H., Zhao, L., Han, D. H., Gao, J., Yuan, H., & Wang, Y. (2020). Experimental study on frequency-dependent elastic properties of weakly consolidated marine sandstone: effects of partial saturation. *Geophysical Prospecting*, *68*(9), 2808-2824.

Lockner, D. A., Walsh, J. B., & Byerlee, J. D. (1977). Changes in seismic velocity and attenuation during deformation of granite. *Journal of Geophysical Research*, *82*(33), 5374-5378.

Masson, Y. J., & Pride, S. R. (2011). Seismic attenuation due to patchy saturation. *Journal of Geophysical Research: Solid Earth*, *116*(B3).

Mavko, G., & Nur, A. (1975). Melt squirt in the asthenosphere. *Journal of Geophysical Research*, *80*(11), 1444-1448.

Mavko, G., & Jizba, D. (1991). Estimating grain-scale fluid effects on velocity dispersion in rocks. *Geophysics*, *56*(12), 1940-1949.

Mavko, G., & Jizba, D. (1994). The relation between seismic P-and S-wave velocity dispersion in saturated rocks. *Geophysics*, *59*(1), 87-92.

Mavko, G., Mukerji, T., & Dvorkin, J. (2020). *The rock physics handbook*. Cambridge university press.

Mavko, G. M., & Nur, A. (1979). Wave attenuation in partially saturated rocks. *Geophysics*, *44*(2), 161-178.

Mavko, G., & Vanorio, T. (2010). The influence of pore fluids and frequency on apparent effective stress behavior of seismic velocities. *Geophysics*, *75*(1), N1-N7.

McKavanagh, B., & Stacey, F. D. (1974). Mechanical hysteresis in rocks at low strain amplitudes and seismic frequencies. *Physics of the Earth and Planetary Interiors*, *8*(3), 246-250.

Mikhaltsevitch, V., Lebedev*, M., & Gurevich, B. (2015). A laboratory study of attenuation and dispersion effects in glycerol-saturated Berea sandstone at seismic frequencies. In *SEG Technical Program Expanded Abstracts 2015* (pp. 3085-3089). Society of Exploration Geophysicists.

Mikhaltsevitch, V., Lebedev, M., & Gurevich, B. (2016). A laboratory study of the elastic anisotropy in the Mancos shale at seismic frequencies. In *SEG Technical Program Expanded Abstracts 2016* (pp. 3174-3178). Society of Exploration Geophysicists.

Müller, T. M., Gurevich, B., & Lebedev, M. (2010). Seismic wave attenuation and dispersion resulting from wave-induced flow in porous rocks—A review. *Geophysics*, *75*(5), 75A147-75A164.

Murphy III, W. F. (1982). Effects of partial water saturation on attenuation in Massilon sandstone and Vycor porous glass. *The Journal of the Acoustical Society of America*, *71*(6), 1458-1468.

O'Connell, R. J., & Budiansky, B. (1974). Seismic velocities in dry and saturated cracked solids. *Journal of geophysical Research*, *79*(35), 5412-5426.

O'Connell, R. J., & Budiansky, B. (1977). Viscoelastic properties of fluid-saturated cracked solids. *Journal of Geophysical Research*, *82*(36), 5719-5735.

Peselnick, L., & Liu, H. P. (1987). 2. Laboratory measurement of internal friction in rocks and minerals at seismic frequencies. In *Methods in Experimental Physics* (Vol. 24, pp. 31-56). Academic Press.

Pimienta, L., Fortin, J., & Guéguen, Y. (2014). Investigation of elastic weakening in limestone and sandstone samples from moisture adsorption. *Geophysical Journal International*, *199*(1), 335-347.

Pimienta, L., Fortin, J., & Guéguen, Y. (2015). Bulk modulus dispersion and attenuation in sandstones. *Geophysics*, *80*(2), D111-D127.

Pimienta, L., Borgomano, J. V. M., Fortin, J., & Guéguen, Y. (2016). Modelling the drained/undrained transition: Effect of the measuring method and the boundary conditions. *Geophysical Prospecting*, *64*(4-Advances in Rock Physics), 1098-1111.

Pimienta, L., Borgomano, J. V., Fortin, J., & Guéguen, Y. (2017). Elastic dispersion and attenuation in fully saturated sandstones: Role of mineral content, porosity, and pressures. *Journal of Geophysical Research: Solid Earth*, *122*(12), 9950-9965.

Plona, T. J. (1980). Observation of a second bulk compressional wave in a porous medium at ultrasonic frequencies. *Applied physics letters*, *36*(4), 259-261.

Pride, S. R. (2005). Relationships between seismic and hydrological properties. In *Hydrogeophysics* (pp. 253-290). Springer, Dordrecht.

Pride, S. R., & Berryman, J. G. (2003a). Linear dynamics of double-porosity dual-permeability materials. I. Governing equations and acoustic attenuation. *Physical Review E*, *68*(3), 036603.

Pride, S. R., & Berryman, J. G. (2003b). Linear dynamics of double-porosity dual-permeability materials. II. Fluid transport equations. *Physical Review E*, *68*(3), 036604.

Pride, S. R., Berryman, J. G., & Harris, J. M. (2004). Seismic attenuation due to wave-induced flow. *Journal of Geophysical Research: Solid Earth*, *109*(B1).

Rapoport, M. (2013). Useful data lurk in seismic inelasticity, nonlinearity. *Oil & gas journal*, *111*(6), 46-53.

Rubino, J. G., & Holliger, K. (2012). Seismic attenuation and velocity dispersion in heterogeneous partially saturated porous rocks. *Geophysical Journal International*, *188*(3), 1088-1102.

Sarout, J. (2012). Impact of pore space topology on permeability, cut-off frequencies and validity of wave propagation theories. *Geophysical Journal International*, *189*(1), 481-492.

Sarout, J., David, C., & Pimienta, L. (2019). Seismic and microseismic signatures of fluids in rocks: Bridging the scale gap. *Journal of Geophysical Research: Solid Earth*, *124*(6), 5379-5386.

Spencer Jr, J. W. (1981). Stress relaxations at low frequencies in fluid-saturated rocks: Attenuation and modulus dispersion. *Journal of Geophysical Research: Solid Earth*, *86*(B3), 1803-1812.

Spencer, J. W., & Shine, J. (2016). Seismic wave attenuation and modulus dispersion in sandstones. *Geophysics*, *81*(3), D211-D231.

Ram, A. V. A. D. H., & Narayan, J. P. (1997). Synthetic seismograms for a layered earth geological model using the absorption and dispersion phenomena. *pure and applied geophysics*, *149*(3), 541-551.

Subramaniyan, S., Quintal, B., Madonna, C., & Saenger, E. H. (2015). Laboratory-based seismic attenuation in Fontainebleau sandstone: Evidence of squirt flow. *Journal of Geophysical Research: Solid Earth*, *120*(11), 7526-7535.

Tisato, N., & Quintal, B. (2013). Measurements of seismic attenuation and transient fluid pressure in partially saturated Berea sandstone: evidence of fluid flow on the mesoscopic scale. *Geophysical Journal International*, *195*(1), 342-351.

Tisato, N., & Quintal, B. (2014). Laboratory measurements of seismic attenuation in sandstone: Strain versus fluid saturation effects. *Geophysics*, *79*(5), WB9-WB14.

Tittmann, B. R., Clark, V. A., Richardson, J. M., & Spencer, T. W. (1980). Possible mechanism for seismic attenuation in rocks containing small amounts of volatiles. *Journal of Geophysical Research: Solid Earth*, *85*(B10), 5199-5208.

Toll, J. S. (1956). Causality and the dispersion relation: logical foundations. *Physical review*, *104*(6), 1760.

Vanorio, T., Prasad, M., & Nur, A. (2003). Elastic properties of dry clay mineral aggregates, suspensions, and sandstones. *Geophysical Journal International*, *155*(1), 319-326.

Walsh, J. B. (1966). Seismic wave attenuation in rock due to friction. *Journal of Geophysical Research*, *71*(10), 2591-2599.

Walsh, J. B. (1995). Seismic attenuation in partially saturated rock. *Journal of Geophysical Research: Solid Earth*, *100*(B8), 15407-15424.

Wang, Y., Han, D. H., Li, H., Zhao, L., Ren, J., & Zhang, Y. (2020). A comparative study of the stress-dependence of dynamic and static moduli for sandstones. *Geophysics*, *85*(4), MR179-MR190.

Wei, Q., Wang, Y., Han, D. H., Sun, M., & Huang, Q. (2021). Combined effects of permeability and fluid saturation on seismic wave dispersion and attenuation in partially-saturated sandstone. *Advances in Geo-Energy Research*, *5*(2), 181-190.

White, J. E. (1965). *Seismic waves: Radiation, transmission, and attenuation*. McGraw-Hill.

White, J. E. (1975). Computed seismic speeds and attenuation in rocks with partial gas saturation. *Geophysics*, *40*(2), 224-232.

Wideman, C. J., & Major, M. W. (1967). Strain steps associated with earthquakes. *Bulletin of the Seismological Society of America*, *57*(6), 1429-1444.

Winkler, K., Nur, A., & Gladwin, M. (1979). Friction and seismic attenuation in rocks. *Nature*, *277*(5697), 528-531.

Winkler, K. W. (1985). Dispersion analysis of velocity and attenuation in Berea sandstone. *Journal of Geophysical Research: Solid Earth*, *90*(B8), 6793-6800.

Yao, Q. (2013). *Velocity dispersion and wave attenuation in reservoir rocks* (Doctoral dissertation).

Yin, C. S., Batzle, M. L., & Smith, B. J. (1992). Effects of partial liquid/gas saturation on extensional wave attenuation in Berea sandstone. *Geophysical Research Letters*, *19*(13), 1399-1402.

Yin, H., Borgomano, J. V., Wang, S., Tiennot, M., Fortin, J., & Guéguen, Y. (2019). Fluid substitution and shear weakening in clay-bearing sandstone at seismic frequencies. *Journal of Geophysical Research: Solid Earth*, *124*(2), 1254-1272.

Zener, C. (1948). *Elasticity and anelasticity of metals*. University of Chicago press.

Zhao, L., Yuan, H., Yang, J., Han, D. H., Geng, J., Zhou, R., ... & Yao, Q. (2017). Mobility effect on poroelastic seismic signatures in partially saturated rocks with applications in time-lapse monitoring of a heavy oil reservoir. *Journal of Geophysical Research: Solid Earth*, *122*(11), 8872-8891.

Zhao, L., Cao, C., Yao, Q., Wang, Y., Li, H., Yuan, H., ... & Han, D. H. (2020). Gassmann consistency for different inclusion-based effective medium theories: Implications for elastic interactions and poroelasticity. *Journal of Geophysical Research: Solid Earth*, *125*(3), e2019JB018328.